UDK 621.3:(53+54+621+66)(05)(497.1)=00 ISSN 0352-9045

INFORMACIJE MIDEM 2·2003

Strokovno društvo za mikroelektroniko elektronske sestavne dele in materiale

Strokovna revija za mikroelektroniko, elektronske sestavne dele in materiale
Journal of Microelectronics, Electronic Components and Materials

INFORMACIJE MIDEM, LETNIK 33, ŠT. 2(106), LJUBLJANA, junij 2003

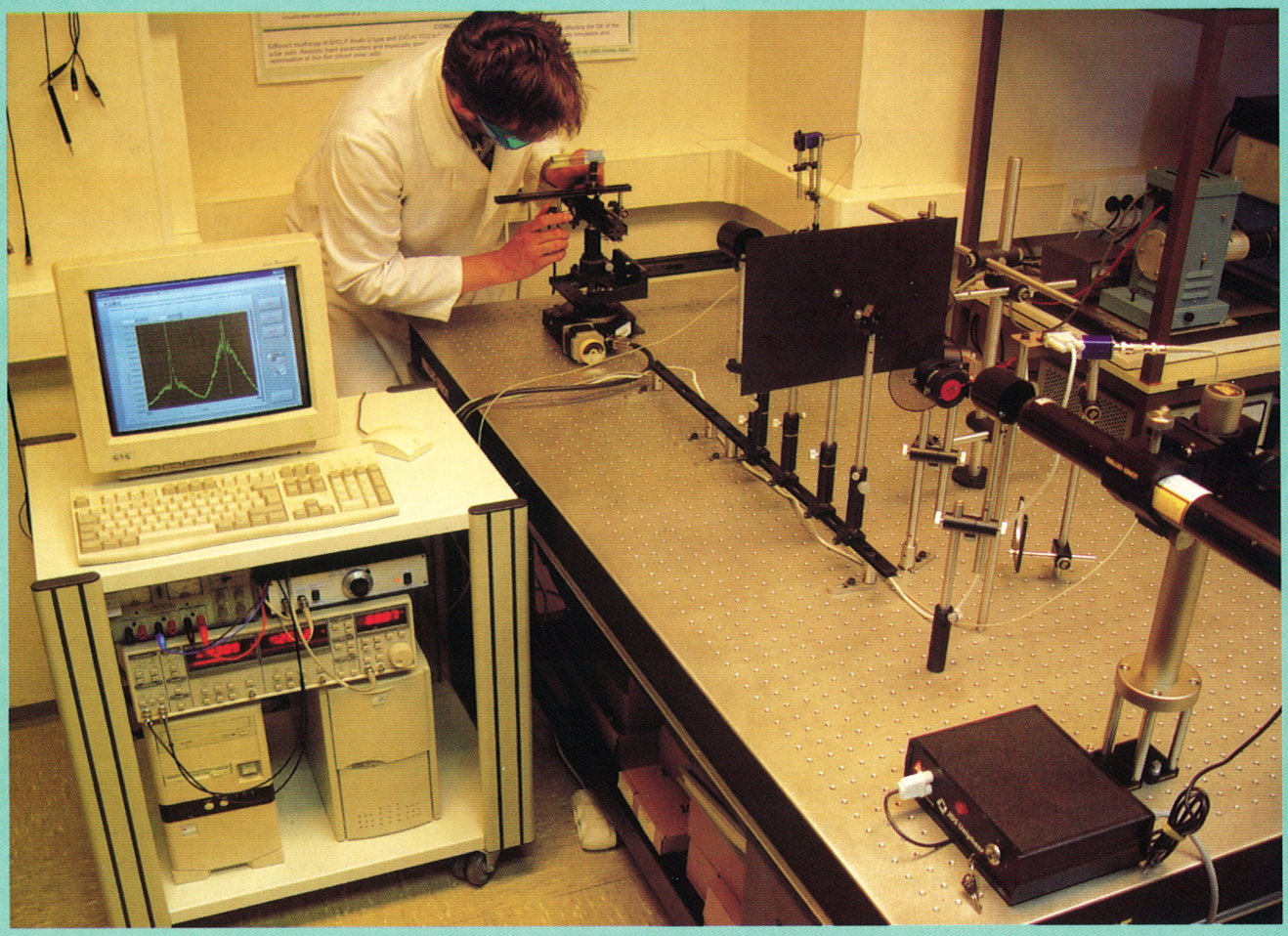

UNIVERSITY OF LJUBLJANA

FACULTY OF ELECTRICAL ENGINEERING

LSD

LABORATORY OF SEMICONDUCTOR DEVICES

UDK 621.3:(53+54+621+66)(05)(497.1)=00 ISSN 0352-9045

INFORMACIJE MIDEM 2 ◦ 2003

INFORMACIJE MIDEM LETNIK 33, ŠT. 2(106), LJUBLJANA, JUNIJ 2003
INFORMACIJE MIDEM VOLUME 33, NO. 2(106), LJUBLJANA, JUNE 2003

Revija izhaja trimesečno (marec, junij, september, december). Izdaja strokovno društvo za mikroelektroniko, elektronske sestavne dele in materiale - MIDEM.
Published quarterly (march, june, september, december) by Society for Microelectronics, Electronic Components and Materials - MIDEM.

Naslov uredništva
Headquarters
Uredništvo Informacije MIDEM
MIDEM pri MIKROIKS
Stegne 11, 1521 Ljubljana, Slovenija
tel.: + 386 (0)1 51 33 768
fax: + 386 (0)1 51 33 771
e-mail: Iztok.Sorli@guest.arnes.si
http://paris.fe.uni-lj.si/midem/

Letna naročnina znaša 12.000,00 SIT, cena posamezne številke je 3000,00 SIT. Člani in sponzorji MIDEM prejemajo Informacije MIDEM brezplačno.
Annual subscription rate is EUR 100, separate issue is EUR 25. MIDEM members and Society sponsors receive Informacije MIDEM for free.

Znanstveni svet za tehnične vede I je podal pozitivno mnenje o reviji kot znanstveno strokovni reviji za mikroelektroniko, elektronske sestavne dele in materiale. Izdajo revije sofinanci rajo Ministrstvo za znanost in tehnologijo in sponzorji društva.
Scientific Council for Technical Sciences of Slovene Ministry of Science and Technology has recognized Informacije MIDEM as scientific Journal for microelectronics, electronic components and materials.
Publishing of the Journal is financed by Slovene Ministry of Science and Technology and by Society sponsors.

Znanstveno strokovne prispevke objavljene v Informacijah MIDEM zajemamo v podatkovne baze COBISS in INSPEC.

Prispevke iz revije zajema ISI® v naslednje svoje produkte: Sci Search®, Research Alert® in Materials Science Citation Index™

Scientific and professional papers published in Informacije MIDEM are assessed into COBISS and INSPEC databases.

The Journal is indexed by ISI® for Sci Search®, Research Alert® and Material Science Citation Index™

Po mnenju Ministrstva za informiranje št.23/300-92 šteje glasilo Informacije MIDEM med proizvode informativnega značaja.

Grafična priprava in tisk
Printed by
BIRO M, Ljubljana

Naklada
Circulation
1000 izvodov
1000 issues

Poštnina plačana pri pošti 1102 Ljubljana
Slovenia Taxe Percue

UDK621.3:(53+54+621+66), ISSN0352-9045 Informacije MIDEM 33(2003)2, Ljubljana

ZNANSTVENO STROKOVNI PRISPEVKI		PROFESSIONAL SCIENTIFIC PAPERS
V.Matko: Senzor poroznosti	73	V.Matko: Porosity Sensor
R.Osredkar: Osnove teorije optičnih preslikav, prirejene za potrebe simulacij fotolitografskega procesa	79	R.Osredkar: Basics of Optical Imaging Theory Applied to the Photolithographic Process Simulation
M.Verderber, A.Žemva: Strojno in programsko razdeljena optimizacija in FPGA implementacija MPEG-2 video dekoderja	86	M.Verderber, A.Žemva: HW/SW Partitioned Optimization and VLSI-FPGA Implementation of the MPEG-2 Video Decoder
B.Kodek: Montaža plošč tiskanih vezij z zlitinami brez svinca	92	B.Kodek: Assembling of Printed Circuits Boards with the Lead Free Alloys
L. Knez: Induktivni senzorji	96	L. Knez: Inductive Sensors
A.Šoštarič, B.Imperl, B.Jerabek: Hišna avtomatizacija na pohodu	100	A.Šoštarič, B.Imperl, B.Jerabek: Home Automation On The Move
F.Koplan: ABS-senzorji na osnovi AlNiCo-magnetov	105	F.Koplan: ABS Sensor Applications Based on AlNiCo Magnets
A.Pleteršek: 12-bitni bliskovni DAC	110	A.Pleteršek: A 12-bit Flash ADC
V. Kunc, M. Atanasijević Kunc: Avtomatsko nastavljanje ojačenja v brezkontaktnih komunikacijskih sistemih	115	V. Kunc, M. Atanasijević Kunc: Automatic Gain Adjustment in Contactless Communication Systems
A.Pevec, J.Trontelj: Mikrosistem za merjenje električnega toka	118	A.Pevec, J.Trontelj: Microsystem For Electrical Current Sensing
M.Topič: Čestitka prof. dr. Mariji Kosec za priznanje Ambasador Republike Slovenije v znanosti za leto 2003	122	M.Topič: Congratulations to prof.dr.Marija Kosec - Ambassador of Science of the Republic of Slovenia for year 2003
I.Pompe: Posvet o novih tehnologijah	125	I.Pompe: Symposium on New Technologies
MIDEM prijavnica	127	MIDEM Registration Form
Slika na naslovnici:		Front page:

Obnovitev članstva v strokovnem društvu MIDEM in iz tega izhajajoče ugodnosti in obveznosti

Spoštovani,

V svojem več desetletij dolgem obstoju in delovanju smo si prizadevali narediti društvo privlačno in koristno vsem članom.Z delovanjem društva ste se srečali tudi vi in se odločili, da se v društvo včlanite. Življenske poti, zaposlitev in strokovno zanimanje pa se z leti spreminjajo, najrazličnejši dogodki, izzivi in odločitve so vas morda usmerili v povsem druga področja in vaš interes za delovanje ali članstvo v društvu se je z leti močno spremenil, morda izginil. Morda pa vas aktivnosti društva kljub temu še vedno zanimajo, če ne drugače, kot spomin na prijetne čase, ki smo jih skupaj preživeli. Spremenili so se tudi naslovi in način komuniciranja.

Ker je seznam članstva postal dolg, očitno pa je, da mnogi nekdanji člani nimajo več interesa za sodelovanje v društvu, se je Izvršilni odbor društva odločil, da stanje članstva uredi in **vas zato prosi, da izpolnite in nam pošljete obrazec priložen na koncu revije.**

Naj vas ponovno spomnimo na ugodnosti, ki izhajajo iz vašega članstva. Kot član strokovnega društva prejemate revijo »Informacije MIDEM«, povabljeni ste na strokovne konference, kjer lahko predstavite svoje raziskovalne in razvojne dosežke ali srečate stare znance in nove, povabljene predavatelje s področja, ki vas zanima. O svojih dosežkih in problemih lahko poročate v strokovni reviji, ki ima ugleden SCI faktor.S svojimi predlogi lahko usmerjate delovanje društva.

Vaša obveza je plačilo članarine 25 EUR na leto. Članarino lahko plačate na transakcijski račun društva pri A-banki : 051008010631192. Pri nakazilu ne pozabite navesti svojega imena!

Upamo, da vas delovanje društva še vedno zanima in da boste članstvo obnovili. Žal pa bomo morali dosedanje člane, ki članstva ne boste obnovili do konca leta 2003, brisati iz seznama članstva.

Prijavnice pošljite na naslov:

MIDEM pri MIKROIKS
Stegne 11
1521 Ljubljana

Ljubljana, april 2003

Izvršilni odbor društva

POROSITY SENSOR

Vojko Matko

University of Maribor, Faculty of Electrical Engineering and Computer Science, Maribor, Slovenia

Key words: porosity, soils, glass test tube, capacitive-dependent crystal, direct digital method.

Abstract: In response to a need for a more accurate porosity measuring method for small solid samples (approximately 1 g in mass) the porosity measurement sensor using a sensitive capacitive-dependent crystal was developed. This paper presents the new sensor and the probe sensitivity, frequency dependence on the volume. In addition, the new idea of excitation of the entire sensor with stochastic test signals is described, and the porosity measuring method is provided. The latter includes the influence of test signals on the weighting function uncertainty. The experimental results of the porosity determination in volcanic rock samples are presented. The uncertainty of the porosity measurement is less than 0.1 % in the temperature range 10 - 30 °C.

Senzor poroznosti

Ključne besede: poroznost, zemljine, steklena merilna epruveta, kapacitivno odvisni kristali, direktna digitalna metoda.

Izvleček: V iskanju bolj natančnega merjenja poroznosti malih trdnih delcev (mase približno 1g) je bila razvita metoda, ki uporablja kapacitivno odvisne kristale. V delu je prikazan novi senzor in njegova frekvenčna odvisnost od volumna. V nadaljevanju je prikazana nova ideja vzbujanja senzorja s stohastičnimi signali in zmanjšanje merilne negotovosti vpliva sistema (senzorja). Prikazani so eksperimentalni rezultati merjenja poroznosti vulkanskega pepela s pogreškom 0.1% v temperaturnem območju 10 - 30°C.

1 Introduction

Porosity is defined as the ratio of the volume of voids to the total volume of the material.

Solid rock is often not so solid. Sandstone might have started out as a sand dune or a beach, which got buried and compressed. But spaces and pores, remain between the particles. Soils, too, contain pores, which can be classified as micro and macro. Pore diameters larger than 0.06 mm are called macropores and those less as micropores. Soils may be considered as a porous four-phase system composed of air, water, solids and admixtures. The latter are a mixture of water and solids and are soft. In this four-phase soil system, the density ρ of soils is defined as the ratio of the sum of mass m to the sum of volume V of various soil phases /1/-/3/

$$\rho = \frac{\sum m_i}{\sum V_i} = \frac{m_s + m_w + m_a + m_{ad}}{V_s + V_w + V_a + V_{ad}}, \quad (1)$$

$$\sum_i m_i = m_s + m_w + m_a + m_{ad}, \quad (2)$$

$$\sum_i V_i = V_s + V_w + V_a + V_{ad} \quad (3)$$

where

s	solid phase
w	water phase
a	air phase
ad	admixture.

Equation (1) can also be rewritten as

$$\rho = \frac{\rho_s V_s + \rho_w V_w + \rho_a V_a + \rho_{ad} V_{ad}}{V_s + V_w + V_a + V_{ad}}, \quad (4)$$

where solid particle density is

$$\rho_s = \frac{m_s}{V_s}, \quad (5)$$

water phase density is

$$\rho_w = \frac{m_w}{V_w}, \quad (6)$$

air phase density is

$$\rho_a = \frac{m_a}{V_a}, \quad (7)$$

and soil admixture density is

$$\rho_{ad} = \frac{m_{ad}}{V_{ad}}. \quad (8)$$

Instead of density, the specific gravity can be written. From equation (4) we can write

$$\gamma = \frac{(\rho_s V_s + \rho_w V_w + \rho_a V_a + \rho_{ad} V_{ad}) \cdot g}{V_s + V_w + V_a + V_{ad}}, \quad (9)$$

In practice, we can define mass as the ratio of weight of soil to gravity

$$m = \frac{W}{g}. \quad (10)$$

During weighting in air the mass must be increased due to the presence of the air (Avogadro's law)

$$m_s = \frac{W_s}{g} + \rho_a \cdot V_s, \quad (11)$$

$$m_w = \frac{W_w}{g} + \rho_a \cdot V_w, \quad (12)$$

$$m_{ad} = \frac{W_{ad}}{g} + \rho_a \cdot V_{ad}. \quad (13)$$

Porosity of soil is defined by two parameters - void ratio e and porosity parameter η. The total void ratio e is defined as the ratio of volume of pores to volume of solid particles

$$e = \frac{V_w + V_a}{V_s} \quad (14)$$

and phases void ratio as

$$e_w = \frac{V_w}{V_s}, \quad (15)$$

$$e_a = \frac{V_a}{V_s}. \quad (16)$$

The porosity parameter η is defined as the ratio of volume of water plus volume of air to volume of soil samples.

Total:

$$\eta = \frac{V_w + V_a}{V} = \frac{V_w + V_a}{V_s + V_w + V_a}. \quad (17)$$

Phases:

$$\eta_w = \frac{V_w}{V} = \frac{V_w}{V_s + V_w + V_a}, \quad (18)$$

$$\eta_a = \frac{V_a}{V} = \frac{V_a}{V_s + V_w + V_a}. \quad (19)$$

The water content w_a is defined as the ratio of the weight of water to the weight of soil particles

$$w = \frac{W_w}{W_s} = \frac{W - W_a - W_s - W_{ad}}{W_s}. \quad (20)$$

The absolute water content w_a is defined as the ratio of the weight of water to the total weight of sample

$$w_a = \frac{W_w}{W} = \frac{W - W_a - W_s - W_{ad}}{W}. \quad (21)$$

The degree of saturation S_r is defined as the ratio of the volume of pores saturated with water to the volume of all pores

$$S_r = \frac{V_w}{V_w + V_a} = \frac{\eta_w}{\eta_w + \eta_a}. \quad (22)$$

1.1 Porosity determination methods

The simplest method is the determination of porosity by saturation method (Fig. 1) /4/. In this standardised procedure, the beakers are first filled to the same mark with gravel, sand, silt or mixture of these three materials. Then the water is poured into each of the beakers until it reaches the top of each material.

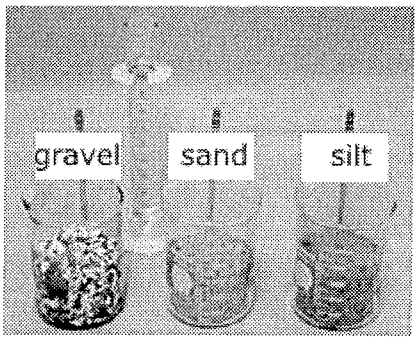

Fig. 1. Determination of porosity by saturation.

Porosity is determined by dividing the volume of water that you were able to pour into the material by the total volume of that material. The result is expressed as a percentage. It dictates how much water a saturated material can contain and has an important influence on bulk properties of material, e.g. bulk density, heat capacity, seismic velocity, etc.

$$\eta = \frac{V_{void}}{V_{total}} \cdot 100\ \% \quad (23)$$

where

V_{void} pore space volume

V_{total} total volume

There are many different porosity measurement methods. The imaging porosity method aims to identify and quantify different pore systems to determine the nature and abundance of matrix and macroporosity. Matrix porosity is characterised from digital images obtained from thin sections cut from core plugs /5/.

The helium pycnometer method uses helium. The pycnometer consists of two chambers, connected by a tube with a valve in it. The idea is to measure the pressure difference between the two containers, one of which has the sample material in it. The degree of porosity is determined by the difference in the pressures (due to porosity) caused by the opening of the valve at constant temperature. The porosity of the sample is the percentage difference between the grain volume and bulk volume, divided by the bulk volume /6/.

Porosity can also be determined by other conventional methods such as adsorption method, infrared scattering, mercury porosimetry, capillary method, dielectric method, analytical method, proton nuclear magnetic resonance, chromatography and ultrasound method /7/, /8/.

The new porosity measuring method described in this paper uses a highly sensitive sensor with improved uncertainty of measuring results and reduced influence of disturbing noise signals /9/. In comparison to the helium pycnometer method it is a lot simpler. In addition, the water is not poured on the material. Instead, the soil or rock sample is immersed in the water.

Most capacitive bridge methods can be adapted to three-terminal measurements by the addition of components to balance the ground admittances /10/, /11/. However, the balance conditions for these and the main bridge being interdependent, the balancing process can become very tedious. Also, the ratio signal/noise is supposed to be high.

The well-known method is Miller's etalon /12/ which is designed to sense small changes in the ≅ 4 pF capacitor from the phase change of a series-resonant circuit. The weakness of Miller's etalon is a greater sensitivity to phase noise than with the bridge method, which is due to higher frequencies (up to 45 MHz).

An alternative approach has been described by Van Degrift /13/ who used very sensitive tunnel-diode oscillator systems for measuring extremely small capacitance changes. This gain in sensitivity is somewhat offset by a loss in stability.

2 The porosity sensor

The porosity sensor uses sensitive capacitive-dependent crystals (40 MHz with stability of ±1 ppm in the temperature range from -5 to +55 °C) due to stability and the long-term repetition (Fig. 2). Two pseudo stochastic three-state signals $x_1(t)$ and $x_2(t)$ are used to influence the frequencies of the two quartz oscillators /14/, /15/. The frequency of oscillator 1 is 40 MHz and that of oscillator 2 is 40.001 MHz /16/, /17/. The output of the pulse-width modulator (EXOR) is a pulse-width signal which is compensated for temperature and voltage drift.

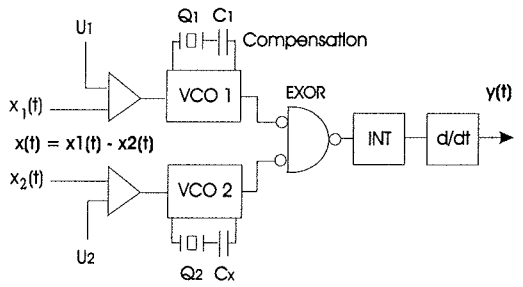

Fig. 2. Sensor structure.

The sensor probe C_x is a capacitor on the outer surface of the glass test tube (Fig. 3) /18/. The crystal is used as a stable oscillation element whose substitutional electrical structure only is being changed through the variation of the series capacitance C_x. The values in the quartz substitutional electrical structure and the capacitance C_x = 5 pF are measured with impedance/gain phase analyser HP 4194A.

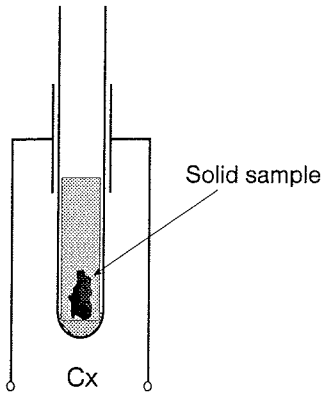

Fig. 3. Glass test tube.

The change of the water level causes the change of capacitance and frequency change in oscillator 2 (Fig. 2, Fig. 3). The probe dependence *df* on the volume is shown in Fig. 4. The frequency measurement uncertainty is ±0.1 Hz. The results suggest that the change in frequency is proportional to the volume in the range 0 - 1ml.

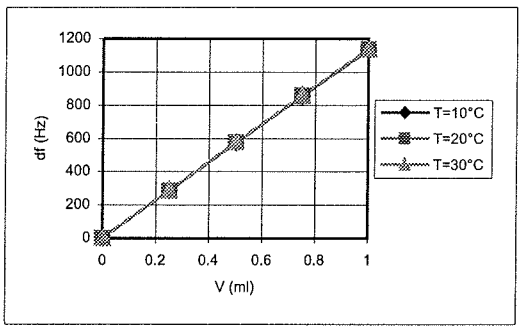

Fig. 4. The probe dependence df on the volume with signals $x_1(t)$ *and* $x_2(t)$.

3 Reduction of the measurement uncertainty

The uncertainty of the measuring results is improved by the direct digital method (DDM), which reduces the influence of disturbances /9/. Linear time-invariant system has been chosen due to signals $x_1(t)$ and $x_2(t)$, which form a special correlation function that is real-time independent.

$$\Phi_{xy}(\tau) = \sum_{u=0}^{T} g(u) \cdot \Phi_{xx}(\tau - u) \qquad (24)$$

$\Phi_{xy}(\tau)$ - cross-correlation function

$g(u)$ - weighting function

$\Phi_{xx}(\tau - u)$ - auto-correlation function

T - measuring period

For every value of τ, one equation with various numbers of elements is obtained. To calculate the value of the weighting functions g(0), g(1),..., g(L), the equations are united in the system with $L + 1$ equations

$$\begin{bmatrix} \Phi_{xy}(-P+L) \\ \cdot \\ \cdot \\ \Phi_{xy}(-1) \\ \Phi_{xy}(0) \\ \Phi_{xy}(+1) \\ \cdot \\ \cdot \\ \Phi_{xy}(M) \end{bmatrix} = \begin{bmatrix} \Phi_{xx}(-P+L) & \cdots & \Phi_{xx}(-P) \\ \cdot & \cdots & \\ \cdot & \cdots & \\ \Phi_{xx}(-1) & \cdots & \Phi_{xx}(-1-L) \\ \Phi_{xx}(0) & & \Phi_{xx}(-L) \\ \Phi_{xx}(+1) & & \Phi_{xx}(1-L) \\ \cdot & \cdots & \\ \cdot & & \\ \Phi_{xx}(M) & & \Phi_{xx}(M-L) \end{bmatrix} \cdot \begin{bmatrix} g(0) \\ \cdot \\ \cdot \\ \cdot \\ \cdot \\ \cdot \\ \cdot \\ \cdot \\ g(L) \end{bmatrix}$$

or its mathematical equivalent

$$\underline{\hat{\Phi}_{xy}} = \underline{\hat{\Phi}_{xx}} \cdot \underline{g}. \tag{25}$$

The biggest negative time move $\tau_{min} = -P$ and the biggest positive one $\tau_{max} = M$ were used. The system of equations has thus $P - L + M + 1$ number of equations. If $M = -P + 2L$ is chosen, $L + 1$ number of equations remain, so that $\hat{\Phi}_{xx}$ becomes a square matrix and we get

$$\hat{g} = \hat{\Phi}_{xx}^{-1} \cdot \hat{\Phi}_{xy}. \tag{26}$$

If $P = L$ is determined, then the same number of values (symmetrical auto-correlation functions (AKF) because $\tau_{min} = -P = -L$ and $\tau_{max} = M = L$ for the positive and negative τ) is used to calculate $\Phi_{xx}(\tau)$. The calculation of the weighting function is simplified if the input signal is white noise with the auto-correlation function as

$$\Phi_{xx}(\tau) = \sigma_x^2 \cdot \delta(\tau) = \Phi_{xx}(0) \cdot \delta(\tau), \tag{27}$$

$$\delta(\tau) \begin{cases} 1 \ for \ \tau = 0 \\ 0 \ for \ |\tau| \neq 0 \end{cases}. \tag{28}$$

It follows that

$$\hat{g}(\tau) = \frac{1}{\hat{\Phi}_{xx}(0)} \cdot \hat{\Phi}_{xy}(\tau). \tag{29}$$

Having formulated (26) and having considered the measurement time t_{meas} which is to be as long as possible, we get the weighting function $\hat{g}(\tau)$ (29) /9/.

4 Porosity measurement

Due to the specially chosen test signals $x_1(t)$ and $x_2(t)$ the function $\Phi_{xy1}(\tau)$ begins in the origin of coordinates and ends on the X axis when $\tau = t_{meas}$ (Fig. 5).

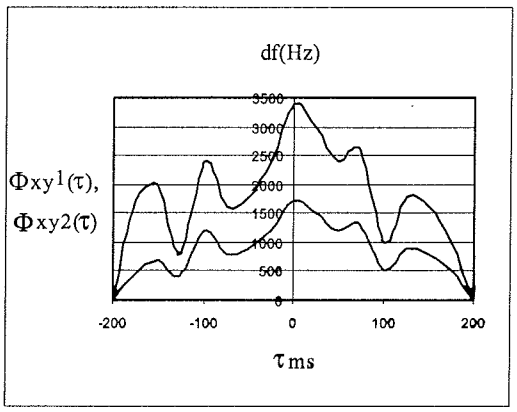

Fig. 5. Functions $\Phi_{xy1}(\tau)$ and $\Phi_{xy2}(\tau)$.

Consequently, the porosity is defined as a change of area between the functions $\Phi_{xy2}(\tau)$ and $\Phi_{xy1}(\tau)$, whose change is defined by capacitance C_x and specially chosen test signals $x_1(t)$ and $x_2(t)$. In this way the test signal has been considered throughout the entire t_{meas} period, as well as the sign change compensation in the calculation of the cross-correlation function. Comparing to the measurements that are not DDM method based the improvement of the ratio signal/noise by ≅ 30 dB is the most significant gain.

4.1 Calibration

The frequency is simultaneously converted into volume units by calibrating the ratio between the frequency and the volume for each glass tube. Mercury, whose mass is measured at an error of 0.01 % (at known temperature) is used for calibration /19/. The mechanical nonlinearities of the glass tube diameter along the whole tube are taken into account. According to the producer's data these do not exceed 0.01 %. The dependence can be linearized by using the spline method.

4.2 The influence of temperature and measurement error

The influence of temperature on measurements is considered in three ways. We must know the influence of the temperature on the measuring equipment, on the measuring medium in which the measurement is performed (i.e. the fluid in which the test is carried out), and the influence of the soil's temperature on its physical properties /19/.

The temperature of the environment affects the linearity of the measuring sensor. Calibration is used to establish the measurement error of the sensor which is 0.03 %. If the relation between the output frequency and the volume is known (Fig. 4), we get

$$V(T) = V(T_0) + \Delta V(T). \tag{30}$$

Equation (30) gives the correction of the measurement with respect to temperature changes. Temperature changes also affect the volume of the measured medium, i.e. of the

soil sample. Consequently, the change of volume due to temperature changes is expressed in the determination of the soil's specific gravity as follows

$$\gamma(T)=\gamma(T_0)+\Delta\gamma(T). \tag{31}$$

In conditions of linear temperature relationship inside a certain temperature range it holds true that

$$V(T)=V_s(T_0)\cdot\left(1+\alpha_{V_s}(T-T_0)\right) \tag{32}$$

where α_S is the temperature coefficient of soil.

The change of volume due to temperature changes in naturally humid soils is expressed as the sum of volume changes of all soil phases

$$dV(T)=dV_s(T)+dV_w(T)+dV_{ad}(T). \tag{33}$$

The total measurement error of the porosity sensor in relation to known individual partial influences such as glass tube nonlinearity, calibration with mercury, the influence of temperature on the sensor (Fig. 4), linearization of *df* on *V*, frequency measurement *y(t)* (Fig. 2), specific soil weight (31), change of water volume in the test tube and the change of sample volume *dV(T)* (33) does not exceed 0.1 % (10 - 30°C). This value was calculated on the basis of calibration data and the influence of temperature and measurement error.

5 Experimental porosity measurement

To test the new method, volcanic rock samples, which are known for their porosity, were selected for experimental determination of porosity. Four characteristic samples approximately 1 ml in size and 1 g in weight were gathered near Puerto de Santiago, Mount Teide volcano (3715 m), Tenerife (Fig. 6).

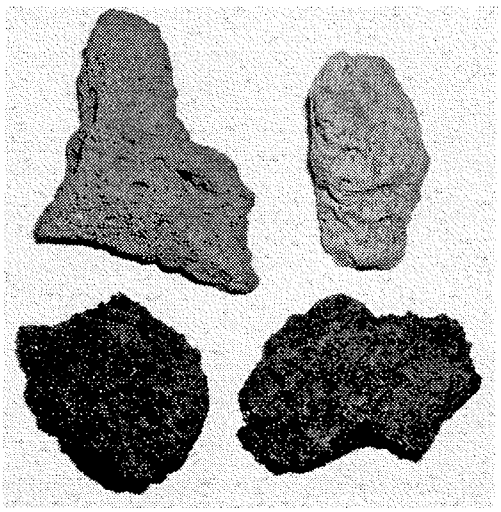

Fig. 6. Four typical porous volcanic rock samples of about 1 ml in size and 1 g in mass.

All test samples were randomly selected. To determine the porosity of a random solid sample (at 20 °C), the sample is immersed in water contained in a test tube around which the capacitor C_x is placed (Fig. 3). The volume of the sample is measured. In the first case, the glass solid sample with ~ 0 % porosity was immersed (Fig. 7).

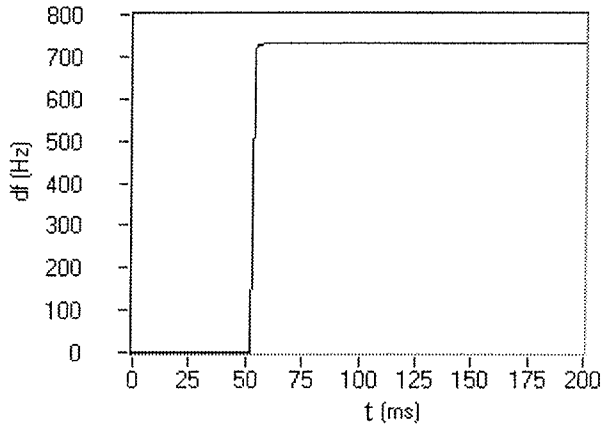

Fig. 7. Measurement of sample having ~ 0 % porosity.

The frequency remained unchanged after immersion, which indicates that there was no air leak. In the second case, a dry randomly selected volcanic rock sample (weighting 0.821 g) was immersed in the water. Since the sample was porous, the air leaked, which was reflected in the dynamic change of frequency (Fig. 8). The transitional phenomenon caused by immersion ends in 1 ms.

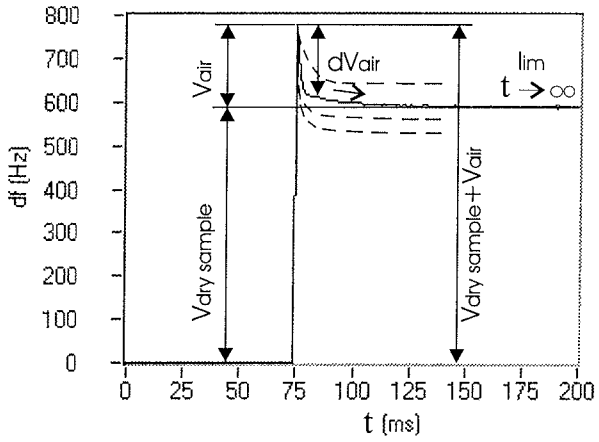

Fig. 8. Air leak after sample immersion.

The measurement is performed until the final state towards which the measurement limits is reliably predicted. Depending on the degree of porosity, this saturation limit is higher or lower as shown for the other three samples (Fig. 8).

At known temperature the sample porosity can be determined

$$\eta=\frac{V_{air}}{V_{drysample}+V_{air}}. \tag{34}$$

The sample porosity on Fig. 8 was 23.8 %. The fastest measurement time without test signals is 1 μs.

6 Conclusion

The porosity sensor using the capacitive-dependent crystals has been described and the dependence of *df* on the volume of the sensor probe has been presented. The porosity determination procedure includes the influence of test signals on the weighting function uncertainty.

The formation of the cross-correlation function between the test signal *x(t)* and the system response *y(t)* decreases the influence of all disturbing signals that are not correlated to the test signal x(t) for ≅ 30 dB /9/. Other advantages of the proposed method are high sensitivity, high stability, a series resonant circuit which is not composed of the elements *L* and *C*, the ratio signal/noise does not affect the accuracy of measurements, reduced disturbances due to the structure and the method, the long-term repetition, reduced hysteresis /17/ and low cost. It should be noted, however, that pairs of crystals with similar temperature characteristics should be used. The accuracy and repeatability are determined only with the temperature frequency difference of the crystal pairs /19/.

7 References

/1/ P. Sheng, „Effective medium theory of sedimentary rocks," Phys. Rev. B., vol. 41, pp. 4507, 1993.

/2/ S. Sakai, "Determination of pore size and pore size distribution," Journal of membrane science, vol. 96, pp. 91, 1994.

/3/ K. Meyer, P. Lorenz, B. Böhl-Kuhn, and P. Klobes, "Porous solids and their characterization," Cryst. Res. Techn., vol. 29, pp. 903, 1994.

/4/ A. Netto, "Pore-size distribution in sandstones," Bull. Appl. Math., vol. 77, pp. 1101, 1993.

/5/ J. Fredrich, B. Menendez, and T. Wong, "Imaging the pore structure of geomaterials," Science, vol. 268, pp. 276, 1995.

/6/ H. Franz, "Herstellung von Drucksensoren," Feinwerktechnik & Meâtechnik 95, H. 3, pp. 145-151, 1987.

/7/ J. Fripiat, „Porosity and adsorption isotherms," Fractal Approach to Heterogeneous Chemistry, Wiley, pp. 28, 1989.

/8/ G. P. P. Gunarathne and K. Christidis, "Measurements of Surface Texture Using Ultrasound," IEEE Trans. Instrum. Meas., 50 (5), October , pp. 1144-1148, 2002.

/9/ K. W. Bonfig, "Das Direkte Digitale Messverfahren (DDM) als Grundlage einfacher und dennoch genauer und störsicherer Sensoren," Sensor Nov., pp. 223-228, 1988.

/10/ M. C. McGregor, J. F. Hersh, R. D. Cutkosky, F. K. Harris, and F.R.Kotter, "New Apparatus at the National Bureau of Standards for Absolute Capacitance Measurement," IRE Trans. Instr. 1-7 (3-4), pp. 253-61, 1958.

/11/ A. M. Thompson, "The Precise Measurement of Small Capacitances," IRE Trans. Instr. 1-7(3-4), pp. 245-53, 1958.

/12/ G. L. Miller and E. R. Wagner, "Resonant phase shift technique for the measurement of small changes in grounded capacitors," Rev. Sci. Instrum. 61(4), pp.1267, 1990.

/13/ C. T. Van Degrift, "Modeling of tunnel diode oscillators," Rev. Sci .Instrum. 52(5), May, pp. 712-723, 1981.

/14/ K. Dmowski, "A new correlation method for improvement in selectivity of bulk trap measurements from capacitance and voltage transients," Rev. Sci. Instrum. 61(4), April, pp.1319-1325, 1990.

/15/ M. Bertocco, A. Flammini, D. Marioli, and A. Taroni, "Fast and Robust Estimation of Resonant Sensors Signal Frequency," IEEE Trans. Instrum. Meas., 51 (2), April, pp. 326-330, 2002.

/16/ V. Matko and J. Koprivnikar - a, "Capacitive sensor for water absorption measurement in glass-fiber resins using quartz crystals," IAAMSAD:South African branch of the Academy of Nonlinear Sciences, Proceedings, Durban, South Africa, pp. 440 -443, 1998.

/17/ V. Matko and J. Koprivnikar - b, "Quartz sensor for water absorption measurement in glass-fiber resins," IEEE Trans. Instrum. Meas., 47 (5), Oct., pp. 1159-1162, 1998.

/18/ M. Stucchi and K. Maex, "Frequency Dependence in Interline Capacitance Measurements," IEEE Trans. Instrum. Meas., 51 (3), Jun., pp. 537-543, 2002.

/19/ R. C. Weast, "CRC Handbook of Chemistry and Physic," 67 th edition, Boca Raton, Florida, pp. E49-E52, 1987.

Izr. prof. dr. Vojko Matko
University of Maribor, Faculty of Electrical Engineering and Computer Science,
Smetanova 17, 2000 Maribor, Slovenia
E-mail: vojko.matko@uni-mb.si

Prispelo (Arrived): 11.11.2002 *Sprejeto (Accepted): 25.05.2003*

OSNOVE TEORIJE OPTIČNIH PRESLIKAV, PRIREJENE ZA POTREBE SIMULACIJ FOTOLITOGRAFSKEGA PROCESA

R. Osredkar

Faculty of Computer Sciences and Faculty of Electrical Eng.,
University of Ljubljana, Slovenia

Ključne besede: Fourireova optika, Frauenhoferjev uklon, MTF, fotolitografija, projekcijski poravnalniki, mikroelektronika

Izvleček: V prispevku so predstavljene osnove teorije optičnih preslikav. Obravnavani so tisti aspekti Fourierove optike, Abbejeve teorije preslikav in teorije modulacijskih prenosnih funkcij (MTF), ki se nanašajo na preslikavo vzorcev s fotolitografske maske na s fotopolimerom prevlečeno rezino s projekcijskimi poravnalniki.

Basics of Optical Imaging Theory Applied to the Photolithographis Process Simulation

Key words: Fourier optics, Frauenhofer diffraction, MTF, photolithography, projection aligners, microelectronics

Abstract: Lithography is the cornerstone of modern IC manufacturing, and lithography tools and process characterization at the core of the lithography process engineering. Most of the ICs today are manufactured by optical photolithography. As the dimensions of the features to be fabricated on the wafer approach 0.1 μm the classical limits of resolution of optical tools used in photolithography are approached. Understanding and optimization of the performance of the lithographic process are thus becoming less accessible by the empirical methods traditionally used in IC manufacturing process development and have to be complemented by different computer simulation tools. Such tools are based on Fourier optics to describe the performance of exposure systems, and for their use a basic understanding of the underlying optical theory is required. In this tutorial these basics are covered, with the intenion to facilitate a study of more advanced literature.

All of the projection exposure systems used in IC manufacturing industry today are diffraction limited optical instruments. Consequently Frauenhofer diffraction theory is used to describe their performance. This has important consequences for imaging the fine mask patterns on the photoresist covered wafer. In order to understand the ralation between the (spatial) Fourier transform of the mask pattern and the diffraction image formed by the objective lens in its focal plane, it is instructive to compare the Fourier transform of a pulse function and the analytical expression for the diffraction image of a line source. It can immediately be seen, that they are equal. This conclusion can be generalized to the more complex case of mask imaging. Thus the far-field electric field intensity $E(y_{ff},z_{ff})$ is given by

$$E(y_{ff},z_{ff}) = F[f(y,z)]$$

where f(y,z) is mask transmittance function, and F Fourier transform operator. The objectve lens perfoms an inverse Fourier transform of $E(y_{ff},z_{ff})$, resulting in an image of the mask in the image plain of the objective lens, where the wafer is positioned. Field intensity distribution $E(y_i,z_i)$ of the image in the wafer plane is

$$E(y_i,z_i) = F^{-1}[E(y_o,z_o)\, P_o(f_y, f_z)] = F^{-1}\{F[E(y,z)]\, P_o(f_y, f_z)\}$$

where F^{-1} inverse Fourier trasform operator. The pupil function $P_o(f_y, f_z)$ of the objective lens is introduced into the expression in order to take account of finite dimensions of the lens. From this expression the well known resolution criteria of a projection system can be extracted.

Another basic optics concept allowing modeling of the aerial image on the surface of the photoresist film is the modulation transfer function (MTF). MTF is basically a measure of the contrast in the aerial image produced by the exposure system. It is also governed by the diffraction effects and MTF is therefore a function of the normalized spatial frequency ξ of the image. The resolution and the MTF(ξ) characterise performace of an exoposure tool, and have to be incorporated in a simulation. An implementation of these ideas in FOLIS, a photolithograhy simulation tool developed at the Microelectronics laboratory of the Faculty of Electrical Eng., University of Ljubljana, is reporte elsewhere /5/.

Uvod

Fotolitografija je eden od temeljev modernih postopkov izdelave integriranih elektronskih vezij in fotolitografska osvetljevalna orodja njeno središče. Velika večina takšnih orodij so danes projekcijski poravnalniki. Minimalne (tako imenovane kritične) dimenzije na sodobnih integriranih vezij segajo v področje velikosti 0,1 μm, kar je povsem na meji, če ne celo pod njo, ločljivosti osvetljevalnih orodij. Zato predstavljajo postopki preslikave in osvetljevanja velik izziv za razvijalce mikroelektronskih postopkov in dodobra uveljavljeni, empirični pristop k reševanju litografskih problemov, ki se pojavljajo pri njihovem delu, jim v resnici ni več povsem kos. Toda uspešno ga lahko dopolnijo različna programska orodja za simulacijo fotolitografskega postopka. Njihova uporaba pa zahteva vsaj osnovno poznavanje optične teorije.

Vsi projekcijski osvetljevalni sistemi, ki se danes uporabljajo v mikroelektronski industriji, so naprave, ki jim kvaliteto preslikave omejujejo uklonski pojavi. Te obravnava teorija Frauenhoferjevega uklona (uklona v daljnem polju), ki ga najpreprosteje simuliramo v okvirih Fourierove optike. Tudi če fotolitografsko preslikavo okarakteriziramo s prenosno funkcijo sistema, se upoštevanju uklonskih pojavov pri preslikavi ne moremo izogniti. Vse omenjene teme so v teoriji optike dobro in že dolgo časa poznane ter jih obravnava vrsta knjig /na primer 1, 2/ ter priročnikov /3/. Vendar se zdi, da je v praksi njihova uporaba omejena, morda v duhu pregovora, da v gozdu ni videti dreves. Fizikalni temelji sicer kompleksne optične teorije pa so razmeroma lahko razumljivi tudi v okviru znanj, ki jih razvojni inženir, delujoč na področju mikroelektronske fotolitografije, že ima. Namen tega prispevka je, da prav v tem okviru predstavi osnove relevantne optične teorije in tako olajša prvi korak pri poglobljenem študiju zahtevnejše literature. V prispevku zato ni govora o tehničnih podrobnostih projekcijskih osvetljevalnih naprav itd. Te so na voljo v literaturi /na primer v izboru literature v 4/. Prav tako v njem ni govora o simulacijskih orodjih, ki jih obravnavamo drugje /5/, pač pa so poudarjeni prav osnovni fizikalni pojmi optične teorije preslikav.

Fourierova transformacija pulzne funkcije

Fourierov integral neke funkcije f(x) je definiran /6/ kot

$$f(x)=\frac{1}{\pi}\left[\int_0^\infty A(k)\cos kx\,dk+\int_0^\infty B(k)\sin kx\,dk\right]$$

kjer sta

$$A(k)=\int_{-\infty}^{\infty} f(x)\cos kx\,dx \quad \text{in}$$

$$B(k)=\int_{-\infty}^{\infty} f(x)\sin kx\,dx$$

Podobnost gornjih izrazov z morda nekoliko bolj domačimi izrazi za Fourierovo vrsto je očitna, če se le spomnimo, da je integral limita vsote neskončne vsote. Količini A(x) in B(x), ki ju lahko razumemo kot amplitudi kosinusnih in sinusnih prispevkov k funkciji f(x) v intervalu od k do k+dk, se imenujeta kosinusna in sinusna transformacija funkcije f(x).

Oglejmo si Fourierovi transformaciji funkcije, ki predstavlja pravokoten pulz z dolžino L:

$f(x)$ = E_o, če je $|x| \le L/2$
0, če je $|x| > L/2$

Ker je f(x) soda funkcija, je njena sinusna transformacija B(k) enaka 0, medtem ko je

$$A(k)=\int_{-\infty}^{\infty} f(x)\cos kx\,dx=\int_{-L/2}^{L/2} E_o\cos kx\,dx=\frac{2E_o}{k}\sin kL/2$$

Če v zadnjem izrazu ulomek v števcu in imenovalcu pomnožimo z L ter člene nekoliko preuredimo, je končni izraz za Fourierovo transformacijo pulzne funkcije

$$A(k)=E_oL\frac{\sin kL/2}{kL/2}$$

Funkcijo $\frac{\sin kL/2}{kL/2}$ v optiki srečujemo tako pogosto, da zanjo običajno uporabljajo poseben simbol, sinc *kL/2*. Fourierovo transformacijo pulzne funkcije torej zapišemo kot

$$A(k) = E_oL \text{ sinc } kL/2$$

Na sliki 1 sta prikazani pulzna funkcija *f(x)* in njena Fourierova transformacija.

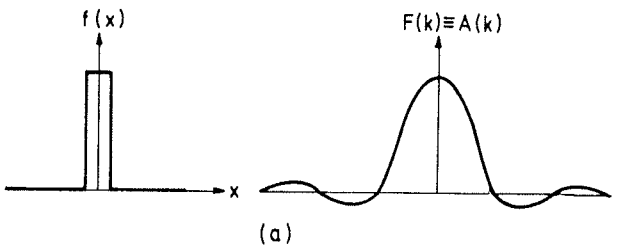

Slika 1: Pulzna funkcija in njena Fourierova transformacija.

Uklon

Če neko EM valovanje (svetlobo) prestrežemo z ravnim zaslonom v katerem je izrezana dolga, ravna reža, se skoznjo del vpadnega valovanja širi v polprostor za zaslonom. Kako to valovanje opišemo? Nalogo poskušamo rešiti s pomočjo Huygens-Fresnelovega načela /1/, ki zagotavlja, da širjenje valovanja lahko opišemo tako, da si neko valovno čelo valovanja zamišljamo razdeljeno na primerno majhne dele, ki so vsak izvor sekundarnih, krogelnih valovanj. Ta imajo isto valovno dolžino kot vpadno valovanje, kjer koli v prostoru za izbranim valovnim čelom pa je nato vrednost nihajoče količine (pri EM valovanje na primer velikost električnega polja, oz. električna poljska jakost E) določena s superpozicijo (nekoliko grobo rečeno, vsoto) prispevkov sekundarnih valov. Pri seštevanju moramo seveda upoštevati amplitude in faze posameznih prispevkov, kar nalogo v splošnem zelo zaplete. Sorazmerno preprosto jo lahko rešimo pravzaprav le v dveh primerih. Prvi je tisti pri katerem točka v kateri iščemo valovanje, od izbrane valovne fronte ni preveč oddaljena (v tako imenovanem bližnjem polju), drugi pa, če je točka od nje zelo oddaljena (v daljnem polje). V zvezi s projekcijskim osvetljevanjem nas zanima le drugi primer.

Preden se resnično lotimo seštevanja prispevkov sekundarnih valov k polju v toči T, definirajmo geometrijo problema:

na zaslon padajoče valovanje naj se širi v smeri x, zaslon pri x = 0 naj leži v ravnini y,z, torej naj bo vzporeden valovnim frontam upadlega valovanja in reža v njem, ki ima širino L, naj leži, simetrično na os x, v smeri z. Če je dolžina reže mnogo večja od njene širine, je očitno, da mora biti rešitev neodvisna od koordinate z. Z drugimi besedami, rešitev iščemo le v ravnini x,y, kar 3-dimenzionalno nalogo praktično prevede v 2-dimenzionalno in jo znatno poenostavi. Za valovno čelo, ki je izhodišče računa, izberemo ravnino zaslona. Režo si moramo torej zamisliti razdeljeno na primerno majhne dele, ki so izvori sekundarnih valov in v neki točki T za zaslonom sešteti njihove prispevke k polju E.

Električno polje ravnega EM valovanja, ki potuje v pozitivni smeri osi x pred zaslonom, opisuje enačba

$$E(x) = E_o \sin(\omega t - kx)$$

kjer sta ω krožna frekvenca ($2\pi\nu$) in k valovni vektor ($2\pi/\lambda$, λ je valovna dolžina valovanja). Valovanje, ki se širi iz točkastega izvora, pa opisuje enačba

$$E = (\Lambda/r) \sin(\omega t - kr)$$

kjer sta Λ tako imenovana jakost izvora in r razdalja od izvora do točke T v kateri valovanje opazujemo. V primeru, ki ga obravnavamo, r leži v ravnini x,y. Podobnost izrazov za ravno in krogelno valovanje je očitna, pomembna razlika med njima je le v faktorju 1/r, ki pri slednjem opisuje zmanjševanje amplitude polja z razdaljo. Režo si mislimo po širini razdeljeno na majhne dele dy. Prispevek vsakega izmed njih k skupnemu polju v točki T je

$$dE = (\Lambda_L/r) \sin(\omega t - kr)\, dy$$

kjer je Λ_L linearna jakost izvora, Λ/L. Da bi dobili celotno polje, moramo gornje prispevke integrirati po celotni širini reže. V primeru daljnega polja, pri katerem je širina reže L mnogo manjša od r, faktor 1/r brez zadrege lahko zamenjamo z 1/R, kjer je R razdalja od koordinatnega izhodišča (sredine reže) do točke v kateri računamo polje valovanja. Tega pa ne moremo storiti pri prostorsko spremenljivi fazi valovanja kr (torej v izrazu $2\pi r/\lambda$), saj pri njej razdalje očitno merimo v enotah valovne dolžine in je zato faza na majhne spremembe razdalje mnogo občutljivejša kot amplituda. Vendar pa pri računu daljnega polja r v izrazu za fazo lahko zamenjamo s približkom

$$r = R - y \sin\Theta$$

pri čemer je y koordinata izvora dy v reži (slika 2). Po tej zamenjavi je izraz za skupno električno polje v točki T

$$E = \frac{\Lambda_L}{R} \int_{-L/2}^{L/2} \sin[\omega t - k(R - y\sin\theta)]\, dy$$

in ga (z zamenjavo spremenljivk) zlahka integriramo:

$$E = \frac{\Lambda_L}{R} \frac{\sin[(kL/2)\sin\theta]}{(kL/2)\sin\theta} \sin(\omega t - kR), \text{ oziroma}$$

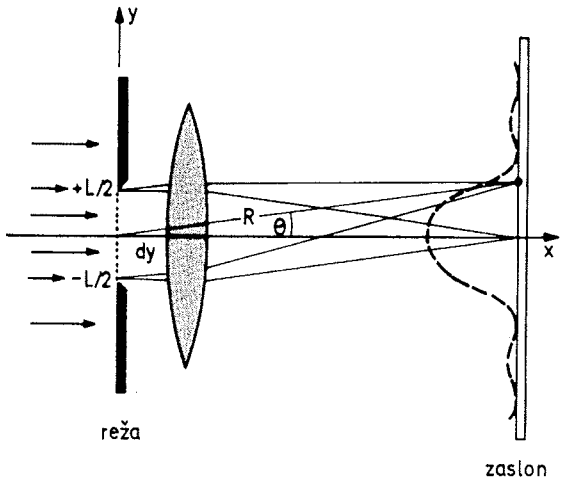

Slika 2: Uklon svetlobe na reži s širino L.

$$E = \frac{\Lambda_L}{R} \frac{\sin\beta}{\beta} \sin(\omega t - kR) = \frac{\Lambda_L}{R} \text{sinc}\beta \sin(\omega t - kR)$$

kjer smo $(kL/2)\sin\Theta$ zapisali kot β.

Primerjava izrazov za električno polje svetlobe, ki jo sevata reža in točkast izvor, pokaže, da je EM valovanje, ki izhaja iz reže, glede časovne odvisnosti in upadanja amplitude z razdaljo podobno valovanju točkastega izvora, vendar pa ni izotropno - v smereh, torej pri kotih Θ, v katerih ima funkcija sincβ vrednost 0 ga enostavno ni. Iz slike 1 je razvidno, da se to prvič zgodi, ko je vrednost njenega argumenta π, torej pri

$$\pi = (kL/2)\sin\Theta = (2\pi/\lambda)(L/2)\sin\Theta, \text{ oz.}$$

$$L\sin\Theta = \lambda$$

V slednjem takoj prepoznamo izraz, ki ga za smer uklonskega minima prvega reda za uklon svetlobe na ozki reži s širino L daje elementarna teorija uklona /7/.

Moteči časovni odvisnosti električnega polja se izognemo tako, da v izrazu zanj $\sin(\omega t - kR)$ zamenjamo z njegovo časovno povprečno vrednostjo, ki je $\frac{1}{\sqrt{2}}$. Po takšni zamenjavi postane enakost (do multiplikacijskega faktorja) izrazov za električno polje valovanja, ki ga seva ozka reža v zaslonu, in tistega za Fouriereovo transformacijo pulzne funkcije očitna. Enakost ni naključna. Z razširitvijo gornje izpeljave na 2-dimenzionalne reže v zaslonu in njeno manjšo posplošitvijo se da pokazati, da je uklonska slika svetlobe, ki prehaja skozi zaslon s poljubno razporeditvijo in obliko rež, v daljnem polju, vedno enaka Fourierovi transformaciji funkcije, ki opisuje porazdelitev, obliko in propustnost rež na zaslonu. Ugotovitev je za analizo in modeliranje preslikav v projekcijskih poravnalnikih, ki se uporabljajo v mikroelektronski industriji, ter drugod v optiki ključna. In seveda tudi praktična, ker s pomočjo računalnikov Fourierove transformacije poljubne prostorske funkcije lahko izračunamo brez velikih zapletov.

Transmisijska funkcija

Maske, ki se uporabljajo pri izdelavi integriranih vezij, so navadno ravne, kvarčne plošče prevlečene s tanko plastjo kroma. Na mestih, kjer na maski ni kromove plasti, je ta za UV svetlobo izvora prozorna, na prekritih mestih pa zanjo povsem neprepustna. Kontrast med svetlimi in temnimi deli maske je velik in zato lahko strukturo na maski zelo natančno opišemo z digitalno transmisijsko funkcijo f(x,z), ki ima vrednost 0 kjer maska ni prozorna in 1 na njenih prozornih delih. Porazdelitev električnega polja svetlobe, ki jo določa takšna maska, je v daljnem polju preprosto

$$E(y_{dp},z_{dp}) = F[f(y,z)]$$

kjer F pomeni Fourierovo transformacijo. Električno polje je pri preslikavah navadno manj zanimiva količina od gostote energijskega toka, ki je sorazmerna kvadratu električnega polja. Različnim multiplikacijskim faktorjem v izrazih za gostoto toka se pogosto ognejo z vpeljavo iradiance I, ki je le kvadrat polja. Za kotno odvisnost iradiance v primeru dolge reže torej velja

$$I(\Theta) = I_o \operatorname{sinc}^2 \beta ,$$

kjer je I_o iradianca v smeri optične osi (smeri x). Za masko, ki jo definira transmisijska funkcija maske f(y,z), podaja iradianco v daljnem polju izraz:

$$I(y_{dp},z_{dp}) = |F[f(y,z)]|^2$$

Abbejeva teorija preslikave

Pri osvetljevalnih sistemih, ki jih v industriji uporabljajo za preslikavo vzorcev z mask na silicijeve rezine, nas seveda zanimajo predvsem gostote energijskega toka (ali iradianca) na površini fotopolimera. Uklonska slika maske v daljnem polju je, kot smo videli, enaka Fourierovi transformaciji njene transmisijske funkcije in bi jo, v načelu, lahko prestregli in opazovali na dovolj oddaljenem zaslonu. To razdaljo zelo skrajšamo, če za masko postavimo lečo (objektiv). Ker so vsi žarki, ki iz predmeta izhajajo v smeri, določeni s kotom Θ (torej kotom med smerjo razširjanja valovanja in optično osjo sistema), med seboj vzporedni, se po prehodu skozi objektiv sekajo v eni točki. Z drugimi besedami, v goriščni ravnini objektiva nastane Frauenhoferjeva uklonska slika predmeta. Ker je ta slika Fourierova transformacija maske, včasih o objektivu govorijo kot o transformacijski leči in o ravnini v kateri nastane transformirana slika kot o transformacijski ravnini. V našem primeru sta goriščna ravnina objektiva in njegova transformacijska ravnina seveda ista ravnina. Na zaslonu, ki bi ga postavili v to ravnino, bi interferenčno sliko lahko prestregli in opazovali. Če takšnega zaslona ni, pa se svetloba širi še naprej in v neki drugi ravnini, imenovani ravnina slike, rekonstruira sliko maske. Položaje maske, glavne ravnine objektiva, njegove goriščne ravnine in ravnine slike na optični osi povezuje enačba leče

$$1/f = 1/a + 1/b$$

kjer so f goriščna razdalja objektiva, a razdalja od maske (predmeta) do glavne ravnine objektiva in b razdalja od glavne ravnine objektiva do ravnine slike. Proces nastanka slike si morda najlaže pojasnimo tako, da si točke v goriščni ravnini objektiva, kjer se sekajo vzporedni snopi žarkov z maske, predstavljamo kot še ene izvore Huygensovih sekundarnih valov, ki interferirajo v ravnini slike. Prav ta druga interferenčna slika je slika predmeta, ki jo da objektiv (slika 3). Nastanek slike je torej posledica dvojnega uklonskega procesa: najprej uklona ravnega valovanja na predmetu in nato uklona valovanj, ki po prvem uklonu potujejo v različnih smereh, na objektivu. Tako je jasno, da pri preslikavi objektiv naredi inverzno Fourierovo transformacijo uklonske slike predmeta.

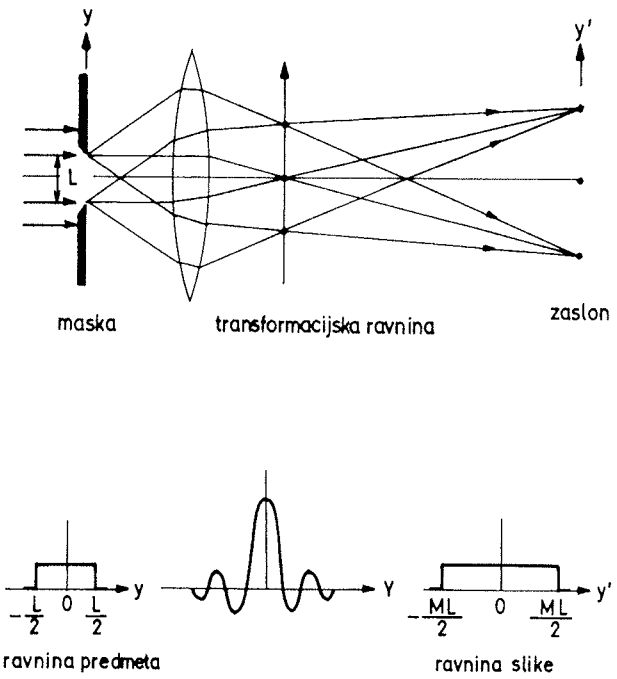

Slika 3: Nastanek slike je dvojni uklonski proces: slika predmeta nastane zaradi interference svetlobe, ki izhaja iz transformacijske ravnine. M je povečava preslikave.

Ločljivost

Najbrž je očitno, da objektiv lahko rekonstruira popolno sliko predmeta le, če zajame njegovo celotno uklonsko sliko. Praktično je to seveda nemogoče, saj pri uklonu glede velikosti kotov Θ ni nobenih omejitev, vsi objektivi pa imajo končne premere. Če leži predmet na razdalji a pred objektivom, ki ima polmer R, je največji kot med žarki, ki izhajajo iz (majhnega) predmeta in jih objektiv še zajame Θ_{max} takšen, da je

$$\operatorname{tg}\Theta_{max} = R/a$$

Razmerje R/a se imenuje numerična apertura (NA) sistema. (NA iz tehničnih razlogov navadno definirajo kot sin Θ_{max} , razlika na tem mestu ni posebno pomembna.) Če želimo z objektivom preslikati nek predmet, recimo režo, s

tako majhno širino L, da je smer prvega uklonskega minimuma, ki ga določa kot Θ ravno enak numerični aperturi objektiva, torej

$$\sin\Theta = \lambda/L = NA$$

smo očitno na meji resolucije objektiva. Pri še manjših predmetih (ožjih režah) objektiv zajame le še svetlobo ničtega uklonskega maksimuma (torej svetlobo, ki se na reži ne ukloni in skozi sistem potuje v smeri optične osi), v tej pa ni nikakršne informacije o velikosti predmeta. Ta se skriva le v položajih minimov v uklonski sliki in če teh v svetlobi, ki jo zajame objektiv, ni, objektiv predmeta ne more rekonstruirati.

Vpliv omejene kotne velikost objektiva navadno vključijo v modeliranje preslikave z zenično (pupilno) funkcijo objektiva, $P_o(f_y, f_z)$, ki ima vrednost 1, če je $(f^2_y + f^2_z)^{1/2} \leq NA/\lambda$ in 0, če je $(f^2_y + f^2_z)^{1/2} > NA/\lambda$, kjer je f_y tako imenovana prostorska frekvenca uklonske slike na objektivu:

$$f_y = y_{ob}/a\lambda$$

f_z je definirana na enak način. Prostorske frekvence, ki jih objektiv lahko transformira (preslika) so očitno omejene z vrednostjo $f_{max} = NA/\lambda$ in zenična funkcija to odraža. Končna velikost objektiva pri preslikavi predmetov z velikimi prostorskimi frekvencami (kar pomeni z majhnimi dimenzijami) igra isto vlogo kot, na primer, nizkopasovni filter pri prenosu ostrih pulznih signalov. Takšen filter signale (seveda v časovni domeni) zaobli, objektiv pa podobno (v prostorski domeni) ne preslika podrobnosti predmeta, ki so skrite v velikih prostorskih frekvencah njihove uklonske slike.

Zenično funkcijo vključimo v izraz za preslikavo in porazdelitev električnega polja na mestu slike zapišemo kot

$$E(y_s,z_s) = F^{-1}[E(y_o,z_o)\, P_o(f_y, f_z)] = F^{-1}\{F[E(y,z)]\, P_o(f_y, f_z)\}$$

kjer je F^{-1} inverzna Fourierova transformacija. Iradianca na mestu slike pa je, kot vedno, $|E(y_s,z_s)|^2$.

Povečanje ločljivosti

Najmanjšo velikost predmetov, ki jih z nekim projekcijskim poravnalnikom lahko preslikamo z maske na fotopolimer in rezino, torej v načelu omejuje končna ločljivost optičnih sistemov. Vendar sta poznana vsaj dva načina kako povečati ločljivost projekcijskih sistemov /4/. Prvi temelji na dejstvu, da je uklonska slika, na primer reže, simetrična glede na ravnino x,z in da zato vključuje informacijo o velikosti reže dvakrat: enkrat v uklonskih minimih v smeri osi +y ter drugič v minimih v smeri -y. Za verno preslikavo pa takšna dvojnost pravzaprav ni potrebna in v načelu za rekonstrukcijo slike zadošča že uklonjena svetloba, ki se od predmeta širi k objektivu le, recimo, nad optično osjo sistema. Če bi objektiv z določeno NA za njegov polmer premaknili vzdolž osi y, bi po premiku njegov spodnji del zajel le še na maski neuklonjeno svetlobo, njegov zgornji del pa dodatno še uklonjeno svetlobo višjih redov. Zaradi vključitve te svetlobe v preslikavo bi bila tudi slika reže ostrejša.

Prav isto bi seveda dosegli z objektivom, ki ima 2 krat večji polmer (in ustrezno večjo NA), ter z zaslonom, ki bi zastrl del objektiva pod optično osjo. Eno ali drugo bi povečalo ločljivost, toda tudi v preslikavo vneslo nesprejemljive aberacije. Podobno bi enako povečanje ločljivosti (iz istega razloga in s podobnimi abracijami) brez premikanja ali zastiranja objektiva dosegli tudi tako, da bi masko osvetlili pod kotom Θ_{max}. Dejansko so koti izvenosnega osvetljevanja, ki še omogočajo nepopačeno preslikavo, hkrati z nekoliko večjo ločljivostjo, mnogo manjši od Θ_{max}, toda tehnika je pri konstrukciji projekcijskih poravnalnikov često uporabljena.

Povsem drugačna tehnika povečevanja ločljivosti projekcijskih osvetljevalnih sistemov temelji na manipulaciji faze, s katero uklonjena svetloba izstopa iz maske /8/ . Za nek del maske lahko postavimo planparalelno ploščico iz snovi z lomnim količnikom n in debelino t, izbrano tako, da del svetlobe, ki gre skozi ploščico, glede na svetlobo, ki gre mimo nje, zaostane za fazni kot π. Debelino t fazne ploščice določa enačba

$$t = \frac{\lambda}{2(n-1)}$$

Deli svetlobe, ki gredo skozi fazno ploščico, pri rekonstrukciji uklonske slike seveda sodelujejo z za π spremenjeno fazo, ali z drugimi besedami, električno polje teh delov svetlobe je pomnoženo s faktorjem -1. S primerno razporeditvijo faznih ploščic po različnih delih maske je mogoče doseči, da se električno polje na določenih delih slike na rezini izniči. S fazno masko torej lahko dosežemo, da ostanejo deli rezine, ki bi bili pri osvetlitvi z navadno masko osvetljeni, neosvetljeni. Princip delovanja faznih mask je prikazan na sliki 4. V okviru Fourierove optike je

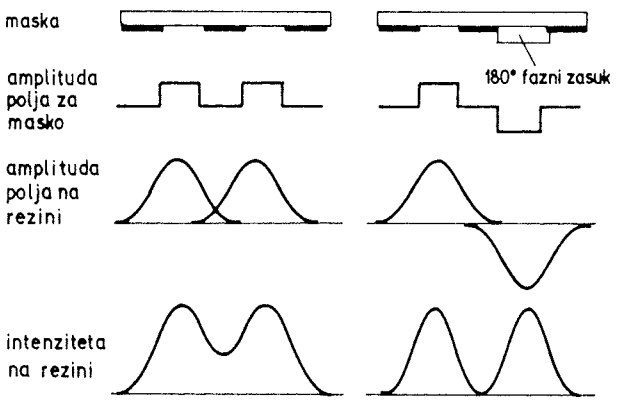

Slika 4: Princip povečanja ločljivosti preslikave z uporabo fazne maske (po /8/).

njihov učinek na ločljivost prav enostavno pojasniti: 180–stopinjski fazni premiki na primerno izbranih delih maske razpolovijo osnovno prostorsko frekvenco vzorca na maski (kar je razvidno iz slike) in zato lahko objektiv z določeno NA, ki sicer deluje na meji ločljivosti, takšne dele maske preslika z velikim kontrastom. Kakšna mora biti razporedi-

tev faznih ploščic na maski s preprosto periodično strukturo je očitno, v splošnem pa načrtovanje fazne maske ni enostavna naloga. Na slikah v /5/ so prikazani primeri simulacije (s programom FOLIS) faznih mask z nekoliko bolj zapleteno strukturo.

MTF

Ločljivost nekega optičnega instrumenta je vsekakor pomembno merilo njegove zmogljivosti, nikakor pa ne edino. Fotolitograske maske tipično niso objekti s preprosto periodično strukturo, katere preslikavo na rezino bi omejevala le ločljivost projekcijskega poravnalnika. Na njih so navadno objekti različnih dimenzij, z bolj ali manj ostrimi vogali itd. in pravi izziv za konstruktorje osvetljevalnih naprav je kontrastna preslikava celotne maske in ne le zadovoljiva preslikava njenih najmanjših delov. Priljubljena analogija preslikavi realne maske je s področja elektroakustike: ocenjevati kvaliteto neke HiFi naprave le po najvišji frekvenci, ki jo zmore reproducirati, je očitno precej pomanjkljivo. Veliko več bi o kvaliteti reprodukcije povedal nek kriterij, ki podaja zmogljivosti naprave v njenem celotnem frekvenčnem območju. Kot takšno merilo kvalitete preslikave se je v optiki uveljavila modulacijska prenosna funkcija (modulation transfer function, MTF) /3/.

Če ob prehodu svetlobe skozi fotolitografsko masko pustimo podrobnosti sipanja itd. povsem ob strani, lahko prehod obravnavamo kot modulacijo curka svetlobe. Na mestih, kjer maska svetlobo prepušča, ostaja gostota svetlobnega toka (oz. iradianca) nespremenjena, na mestih, ki so zakrita s plastjo kroma, pa maska svetlobe sploh ne prepušča. Na osnovi te ugotovitve smo že definirali transmisijsko funkcijo maske in podobno definiramo tudi modulacijo M_M svetlobnega toka, ki prehaja skozi masko, kot

$$M_M = \frac{I_{oM} - I_{tM}}{I_{oM} + I_{tM}}$$

kjer sta I_{oM} največja in I_{tM} najmanjša gostota toka po prehodu svetlobe skozi masko. Povsem enako definiramo modulacijo svetlobe v ravnini slike

$$M_S = \frac{I_{oS} - I_{tS}}{I_{oS} + I_{tS}}$$

MTF optičnega sistema je definirana kot

$$MTF = M_S/M_M$$

in meri kontrastnost slike pri preslikavi. Ker je v praksi transmisijska funkcija maske domala idealno digitalna in je zato M_M zelo natančno enak 1, je prenosna funkcija sistema praktično enaka M_S. Iz opisa mehanizma preslikave bi moralo biti očitno, da je MTF funkcija velikosti struktur na maski, ki jih želimo preslikati. Če so te velike, da preslikava verno, zelo kontrastno sliko predmeta in je vrednost MTF blizu 1. Pri strukturah, ki so istega reda velikosti kot ločljivost projekcijskega poravnalnika, pa je vrednost MTF blizu 0. Velikost struktur na maski opisuje njena prostorska frekvenca u, ki je za masko, podobno uklonski mrežici, navadno podana kar kot število linij na milimeter. Frekvenca u seveda ni enaka (na žalost pa se enako imenuje) prostorski frekvenci predmeta f_x, ki smo jo srečali pri obravnavi uklona. Dejansko MTF navadno podajajo kot funkcijo normalizirane prostorske frekvence ξ, ki je kvocient obeh, to je

$$\xi = u/f_x$$

Izpeljava MTF za nek optični sistem je sorazmerno nazorna in nezahtevna le za lečo, ki je pri projekcijskih osvetljevalnih sistemih pravzaprav nikoli ne srečamo, namreč za idealno cilindrično lečo. Zato nam v to kislo jabolko ni treba ugrizniti, omenimo le, da je pri taki leči izpeljava nezahtevna zaradi preproste, cilindrične simetrije rež na maski in leče. Uklonsko omejena MTF za takšno lečo brez aberacij, pri monokromatski svetlobi je

$$MTF(\xi) = (1 - \xi)$$

Za sferično lečo, pri istih pogojih, je MTF

$$MTF = \frac{2}{\pi}\left[\arccos(\xi) - \xi\sqrt{1-\xi^2}\right]$$

Analogija med obema izrazoma je morda opazna, njuna podobnost na grafu obeh funkcij pa očitna (slika 5). Omeniti je treba, da je pri sferični leči in krožnem predmetu, ki ga leča preslikuje, (kotna) prostorska frekvenca f_r definirana nekoliko drugače kot pri reži,

$$f_r = (2\Theta_{max}\sin\Theta_{max})/\lambda$$

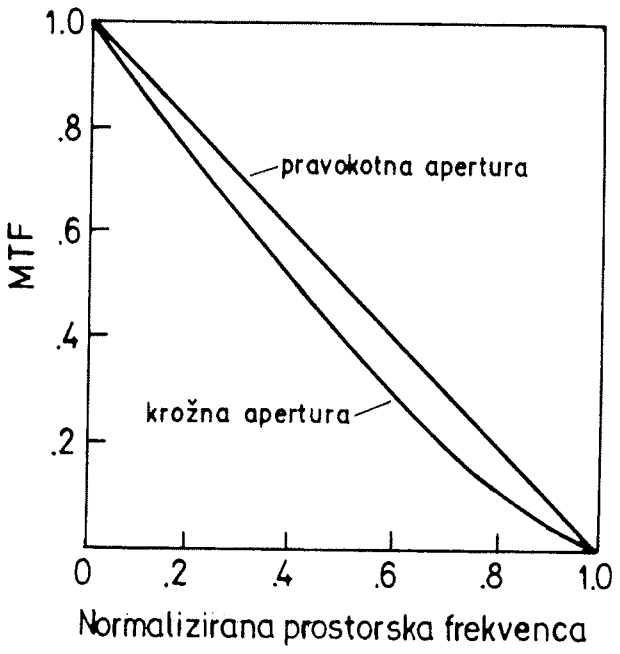

Slika 5: MTF za okroglo in pravokotno zaslonko objektiva.

Definicija prenosne modulacijske funkcije nekega sistema, kot je opisana, strogo velja le za preslikavo s koherentno svetlobo. Koherenčni pogoj za nek izvor svetlobe je

$$d \sin\varphi << \lambda/2$$

kjer sta d premer izvora in φ največji kot med žarkom, ki ga optični sistem še zajame, in optično osjo sistema. Realni izvori končnih dimenzij koherenčnemu pogoju lahko zadostijo le, če ležijo v neskončnosti, pri takšnem položaju izvora pa je gostota energijskega toka na mestu maske seveda 0. V praksi se problem koherence izvora navadno reducira na razmerje numeričnih apertur kondenzorske in projekcijske optike fotolitografskega sistema in je stopnja nekoherence s definirana kot

$$s = NA_{kon}/NA_{pr}$$

s za idealno koherenten izvor, ali izvor v neskončnosti je torej 0. Na prvi pogled bi morda sodili, da je prav takšen najbolj primeren za potrebe optične litografije, vendar ni tako. Videli smo že, da z izvenosnim osvetljevanjem masko, ki nosi strukture z veliki prostorskimi frekvencami (zelo majhne strukture), natančneje preslikamo kot z osvetljevanjem v osi. Tudi delna nekoherenca izvora privede do tega, da vsa svetloba na masko ne pade pod natanko pravim kotom. Zaradi tega se uklonska slika maske razprši v večji kot kakor pri koherentni osvetlitvi, takšen, ki ga NA objektiva ne zajame več. Slika maske je zato na ravnini silicijeve rezine seveda nekoliko bolj razmazana. Zaradi delne izvenosne osvetlitve pa objektiv hkrati zajame tudi del uklonjene svetlobe z drobnih struktur na maski, ki bi jo sicer povsem izločil in jih preslika. Preslikava z delno nekoherentno svetlobo je zato ostrejša.

Stopnjo koherentnosti izvora se da vključiti v MTF /9/, toda analitični izraz za MTF(ξ,s) nespecialistu na žalost ne pove prav ničesar. Ponovno si pomagamo z grafom. Na sliki 6 je prikazana simulacija MTF(ξ,s) s programom FOLIS za nek dejanski projekcijski osvetljevalni sistem. Povsem očitno je, da vrednost MTF(ξ,s) pri normaliziranih prostorskih frekvencah ξ, ki so večje od 0,5, narašča z naraščajočo

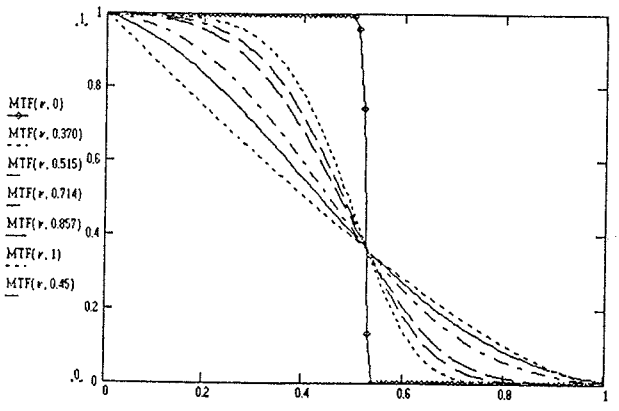

Slika 6: Simulacija MTF s programom FOLIS za projekcijski osvetljevalni sistem UTS 1100 z Wynne-Dysonovo optiko.

stopnjo nekoherentnosti. Praviloma takšno odvisnost MTF(ξ,s) od s opazimo pri vseh projekcijskih poravnalnikih. To pomeni, da je običajno pri velikih prostorskih frekvencah predmeta (maske) kontrastnost slike pri preslikavi z delno koherentno svetlobo večja kot pri preslikavi s koherentno in preslikava majhnih objektov z maske na površino rezine boljša. Le omenimo, da nelinearni odziv fotopolimera na osvetlitev, kontrast v fotopolimer prenesene fizične slike lahko še izboljša. Še boljši približki MTF nekega optičnega sistema vključujejo tudi efekte globine fokusa, aberacij optičnega sistema, odstopanj optičnih elementov sistema od idealne oblike itd. Vse te popravke v MTF navadno vključijo kot fazno aberacijo φ sistema, ki ga torej okarakterizira prenosna funkcija treh spremenljivk, MTF(ξ,s,φ).

Zaključek

Vse predstavljene metode analize optičnih preslikav se v takšni ali drugačni obliki uporabljajo v simulacijskih orodjih za modeliranje fotolitografskega osvetljevanja rezin. V praksi jih dopolnjujejo računalniške metode hitrega Fourirovega obrata (FFT), ki so danes postale povsem vsakdanje, in množica empiričnih modelov različnih podrobnosti preslikave. Združiti vse to v uporabno simulacijsko orodje je zahtevna naloga, ki je brez poznavanja osnov optične teorije nerešljiva. V Laboratoriju za mikroelektroniko, Fakultete za elektrotehniko, Univerze v Ljubljani je bilo razvito simulacijsko orodje FOLIS v katerem je opisana teorija implementirana.

Literatura

/1./ E.Hecht and A. Zajac, Optics, second printing, Addison-Wesley Publishing Co., Reading, MA. USA, 1977

/2./ E. L. O'Neil, Introduction to Statistical Optics, Addison-Wesley Publishing Co., Reading, MA. USA, 1963

/3./ Optics Guide 3, Melles Griot, Irvine, CA, USA, 1985

/4./ J.D. Plummer et al., Silicon VLSI Technology, Prantice Hall, Upper Saddle River, N.J., USA, 2000

/5./ I. Macarol, R. Osredkar, FOLIS, a PC Compatible Photolithography Simulation Tool, to be published in inf. MIDEM, Vol 33, March 2003

/6./ Bronštejn et. al., Matematični priročnik, Tehniška založba Slovenije, Ljubljana, SI, 1997

/7./ J. Strnad, Fizika, drugi del, DZS, Ljubljana, SI, 1978

/8./ M.D. Levenson et al., Improving Resolution in Photolithography with a Phase Shifting Mask, IEEE Trans. Elec. Dev., Vol. ED-29, 1982

/9./ A. Offner, Wavelength and Coherence Effects on the Performance of Real Optical Projection Systems, Photographic Sc. Eng., Vol. 23, No. 6, Nov./Dec., 1979

Radko Osredkar
FRI in FE Univerze v Ljubljani
Tržaška 25, SI 1000, Ljubljana, Slovenia
e-mail: radko.osredkar@fri.uni-lj.si

Prispelo (Arrived): 20.11.2002 *Sprejeto (Accepted): 25.05.2003*

UDK621.3:(53+54+621+66), ISSN0352-9045 Informacije MIDEM 33(2003)2, Ljubljana

HW/SW PARTITIONED OPTIMIZATION AND VLSI-FPGA IMPLEMENTATION OF THE MPEG-2 VIDEO DECODER

Matjaž Verderber, Andrej Žemva

University of Ljubljana, Faculty of Electrical Engineering, Ljubljana, Slovenia

Key words: MPEG-2 video decoder, FPGA implementation, optimization, ISO/IEC 13818-2, power consumption, speeding-up, inverse discrete cosine transform-IDCT, variable length decoding-VLD, Huffman coding, embedded system

Abstract: In this paper, we have proposed optimized real-time MPEG-2 video decoder. The decoder has been implemented in one FPGA device as a HW/SW partitioned system. We made timing/power-consumption analysis and optimization of the MPEG-2 decoder. On the basis of the achieved results, we decided for hardware implementation of the IDCT and VLD algorithms. Remaining parts were realized in software with 32-bit RISC processor. MPEG-2 decoder (RISC processor, IDCT core, VLD core) has been described in high-level Verilog/VHDL hardware description language and implemented in Virtex 1600E FPGA. Finally, the decoder has been tested on the Flextronics prototyping board.

Strojno in programsko razdeljena optimizacija in FPGA implementacija MPEG-2 video dekoderja

Ključne besede: MPEG-2 video dekoder, FPGA implementacija, optimizacija, ISO/IEC 13818-2, poraba moči, pohitritev, inverzna diskretna kosinusna transformacija-DCT, dekodiranje s spremenljivo dolžino-VLD, Huffmanovo kodiranje, vgrajeni sistem

Izvleček: V članku smo predstavili optimiziran MPEG-2 video dekoder namenjen dekodiranju v realnem času. Dekoder smo realizirali v enem FPGA vezju kot kombinacijo programske in strojne rešitve. Opravili smo analizo in optimizacijo hitrosti delovanja ter porabe moči MPEG-2 dekoderja. Na podlagi rezultatov smo se odločili, da časovno in energijsko zahtevne algoritme (inverzna kosinusna transformacija ter dekodiranje s spremenljivo dolžino) realiziramo direktno v strojni opremi, ostale dele dekoderja pa realiziramo z RISC mikroprocesorjem. Celoten MPEG-2 dekoder (RISC procesor, IDCT jedro, VLD jedro) smo opisali v visokonivojskih jezikih Verilog in VHDL in ga implementirali v Virtex 1600 programirljivem FPGA vezju. Vezje dekoderja smo nato preizkusili v realnem testnem okolju na FPGA prototipnem sistemu proizvajalca Flextronics.

1. Introduction

MPEG-2 video standard is an important standard for video compression today /1/. MPEG-2 coding/decoding algorithm can be found in different applications such as digital video broadcast, DVD, cable TV, graphics/image processing cards, set top boxes, digital cameras, SDTV and HDTV. Due to different profiles and levels of the MPEG-2 video standard, every application has specific ratio between performance and quality. Since modern multimedia applications increase both aspects of the MPEG-2 compression, it is necessary to achieve best performance in terms of real-time operation and reduced hardware cost.

The MPEG-2 standard includes several compression techniques such as variable length coding (VLC), discrete cosine transform (DCT), quantization and motion compensation. It was shown that some of these parts can be optimized with parallel structures and efficiently implemented in the hardware-software partitioned system. Recently, several MPEG-2 decoders have been developed either as software based applications /2/ or hardware based ASIC custom chips /3/.

A parallel decoder for the MPEG-2 standard implemented on a shared memory multiprocessor was presented in /2/. The primary goal of this approach was to provide an all-software memory solution for real-time high quality video decoding and to investigate the important properties as they pertain to multiprocessor systems.

In /3/, a VLSI chip for real-time decoding of MPEG-2 video was developed as hardware based ASIC device with unoptimized decoding functions.

In literature, we haven't found any description of combined hardware-software implementation of the MPEG-2 decoder on a single chip. The reason is probably the lack of technology that provides efficient hardware/software implementation. With the recent advantages in technology from leading manufactures of the programmable devices (Xilinx-Microblaze /4/, Altera-Nios /5/), the proposed design gain importance. The VLC decoding algorithm and IDCT algorithm are implemented with fast parallel architectures directly in hardware. Hardware part is described in VHDL/Verilog and implemented together with the RISC processor in a single Virtex 1600E FPGA device. Decoding of the coded bitstream, inverse quantization, motion-compensation are running in software on 32-bit RISC processor which is implemented in FPGA and uses Linux as the operating system. This is so due to the non-existence of efficient parallel architectures for these algorithms. This partitioning was selected in order to achieve better timing properties and lower power consumption.

With the proposed parallel optimization in hardware, up to 40% improvement is achieved compared to the complete software implementation. The main benefit of our MPEG-2 decoder is leveraging best characteristics from hardware and software based solutions. The proposed MPEG-2 video decoder was tested on the Flextronics FPGA based industrial board /6,7/ which serves as a testing environment and forms the intermediate step in VLSI chip design cycle.

This paper is organized as follows: the next section describes timing optimization and optimization of the power consumption of the decoder. The implementation of the MPEG-2 decoder is presented in Section 3. Finally, Section 4 completes the paper with a conclusion and future work.

2. Optimization of the MPEG2 Video Decoder

As illustrated in Figure 1, coded pictures are first variable length (Huffman) decoded and their type is determined from the header information. Pictures are inverse scanned and inverse quantized. Inverse quantization is performed in two steps. Data are first divided with a quantization-step matrix and then scaled with a scale factor.

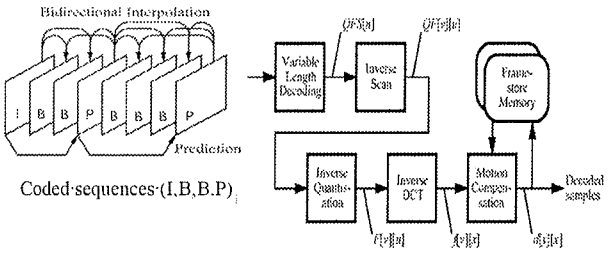

Figure 1: Structure of the ISO/IEC 13818-2 MPEG-2 video decoder

MPEG-2 standard defines 3 types of the coded frames (**I**, **P**, **B** pictures). Intra-coded pictures **I** take advantages of the picture's spatial correlation. They do not reference any other pictures in the coded bit stream. They provide fast random access with only moderate compression. **I** pictures are only DCT decoded while no motion compensation is performed. Inter-coded pictures **P, B** consider also temporal correlation between successive pictures (motion compensation). **P** pictures are decoded using motion-compensated prediction from the past **I** or **P** pictures which are stored in the Frame-Store-Memory. The compression for **P** pictures is better than for **I** pictures, and **P** pictures can be used as reference points for additional motion compensation. Bidirectionally predicted pictures **B** provide the highest degree of compression. They are decoded using motion-compensated prediction from either past and/or future **I** or **P** pictures. Since **B** pictures are not used in the prediction of other **B** or **P** pictures, such pictures accommodate more distortion and hence yielding more compression than **I** or **P** pictures. The ISO/IEC 13818-2 (MPEG-2 video part) standard defines only the frame for different algorithms included in the standard /8/. Therefore, there are various possibilities to optimize particular parts of the decoder.

In order to deal with timing and power-consumption optimization, we have developed a software support in visual C++ programming language. A screenshot of the software tool is shown in Figure 2.

Figure 2: Program for MPEG-2 software simulation

This software allows us to simulate input sequences with different settings (profile/level, bit-rate, I/P frame distance, number of frames in GOP, frame/field pictures and all other coder/decoder parameters). The complete analysis can be performed and timing properties of particular algorithms included in the standard can be simulated. For timing analysis, elapsed time of the decoding parts in mili-seconds is measured for every decoded sequence. Finally, the speed of the program execution is evaluated. Based on the obtained results, we have estimated equivalent decoding speed for real-time decoding.

2.1. Timing Optimization

Figure 3 shows a computational load of the decoding functions in MPEG-2 decoder.

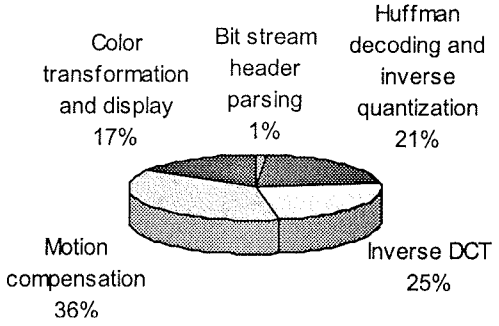

Figure 3: Computational power distribution for MPEG-2 decoding

The data in the Figure 3 are based on simulations of source input format (SIF) (352x244, 25Hz) resolution pictures coded at 4 Mbits/s containing two B-pictures for every P-picture. As illustrated in Figure 3, the most computational expensive parts of the decoder are motion compensation, inverse DCT and VLD decoding.

The main idea of our decoder is to exploit advantages of the parallel structures which can be efficiently implemented in hardware. Hardware implementation of DCT and VLD decoder promises better results compared to software based algorithms. The key point of a parallel hardware structure is reduced number of operation and an ability to work in parallel. On the contrary, hardware implementation of motion compensation does not gain performance versus software based solution. In our decoder, we have therefore built fast hardware cores for IDCT and VLD decoder.

The basic computation element in a DCT-based system is the transformation of an NxN image block from the spatial domain to the DCT domain and vice versa. For the image compression standards, N is usually 8. From a hardware or software implementation point of view, an 8x8 block size does not impose significant memory requirements. Furthermore, the computational complexity of an 8x8 DCT is manageable on most computing platforms. Mathematical formulation for the 2D discrete cosine transform is shown in (1).

$$F(u,v)=\frac{C_u C_v}{4}\sum_{x=0}^{7}\sum_{y=0}^{7} f(x,y)\cos\left(\frac{(2x+1)u\pi}{16}\right)\cos\left(\frac{(2y+1)v\pi}{16}\right)$$

$$C_u, C_v = \frac{1}{\sqrt{2}}(u,v=0)\ldots otherwise \quad 1$$

$$x,y \quad coordinates \quad in \quad pixel \quad domain(0\ldots7)$$

$$u,v \quad coordinates \quad in \quad DCT \quad domain(0\ldots7) \qquad (1)$$

The separable nature of the 2D DCT is exploited by performing the 1D DCT on the eight rows and then the 1D DCT on the eight columns /9/. Several fast algorithms are available for calculation of the 8-point 1D DCT. In our decoder, scaled version of Chen has been used /10/. It was selected due to the minimum required number of additions and multiplication. Structure of Chen DCT is illustrated in Figure 4.

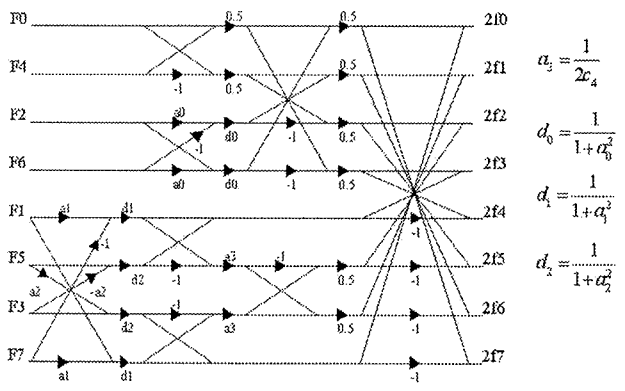

Figure 4: Modified Chen 1D inverse DCT structure

For variable length decoder (VLD), a lookup table based decoder structure proposed by Lei and Sun /11/ has been used. It is one of the fastest known variable length decoders today /1/. It decodes each codeword in a single cycle regardless of its length. The block diagram of the Lei-Sun VLD is illustrated in Figure 5.

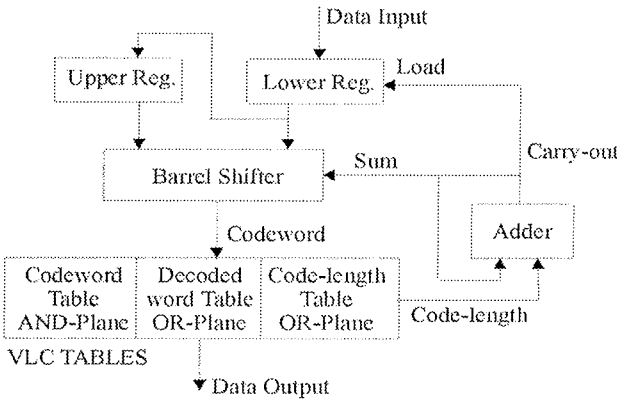

Figure 5: Block diagram of the Lei-Sun variable length decoder

Coded data are always concatenated together and segmented into 16-bit words. When the 16-bit lower and upper register are fully loaded, the decoding process starts. At each cycle, the output of the barrel shifter is matched in parallel with all the entries in the codeword lookup table. The barrel shifter operates like a sliding window on the contents of the two registers. When a match is found, the lookup table outputs the corresponding source symbol and the length of the decoded codeword. The barrel shifter is then shifted to the beginning of the next codeword. As the 4-bit adder overflows 16, this indicates that the upper register has been fully decoded. After the content of the lower register is transferred into the upper register, the VLC decoder loads a new 16-bit segment into the lower register, and operations continue.

Once the IDCT and VLD had been modeled in VHDL, we have performed timing simulation of MPEG-2 decoder. IDCT 1-D Chen structure is described in VHDL at RTL level. Our simulations have shown a delay of 100 ns for 1-D IDCT and 1.6 µs for 2-D 8x8 IDCT targeting the Xilinx FPGAs. In the VLD decoder, every coded symbol can be decoded in only one cycle. Since the prototyping evaluation board operates at 25 MHz, 40 ns delay for each decoded data is required.

Our results show up to 40% improvement of speed for MPEG-2 decoding compared to software based solution. The results before and after optimization are presented in Figure 6.

These results have been obtained with the software decoding speed of 45 MHz. We have calculated equivalent decoding speed for the real-time decoding rate (40 ns for 25 Hz frame rate) which was 72 MHz. As seen in Figure 6, there are great deviations from the average decoding times.

This is a consequence of the irregular CPU tasks and can be ignored.

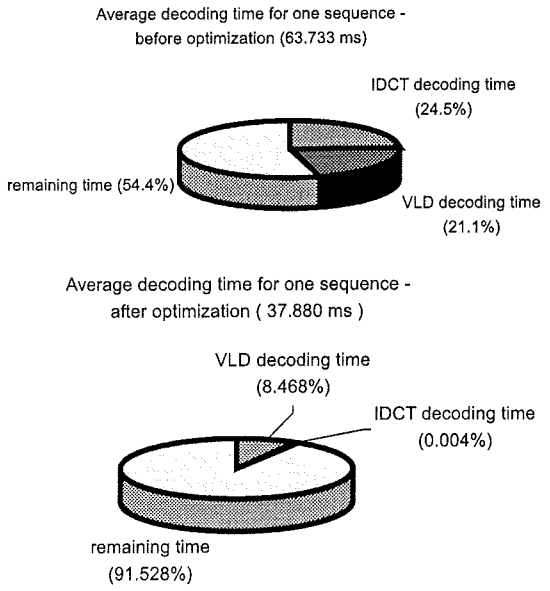

Figure 6: Results of the timing simulation before and after optimization

2.2. Power Consumption Analysis

At this point, we summarize results of the detailed energy conscious study made by Henkel and Li /12/. The study is based on the idea that an application specific hardware can be more energy efficient due to the higher utilization. They made an energy dissipation study by distinguishing five different cases of HW/SW partitioned MPEG-2 encoder (Figure 7). As a reference case a complete software implementation was used. Then, four candidate hardware parts were synthesized (quantization-case 1, two dimensional DCT-case 2, one dimensional DCT-case 3, quantization and two dimensional DCT-case 4) and analyzed. The encoder was intended to run on an architecture composed of the CPU, instruction and data cache, a main memory and an application specific hardware (ASIC). Since every encoder also includes a duplicated decoder, results can be easily adopted for the MPEG-2 decoder. As illustrated in Table 1, each of the selected co-designs in cases 1 to 4 yields an energy savings up to 48% compared to the reference case of software based solution.

Case	Energy [mJ]		
	SW	HW	total
Case 0: All SW Solution	74.32	N/A	74.32
Case 1: Quant. in HW, rest in SW.	49.33	14.09	63.42
Case 2: 2-D DCT in HW, rest in SW.	27.16	0.709	27.869
Case 3: 1-D DCT in HW, rest in SW	49.51	0.156	49.666
Case 4: Quant. and 2-D DCT in HW rest in SW	16.99	22.27	39.26

Table 1: Energy dissipation for selected co-designs

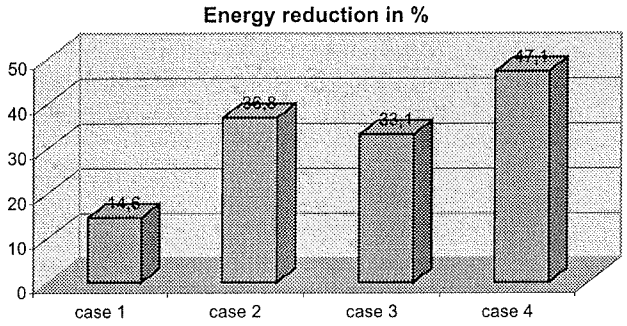

Figure 7: Results of the case study for energy-conscious HW/SW partitioning

3. VLSI-FPGA Implementation of the MPEG-2 Video Decoder

3.1. System Environment

Our HW/SW partitioned MPEG-2 decoder has been tested on the Flextronics /6/ FPGA based prototyping board (Figure 8).

The heart of the board is the Xilinx Virtex 1600E FPGA /13/. Several peripheral devices and connectors (ethernet, VGA, LCD, GSM, UART, IDE, PS2) serve as interfaces from the FPGA to the external world. 32 MByte flash,

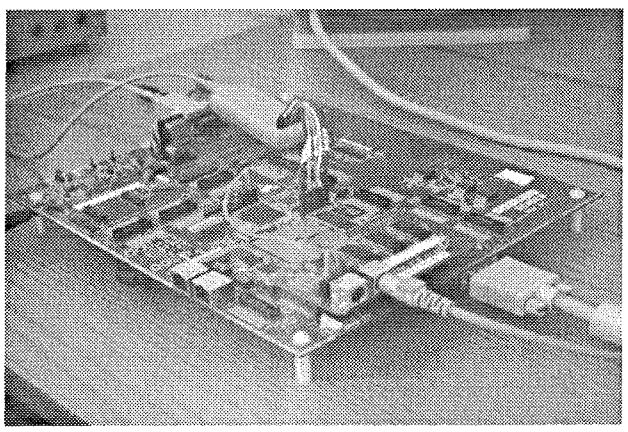

Figure 8: Flextronics prototyping board

64 MByte SDRAM, and 4 MByte SRAM allow implementation of the complex FPGA applications. For the MPEG-2 decoder, we are using flash memory (loaded input sequences), SRAM, UART (display of the MPEG-2 decoding messages) and VGA output to the display.

Every hardware core is first described in Verilog or any other high level hardware description language (HDL). We have used Synplify tool /14/ for circuit synthesis and Xilinx ISE tool /15/ for target implementation. Once the hardware is designed, there are two options how to port software applications on the board. The first is to use Linux operating system. On the RISC processor and various peripheral hardware cores (ethernet, ps2, uart etc), we can port derivative of Linux kernel (uClinux) which is intended for microcontrollers without Memory Management Units (MMUs). The second option is to use the monitor program which is loaded into the RAM of the RISC controller. The latter method is used during the development cycle. When an application meets the requirements, it is compiled for the Linux operating system.

3.2 FPGA Implementation

Our HW/SW partitioned decoder is composed of three parts: a 32-bit RISC processor, IDCT and VLD hardware cores (Figure 9).

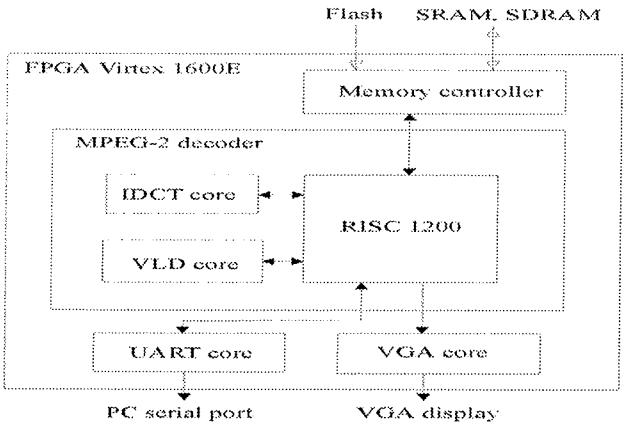

Figure 9: Block diagram of the implemented MPEG-2 decoder

The decoded frames are displayed on the analog monitor. During the MPEG-2 decoding process, we can also see possible decoding errors and warnings ("buffer overrun" for example). For this purpose, we have implemented the VGA Controller core (display of decoded frames) and UART communication core into the FPGA. For the memory accesses from RISC to external memory, the FPGA contains memory controller core.

The RISC processor is based on OpenRISC 1000 /7/ design and is a 32-bit scalar RISC with Harvard microarchitecture, 5 stage integer pipeline, virtual memory support (MMU) and basic DSP capabilities. Default caches are 1-way direct-mapped 8KB data cache and 1-way direct-mapped 8 KB instruction cache, each with 16-byte line size. Both caches are physically tagged. Block diagram is shown in Figure 10.

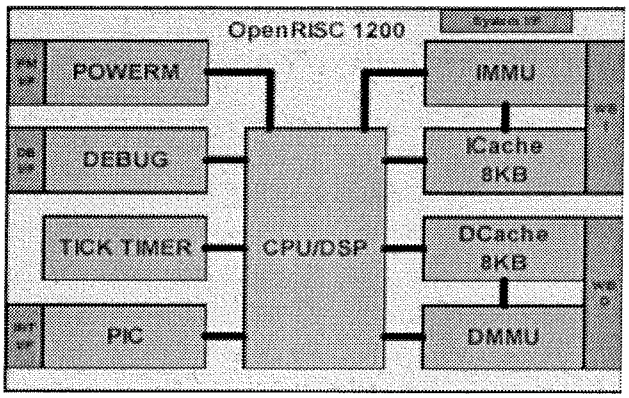

Figure 10: Architecture of the RISC controller

Supplemental facilities include a debugging unit for real-time debugging, a high resolution tick timer, a programmable interrupt controller and power management support. When implemented in a typical 0.18u 6LM process, it provides over 300 dhrystone 2.1 MIPS at 300 MHz and 300 DSP MAC 32x32 operations. OR1200 is intended for embedded, portable and networking applications.

IDCT core follows the Chen IDCT structure described in Section 2.1. The core is described with logic functions at the RTL level. It works with row-column decompositions since 2-D DCT can be computed with 1-D DCT. The simplified architecture is shown in Figure 11.

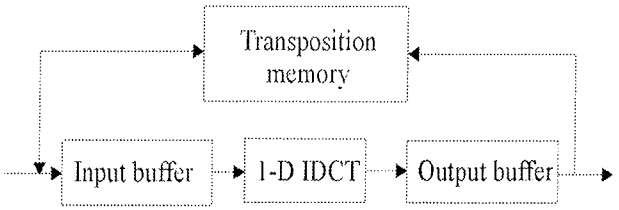

Figure 11: Simplified IDCT core architecture

The architecture of the VLD decoder is described in Figure 5. From the implementation point of view, this core is more complex compared to IDCT core. Due to the need of proper internal logic synchronization, the most complex part is controller of variable length decoding steps. There is also a problem of difficult implementation and routing of the VLD table circuit. MPEG-2 standard specifies 11 different variable length code tables with up to 17 bits wide codewords. Hardware implemented VLD decoding tables require several FPGA look up tables (LUTs), since every Virtex LUT is only 4bit wide. This problem was solved building large (over 12 bits wide) VLD tables with a use of smaller VLD tables.

3.3 Implementation Results

Virtex 1600E device (Figure 12) features a flexible, regular architecture that comprises an 72x108 array of confi-

gurable logic blocks (CLBs) surrounded by programmable input/output blocks (IOBs), all interconnected by a hierarchy of fast, versatile routing resources. CLBs interconnect through a general routing matrix (GRM). The GRM comprises an array of routing switches located at the intersections of horizontal and vertical routing channels. Virtex 1600E also includes 589824 bits of dedicated memory (BlockRAM) and Clock DLLs for clock-distribution delay compensation. For Clock distribution, FPGA uses fast specially dedicated global clocks (GCLKs, GCLKIOBs) or local routing resources GRM. The VersaRing I/O interface provides additional routing resources around the periphery of the device. This routing improves I/O routability and facilitates pin locking.

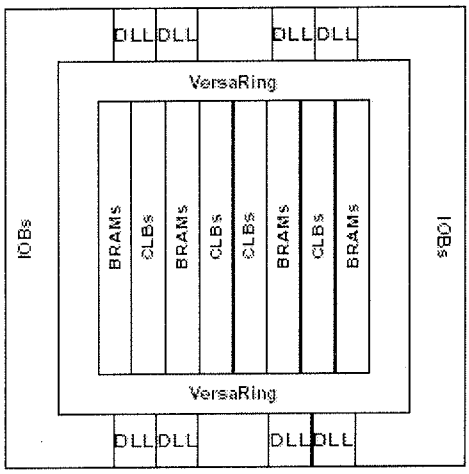

Figure 12: Virtex 1600E architecture

Each CLB is organized in two slices and provides the functional elements for constructing logic. IOBs provide the interface between package pins and the CLBs. Table 2 shows implementation results of the MPEG-2 decoder in the Virtex 1600E FPGA.

Number of:	RISC1200	IDCT	VLD
SLICEs	22%	8%	10%
BlockRAMs	12%	0	0
IOBs	90%	20%	6%
GCLKs	75%	75%	25%
GCLKIOBs	90%	25%	25%

Table 2: Utilization of the FPGA

Results in the Table 2 have been obtained with separate implementation of the particular modules (RISC, IDCT, VLD). The most important data is the number of the SLICEs (basic FPGA structure) and BlockRAMs. In the common implemented MPEG-2 decoder, this resources are merged together. Entire MPEG-2 decoder utilizes 40% of the Virtex device. Other resources (IOBs, GCLKs, global clock IOBs-GCLKIOBs) are shared, so the decoder utilizes 90% IOBs, 75% GCLKs and 90% GCLKIOBs. As we can see in Table 2, there is about 60% free of space for other applications.

4. Conclusion

In this paper, we have proposed an optimized MPEG-2 video decoder. We have considered optimization of speed and power consumption. Both, timing and the power consumption optimization show correlated results by achieving optimized MPEG-2 decoder. We have shown that 40% higher decoding speed and 36% lower power consumption can be obtained with combined hardware and software implementation. From a power-consumption point of view, it would be reasonable to implement quantization in hardware, but this guaranties any improvements of the decoding speed.

We have presented a modern implementation method where the complex embedded system (MPEG-2 decoder) can be efficiently HW/SW partitioned and optimized. In the future work, we will concentrate on timing optimization and HW/SW implementation of the next generation standard (MPEG-4).

Literature

/1/ Vasudev Bhaskaran, Konstantinos Konstantidies "Image and Video Compression Standards, Algorithms and Architectures", Kluwer Academic Publishers, Boston, 1997.

/2/ Eishi Morimatsu, Kiyoshi Sakai, Koichi Yamashita, ... "Development of a VLSI Chip for Real Time MPEG-2 Video Decoder", Proceedings of the 1995 International Conference on Image Processing, IEEE, 1995.

/3/ Angelos Bilas, Jason Fritts, Jaswinder Pal Singh, "Real-time Parallel MPEG-2 Decoding in Software", Proceedings of the 11th International Parallel Processing Symposium, IEEE 1997.

/4/ http://www.xilinx.com/xlnx/xil_prodcat_product.jsp?title=microblaze

/5/ http://www.altera.com/literature/lit-nio.html

/6/ http://www.flextronicssemi.com/semi/flexsemi.nsf

/7/ http://www.opencores.org/

/8/ ISO/IEC 13818-2: 1995 MPEG video standard, ITU-T H.262 Recommendation.

/9/ G. Panneerselvam, P.J.W. Graumann, L.E. Turner, "Implementation of Fast Fourier Transform and Discrete Cosine Transform in FPGAs", FPL'95 conference.

/10/ W.C Chen, C.h Smith and S.C. Fralick, "A fast Computational Algorithm for the Discrete Cosine Transform", IEEE Transactions on Communications, Vol. COM-25, No. 9, pp.1004-1009, Sept.1997.

/11/ Shaw-Min Lei and Ming-Ting Sun, "An Entropy Coding System for Digital HDTV Applications," *IEEE Transactions on Circuits and Systems for Video Technology*, vol. 1, no. 1, pp. 147-155, March 1991.

/12/ Jörg Henkel, Yanbing Li, "Energy-Conscious HW/SW Partitioning of Embedded Systems, A Case Study on an MPEG-2 Encoder", Procedings of the 6th International Workshop on Hardware/Software Codesign, Seatle, 1998.

/13/ The Programmable Logic Data Book, 2002.

/14/ http://www.synplicity.com/products/synplifypro/index.html

/15/ http://www.xilinx.com/ise/ise_promo/finish_faster.htm

Matjaž Verderber, Andrej Žemva
Univerza v Ljubljani, Fakulteta za elektrotehniko,
Ljubljana, Slovenija

Prispelo (Arrived): 29.10.2002 *Sprejeto (Accepted): 25.05.2003*

MONTAŽA PLOŠČ TISKANIH VEZIJ Z ZLITINAMI BREZ SVINCA

Breda Kodek

Razvoj & raziskave, Laboratorijski center, Iskraemeco d.d., Kranj

Ključne besede: plošča tiskanega vezja (TIV), spajkalna pasta, spajka, spajkanje, komponenta, klimatski test, odtržna sila, kot omočenja

Izvleček: Za obdobje spajkanja brez svinca v elektronski industriji smo testirali spoje med elektronskimi komponentami in ploščo tiskanega vezja (TIV). Komponente smo prispajkali na kositrene in zlatene vzorce TIV s spajkalno pasto brez svinca, na TIV izdelane po Hot Air Solder Leveling (HASL) postopku pa z običajno spajkalno pasto s svincem. Vzorce smo starali na pospešenih klimatskih testih, ki simulirajo klimatske obremenitve pri uporabi v naravi. Z merjenjem odtržnih sil in mikroskopskimi preiskavami smo primerjali kvalitete spojev. Rezultati raziskav so pokazali, da se spoji po fizikalnih lastnostih nekoliko razlikujejo od običajnih, narejenih s spajkalno pasto, ki vsebuje svinec, vendar so še dovolj trdni in lahko zadovoljujejo zahteve mednarodnih standardov za elektronsko industrijo. Tudi po pospešenih testih rezultati niso bistveno slabši.

Assembling of Printed Circuits Boards with the Lead Free Alloys

Key words: Printed Circuits Board (PCB), solder paste, solder, soldering, component, climatic test, pull off strength, angle of wettability

Abstract: The soldered joints of assembled printed circuit boards (PCB) for the lead free time were tested. The components were soldered with the lead free solder paste on the tinned and flash gold finished PCBs but with the normal lead solder paste on the Hot Air Solder Leveling (HASL) finished PCB. The samples were exposed to some accelerated climatic tests as a simulation of different climatic changes in use. The quality of the joints was investigated by measuring of the pull off strength and microscopic research. There are some conclusions from this research work that could help us to work in the electronic industry in the lead free time.

The wettability of the lead free solders on the tinned PCBs and the PCBs finished with the flesh gold is good enough to satisfy the demands for a good joint. There are inter-metallic structures in all three investigated types of the joints. The thickness of these structures in the joint on the PCB with the flash gold is almost identical to the one on the HASL finished PCB. The joint has a double thickness of the inter-metallic structure on the tinned PCB. The pull off strength of the components on all three different samples does not differ very much even after the accelerated climatic tests.

The results of this research show that the joints are different from those we have today with the lead solders, but they are still strong enough to satisfy the demands of international standards for the quality of solder joints in the electronic industry.

1. Uvod

Predvideno je, da bo v Evropi nastopilo obdobje spajkanja brez svinca v elektronski industriji po letu 2007. Za to obdobje je na voljo že več vrst materialov za spajkanje, hkrati pa tudi več vrst plošč tiskanih vezij (TIV) /1,2,3,4/. Poiskali smo nekaj vzorcev TIV, ki bodo aktualne takrat in nanje prispajkali SMD komponente s spajkalno pasto brez svinca. Tako smo si preskrbeli TIV z naslednjimi prevodnimi liki:

- Kemijski nikelj / zlato
- Kemijski kositer

Komponente smo spajkali z vzorcem spajkalne paste s sestavo Sn 95,5/ Ag 3,8/ Cu 0,7 in rezultate preiskav primerjali z rezultati dobljenimi s spajkanjem z običajno spajko Sn62/Pb/Ag2. V literaturi lahko zasledimo tudi zlitine Sn/Ag/Cu/Sb in Sn/Ag/Bi, vendar so prve kot zlitine štirih kovin manj primerne za uporabo, pa tudi antimon je ekološko oporečen. Tudi bizmutove spajke se v glavnem ne bodo mogle dosti uporabljati, ker že minimalna prisotnost svinca v bizmutu lahko zelo poslabša spoj /5/. Zanimale so nas naslednje lastnosti spojev:

- Oblika spoja in razlivanje
- Odtržne sile komponent po spajkanju
- Nastanek in debelina intermetalnih plasti takoj po spajkanju in po staranju na pospešenih klimatskih testih.

1. Eksperimentalni del

2.1. Priprava vzorcev

Vzorce smo pripravili tako, da smo SMD komponente SOT 14 vgradili na polagalni liniji z naslednjima spajkalnima pastama:

- Sn 95,5/ Ag 3,8/ Cu 0,7 in
- Sn62/Pb36/Ag2

Spajkalne paste smo pretalili na tri različno izdelane vzorce TIV in sicer:

- Obdelava tiskanine FR-4 s kemijskim Ni/Au
- Obdelava tiskanine FR-4 s kemijskim Sn

- običajne TIV, izdelane po Hot Air Solder Leveling (HASL) postopku

Postopek pretaljevanja je potekal na pretaljevalnem stroju v proizvodnji. Pri pretaljevanju je bil nastavljen ustrezen temperaturni profil (230 - 260°C za spajkalno pasto brez svinca in 210 - 235°C za običajno spajkalno pasto s svincem) /6/. Na prvi dve vrsti TIV smo komponente pretalili s spajkalno pasto brez svinca, na običajne TIV pa s spajkalno pasto s svincem, ki jo uporabljamo danes.

2.2. Klimatski testi

Pripravljene vzorce TIV smo starali na pospešenih klimatskih testih, ki simulirajo nekaj različnih klimatskih obremenitev v uporabi in sicer:

- 6 ciklov testa po IEC 60068-2-30 (tropski test) /7/
- temperaturno cikliranje iz -30°C na +130°C, na vsaki temperaturi po 6 minut; skupaj 15 ciklov

2.3. Ocenjevanje kvalitete spojev

Kvaliteto spojev smo določali z naslednjimi metodami:

- z ocenjevanjem razlivanja spajke v spoju TIV - priključek komponente, oziroma merjenjem kota omočenja
- z oceno mikroskopskega pregleda spoja z mikroskopom OLYMPUS PMG3 pri 2000-kratni povečavi na metalografskih obrusih
- z merjenjem odtržnih sil prispajkane komponente s strižno obremenitvijo na preskusni napravi ZWICK Z 100

3. Rezultati

3.1. Ocenitev oblike spoja in razlivanje spajke po pretaljevanju

Obliko spoja in razlivanje spajke smo ocenili z merjenjem kota omočenja na mikroskopskem posnetku prereza priključka komponente in PTIV. Spajka je bila v vseh primerih lepo razlita, brez napak v strukturi.

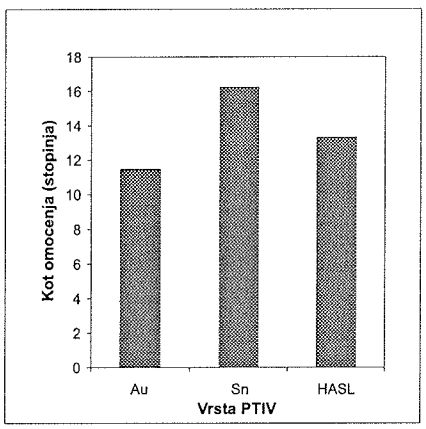

Slika 1: Kot omočenja glede na vrsto PIV (Au - zlatena; Sn - kositrena; HASL - Hot Air Solder Leveling)

Iz zgornje slike 1 je razvidno, da je še najbolj ugoden kot omočenja pri TIV, ki je zlatena (11,5°). Na vseh TIV pa je kot omočenja manjši od 20°, kar pomeni še vedno dobro omočenje in razlivanje spajke

3.2. Rezultati mikroskopskih preiskav

Posnetek na sliki 2 je narejen ob robu vodnika, kjer so se intermetalne faze tvorile najbolj itenzivno. Na bakru je najprej galvanski nanos niklja, nato enakomerna temna intermetalna faza, potem razgibana svetla intermetalna faza in nato spajka. Zlata, ki je nanešen na nikelj, pri mikroskopski preiskavi ne vidimo, ker je debelina le-tega prenizka (pod mejo zaznavnosti optičnega mikroskopa 0,2 μm), ali pa je zlato raztopljeno v spoju.

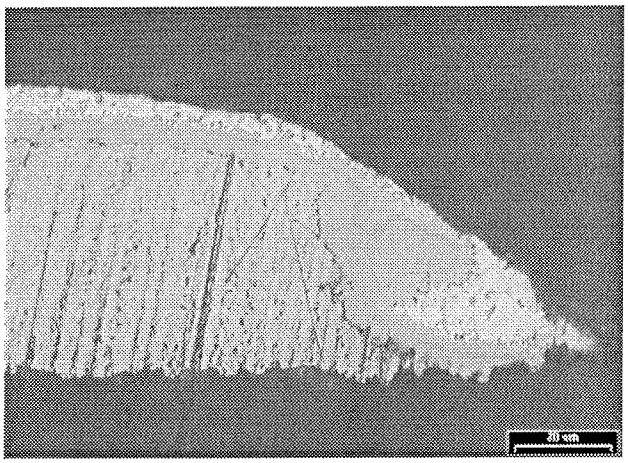

Slika 2: Spoj med pokovinjenjem na TIV (CuNiAu) in spajko brez svinca

Na slikah 3 in 4 vidimo pri preiskavi spojev pri povečavah do 2000-krat med ploščo tiskanega vezja in spajko dve plasti. Temna plast je ob strani plošče, svetla plast pa ob strani spajke. Plasti sta intermetalni fazi, temna plast je najverjetneje intermetalna faza Cu_3Sn, svetla plast pa intermetalna faza Cu_6Sn_5. Kvalitete intermetalnih faz z metalografsko analizo nismo dokazovali. Taka analiza je možna samo z EDS analizo na elektronskem mikroskopu.

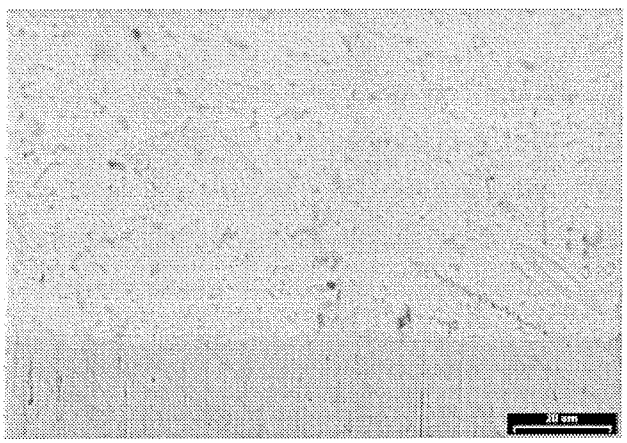

Slika 3: Spoj med pokovinjenjem na TIV (CuSn) in spajko brez svinca

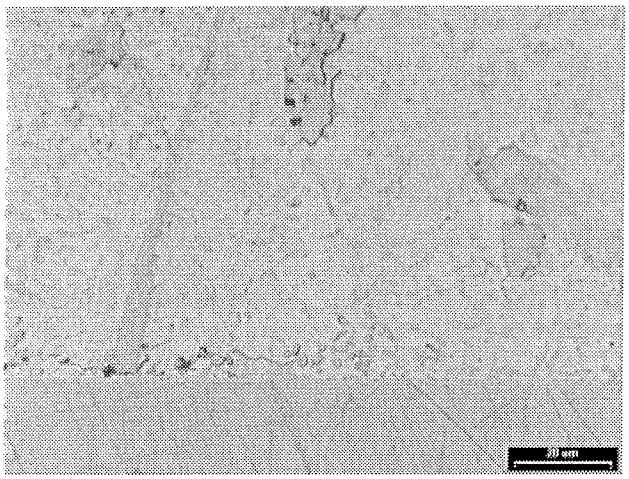

Slika 4: Spoj med pokovinjenjem na TIV (Cu SnPb - HASL) in običajno spajko s svincem

Na sliki 5 so prikazane povprečne debeline intermetalnih plasti za posamezno vrsto spoja. Intermetalne strukture so krhke. Čim večja je njihova debelina, tem slabši je spoj. Iz tega diagrama je razvidno, da je debelina inermetalne plasti na pozlačeni TIV približno identična tisti pri običajnih, po HASL postopku obdelanih TIV, kositrene TIV pa imajo te plasti skoraj dvakrat večje.

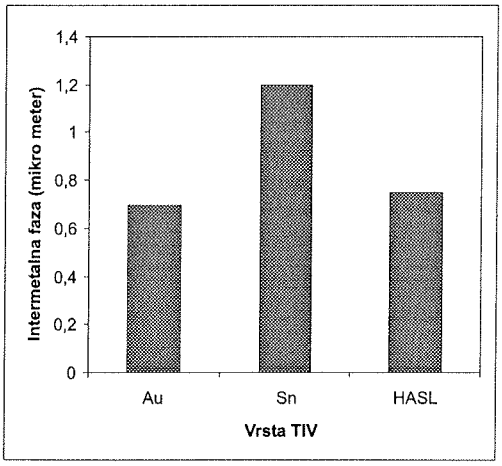

Slika 5: Debeline intermetalnih plasti glede na vrsto TIV(Au - zlatena; Sn - kositrena; HASL - Hot Air Solder Leveling)

3.3. Rezultati odtržnih sil prispajkanih komponent

Rezultate odtržnih sil prispajkanih komponent prikazujejo slike 6,7 in 8. Pri tej raziskavi so nas zanimale tudi spremembe po klimatskih testih.

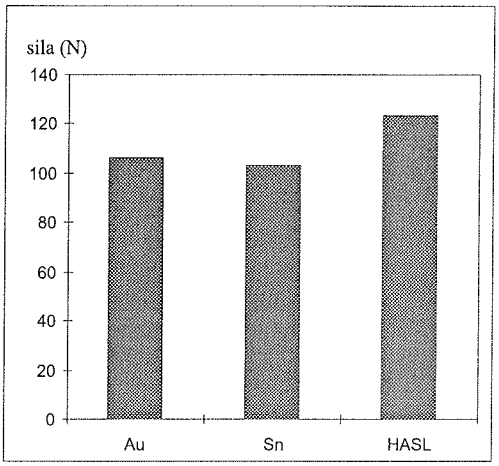

Slika 6: Odtržne sile komponente po pretaljevanju glede na vrsto TIV(Au - zlatena; Sn - kositrena; HASL - Hot Air Solder Leveling)

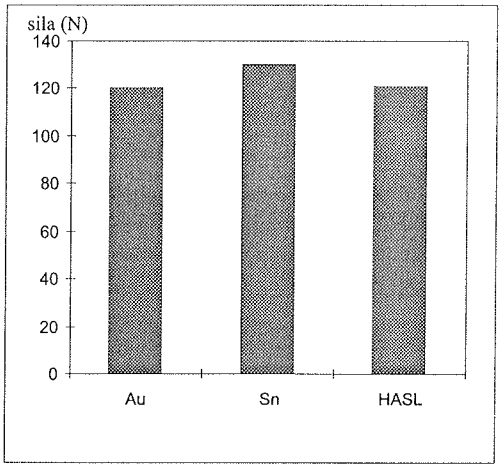

Slika 7: Odtržne sile komponente po tropskem testu glede na vrsto TIV (Au - zlatena; Sn - kositrena; HASL - Hot Air Solder Leveling)

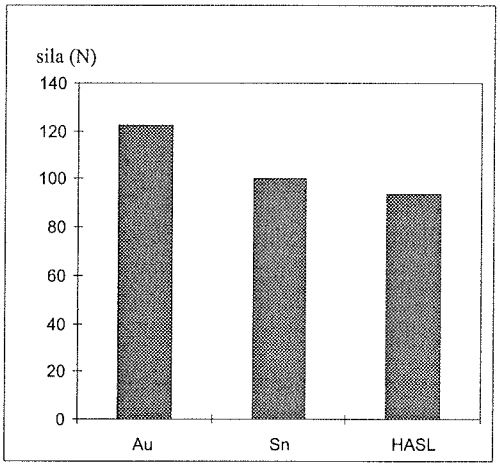

Slika 8: Odtržne sile komponente po cikliranju temperature glede na vrsto TIV(Au - zlatena; Sn - kositrena; HASL - Hot Air Solder Leveling)

Iz zgornjih treh diagramov lahko razberemo naslednje:

- Takoj po pretaljevanju (Slika 6) je očitno, da so odtržne sile na zlatenih in kositrenih TIV malenkost manjše (okrog 10%) od tistih na TIV, izdelanih po HASL postopku. Vendar razlike niso velike.
- Vrsta staranja bistveno ne vpliva na velikost odtržne sile komponente (Slika 7 in Slika 8)
- Po pospešenih klimatskih testih se odtržna sila komponente bistveno ne zmanjša.

4. Zaključek

Iz raziskave lahko naredimo nekaj zaključkov, ki nam bodo koristili pri izbiri materialov in postopkov pri spajkanju v obdobju, ko svinec v elektronski industriji ne bo več dovoljen. To so:

- Spajka brez svinca se na pokositrenih in zlatenih TIV lepo razliva. Kot omočenja je sicer nekoliko večji, vendar še vedno v sprejemljivih mejah.
- Intermetalne strukture nastajajo v vseh treh vrstah spojev. Debeline le-teh so na pozlačenih TIV približno identične tistim pri običajnih, po HASL postopku obdelanih TIV. Kositrene TIV imajo te plasti skoraj dvakrat večje. Krhkost spojev na pokositrenih TIV je torej večja.
- Odtržne sile komponent se glede na vrsto TIV, na katere so prispajkane, po velikosti bistveno ne ločijo.
- Po pospešenih klimatskih testih, ki simulirajo naravne pogoje pri delovanju TIV, se odtržna sila komponent bistveno ne zmanjša
- Vrsta pospešenega testa, ki smo jih izbrali, bistveno ne vpliva na velikost odtržne sile komponent.

5. Literatura:

/1/ CIRCUITS ASSEMBLY; December 2001: Materials and Process Considerations for Lead-Free Electronics Assembly

/2/ CIRCUITS ASSEMBLY; September 2000: The Status of Lead - Free Alloys in Lead-Free Electronics Assembly

/3/ CIRCUITS ASSEMBLY; Avgust 1999: Connecting to Lead-Free Solders

/4/ Paper for "Electronics Goes Green 2000+"; Dipl. Ing. Anton Miric, W.C.Heraeus GmbH & Co., Hanau Germany

/5/ Bob Willys: »Lead free Assembly & Soldering«; Lecture; SMT Nürenberg 2002

/6/ Technische Information: Litton Kester, Producer of soldering materials

/7/ IEC 60068-2-30

Breda Kodek, univ.dipl.kemik
Iskraemeco d.d.
Razvoj & Raziskave
Laboratorijski center
Savska loka 4,
4000 KRANJ

Prispelo (Arrived): 20.11.2002 *Sprejeto (Accepted):25.05.2003*

INDUKTIVNI SENZORJI

Leopold Knez

Iskra Feriti, Ljubljana, Slovenija

Ključne besede: Induktivni senzorji, približevalna stikala, izgubni faktor, temperaturni koeficient permeabilnosti, Curiejeva temperatura, induktivnost tuljave, faktor kakovosti tuljave

Izvleček: Induktivni senzorji so gradniki nekontaktnih stikal. Uporabljamo jih v avtomatiki in profesionalni elektroniki za merjenje razdalj, razpoznavanje kovin in krmiljenje aktuatorjev. Za zanesljivo delovanje je treba izbrati primeren feritni material, ki ima majhne normalizirane izgube $\tan \delta / \mu_i$ in čim manjši temperaturni koeficient permeabilnosti α_F. V članku opisujemo princip delovanja induktivnega senzorja in induktivnega stikala, pojasnjujemo nekatere parametre in sklenemo s praktičnim izračunom senzorske tuljavice. Izračunu dodajamo še meritve induktivnega senzorja za primerjavo.

Inductive Sensors

Key words: inductive sensor, proximity switch, loss factor, temperature coefficient of permeabiliy, Curie temperature, inductance of coil, quality factor

Abstract: Inductive sensors form parts of proximity switches. They are used in automotive and professional electronics for measuring distance, recognising different alloys and control actuators. For reliable operation it is necessary to choose a suitable ferrite material that has a very low loss factor $\tan \delta / \mu_i$ and temperature coefficient of permeability α_F. In the article we describe the working principle of an inductive sensor and a proximity switch. Some important ferrite material parameters are explained and a calculation of the inductivity of an open magnetic coil is added as an example. We conclude with practical measurements of an inductive sensor L14 which are added for comparison.

1 Princip delovanja induktivnih senzorjev

Induktivni senzorji spadajo med robustnejše elemente. Uporabljajo se v industrijski avtomatizaciji, avtomobilski industriji in široki porabi. Delujejo nekontaktno. Če so primerno zaščiteni proti udarcem, prahu in vlagi, imajo zelo dolgo trajnostno dobo. Nepogrešljivi so povsod tam, kjer želimo nedotično ugotavljati pozicijo kovinskega predmeta ali izdelka. Z njimi lahko ugotavljamo premike, leguro materiala, štejemo izdelke ali vrtljaje.

Prerez induktivnega senzorja je podan na sliki 1. Tuljavica je navita na plastični tuljavnik tako, da je njena ravnina natančno poravnana z robom feritnega jedra. To jedro je navadno izdelano v obliki navadnega ali podolgovatega lončka, ki ima odprt magnetni krog. Tako dobimo stresano elektromagnetno polje. Tuljava tvori z vzporedno vezanim kondenzatorjem nihajni krog. Tega napajamo z oscilatorjem. Frekvence osciliranja so navadno med 10 kHz in 1 MHz.

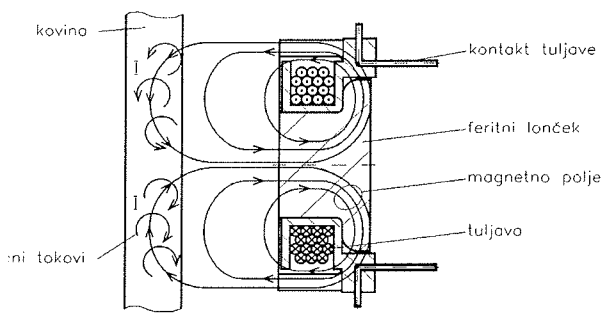

Slika 1. Prerez induktivnega dela senzorja

Smer magnetnega polja se spreminja s smerjo toka. Na sliki 1 je narisana smer polja le v eni pol periodi. V naslednji pol periodi se magnetno polje obrne. Obrne se tudi smer vrtinčnih tokov. Stresano magnetno polje inducira v kovini vrtinčne tokove, ki segrevajo kovino. Velikost vrtinčnih tokov je odvisna od razdalje med kovino in induktivnim senzorjem. Razmere so podobne tistim pri transformatorju, ki ima sekundarno navitje v kratkem stiku.

Električne izgube v kovini krije magnetno polje, ki črpa električno energijo iz vezja. Ker je vir elektromagnetne energije šibak, pri približevanju kovine hitro upade amplituda osciliranja elektromagnetnega polja senzorja. Ob približevanju kovine senzorju prične upadati tudi Q nihajnega kroga. To lastnost izkoriščamo pri prepoznavanju kovancev in njihovih legur. Če so kovanci pristni, so izdelani iz enake legure, na katero je možno umeriti induktivni senzor. Tako ugotavljamo pri novčičnih avtomatih vrsto in pristnost kovanca. Ker je v kovancu več različnih kovin, uporabimo več induktivnih senzorjev, ki so umerjeni na posamezne kovine. Navadno uporabljamo tri do štiri induktivne senzorje, ki so z mikroprocesorjem in programom povezani v sistem štetja in ugotavljanja pristnosti kovancev. Pri sodobnih avtomatih na kovinske žetone uporabljamo podoben princip delovanja.

2 Zgradba induktivnih stikal

Induktivno stikalo (slika 2) je sestavljeno iz kvalitetnega induktivnega senzorja L, ki skupaj z L in C sestavlja nihajni krog, oscilatorja, Schmitovega prožilnika in ojačevalnika. Induktivno stikalo napajamo z enosmernim tokom. Izhod induktivnega stikala je visok ali nizek napetostni nivo. Za

krmiljenje močnejših aktuatorjev je treba dograditi ojačevalnik, ki zagotavlja ustrezne izhodne tokove za njihovo proženje.

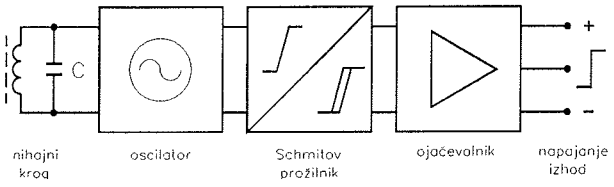

Slika 2. Shema induktivnega stikala

Napetost na sponkah vzporednega nihajnega kroga je v resonanci najvišja. Najvišja pa je tudi kakovost kroga Q. Ob prisotnosti kovine pa Q, kot je bilo pokazano v predhodnem poglavju, močno upade. Zmanjša se tudi induktivnost tuljave ter posledično frekvenca nihajnega kroga. Induktivna stikala so zato lahko umerjena na padec Q -ja ali na spremembo frekvence nihajnega kroga.

Pri približevanju kovinske plošče induktivnemu stikalu torej dosežemo točko, kjer se stikalo vklopi. Pri oddaljevanju plošče dosežemo novo točko, kjer se stikalo izklopi. Razlika razdalj med vklopom in izklopom stikala je histereza, ki pa je tudi potrebna za zanesljivo delovanje induktivnega senzorja.

3 Praktična izvedba induktivnega stikala

Na sliki 3 je prikazana električna shema induktivnega stikala za industrijske aplikacije. Tranzistorska stopnja poveča občutljivost senzorja in zmanjšuje histerezo preklapljanja na 0,6 do 0,7mm pri odmiku 0,5mm. Tipični frekvenci nihajnih krogov sta med 2 in 3MHz. Frekvenci pa se glede na vrednosti induktivnosti lahko spreminjata med 1 in 10MHz. Ko se induktivnemu senzorju približa kovinska plošča, se zaradi izgub v njej, zniža frekvenca nihajnih krogov. Integrirano vezje TCA 105 pretvori spremembe resonančnih frekvenc nihajnih krogov v nizek izhodni nivo. Izhodna logična stanja prožita aktuatorje. Z nastavljivim trimerjem P1 nastavljamo širino histerezne zanke v območju 0,3 do 1mm medtem, ko s trimerjem P2 nastavljamo prag preklapljanja senzorja glede na oddaljenost senzorja od kovinske plošče v območju 3 do 10mm. Frekvenca nihajnih krogov se zmanjšuje ob horizontalnem ali vertikalnem približevanju tuljavic kovinski plošči.

Za kakovostno in zanesljivo delovanje induktivnih senzorjev izberemo primeren feritni material, ki ima čim manjše izgube pri visokih frekvencah in majhen temperaturni koeficient permeabilnosti. Pomembnejše parametre in bistvene razlike med tremi materiali navajamo v tabeli 1.

Podrobnejše karakteristike so dostopne na spletnih straneh http://www.iskra-feriti.si.

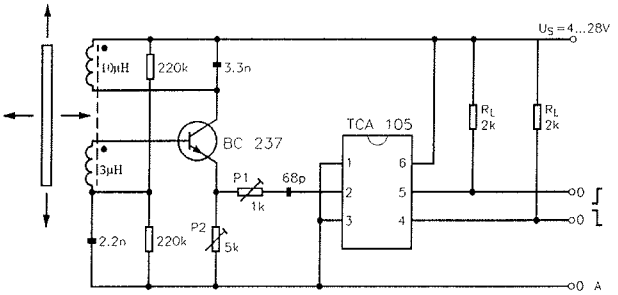

Slika 3. Praktična izvedba induktivnega stikala [1]

Tabela 1. Pomembnejši parametri feritnih materialov za induktivne senzorje

Parameter	Material 10G	Material 16G	Material 26G
Začetna permeabilnost μ_i	750 ± 20 %	2200 ± 20 %	2200 ± 20 %
Normalizirane izgube $\tan\delta/\mu_i$	< 8 10^{-6}; 300 kHz < 20 10^{-6}; 1 MHz	<1.5 10^{-6}; 10 kHz < 3.5 10^{-6}; 100 kHz	<1.0 10^{-6}; 10 kHz < 2.5 10^{-6}; 100 kHz
Temperaturni koeficient permeabilnosti α_F: - 25 do + 55 °C	0 – 2 10^{-6}/K	0.6 – 2.2 10^{-6}/K	0.4 – 1.5 10^{-6}/K
Curiejeva temperatura	> 200 °C	> 150 °C	> 150 °C

4 Definicije pomembnejših parametrov feritnih materialov

4.1 Normalizirane izgube v feritnem materialu

Magnetne izgube so vsota histereznih izgub, izgub zaradi vrtinčnih tokov in preostalih ali remanenčnih izgub. Histerezne izgube so pri majhnih magnetnih gostotah v feritnem materialu zanemarljive. Izgube zaradi vrtinčnih tokov naraščajo s hitrostjo spreminjanja smeri tokov. Pri nizkih frekvencah so zanemarljive. Induktivni senzorji uporabljajo majhne magnetne gostote in višje frekvence magnetnih polj.

Normalizirane izgube $\tan\delta/\mu_i$ so neodvisne od velikosti jedra in zračne reže pri magnetno odprtih jedrih. Določajo ga le izgube zaradi vrtinčnih tokov in preostale izgube v feritnem materialu, zato ne vključuje histereznih izgub. Faktor narašča s frekvenco.

Normalizirane izgube v feritnem materialu merimo z računalniško podprtim merilnim sistemom. Merilni vzorec je toroidno jedro T 22 14 07, na katerega navijemo 20 ovojev dvakrat lakirane bakrene žice premera 0,25 mm. Merilno frekvenco za nizkoizgubne materiale spreminjamo med 10 kHz in 1 MHz. Merilni sistem pri sobni temperaturi 23 ± 2 °C zagotavlja stalno gostoto 0,1 mT v feritnem jedru, izmeri induktivnost tuljave ter njeno enosmerno in efektivno upornost. Na osnovi izmerjenih parametrov izračuna normalizirane izgube feritnega materiala po enačbi (4.1):

$$\frac{\tan\delta}{\mu_i} = \frac{\frac{R_{ef} - R_o}{2 \cdot \pi \cdot f \cdot L}}{\mu_i} = \frac{\tan\delta_e}{\mu_e} \qquad (4.1)$$

pri čemer je R_{ef} efektivna upornost tuljave, navite na feritno jedro, pri frekvenci 100 kHz ali 1 MHz in vključuje enosmerne in celotne izgube izražene v Ω, R_o je čista enosmerna upornost tuljave v Ω, f je merilna frekvenca v Hz, L induktivnost tuljave v H, μ_i začetna permeabilnost toroida in μ_e efektivna permeabilnost jedra z režo. Efektivna permeabilnost je vedno nižja od začetne. Podajamo jo za jedra z zračno režo. Izgubni faktor je za obe permeabilnosti enak, ker se pri jedrih z režo zmanjša tudi kot δ_e.

4.2 Curiejeva temperatura

Curiejeva temperatura T_C je temperaturna meja, nad katero izgubi feritni material svoje magnetne lastnosti. Začetna permeabilnost feritnega materiala μ_i sedaj pade na vrednost 1.

4.3 Temperaturni koeficient permeabilnosti

Temperaturni koeficient permeabilnosti materiala α_F je določen kot sprememba začetne permeabilnosti materiala zaradi spremembe temperature in ga podaja enačba (4.2). To je materialna konstanta, ki je neodvisna od reže. Ta faktor posledično vpliva na spremembo induktivnosti tuljave, če se spremeni temperatura v feritnem materialu. V enačbi nastopa relativna permeabilnost μ_i, ki je brezdimenzijska. Temperaturni koeficient permeabilnosti α_F podaja enačba (4.2):

$$\alpha_F = \frac{\mu_{i2} - \mu_{i1}}{\mu_{i1} \cdot \mu_{i2} \cdot [T_2 - T_1]} \left[\frac{1}{K}\right] \qquad (4.2)$$

pri čemer je μ_{i1} permeabilnost pri temperaturi T_1 in μ_{i2} permeabilnost pri temperaturi T_2 v stopinjah Kelvina.

5 Oblike in velikosti feritnih lončkov za induktivne senzorje

Iz feritnih materialov 10G, 16G in 26G se izdeluje lončaste oblike feritnih jeder, ki so primerni za induktivne senzorje. Črka pri oznaki običajno pomeni lonček, številka pa njegov zunanji premer.

6 Izračun induktivnosti tuljave za senzor induktivnosti

Izračunavanje induktivnosti tuljav z odprtimi magnetnimi krogi je težavno. Za praktične izračune pa enačba (6.1) določa dober rezultat /2/. Natančne vrednosti parametrov induktivnega senzorja ugotavljamo z meritvami. Induktivnost tuljave je določena s številom ovojev in njeno geometrijsko obliko. Vpliv feritnega materiala na induktivnost je izražena s koeficientom k.

$$L = k \cdot \frac{\pi^2 \cdot D^2 \cdot N^2}{l \cdot \left[1 + 0{,}45 \cdot \frac{D}{l} - 0{,}003 \cdot \frac{D^2}{l^2}\right]} [nH] \qquad (6.1)$$

D = notranji premer tuljave v cm
l = dolžina tuljave v cm
N = število ovojev tuljave
k = koeficient (k = *1* za zračno tuljavo, k = *3* za tuljavo s feritnim jedrom)

Induktivnost po enačbi (6.1) lahko računamo, kadar je razmerje notranjega premera tuljave proti dolžini tuljave $\left(\frac{D}{l}\right)$ med 0 in 30.

Kakovost tuljave Q podaja naslednja enačba:

$$Q = \frac{\omega \cdot L}{R} = \frac{2 \cdot \pi \cdot f \cdot L}{R} \qquad (6.2)$$

pri čemer je L induktivnost tuljave v H in R enosmerna upornost v Ω in f frekvenca v Hz.

Kakovost tuljave linearno raste s frekvenco dokler ne začne s frekvenco rasti še njena upornost. Kakovost nihajnega kroga pa se spreminja po značilni zvonasti krivulji. Iz znane induktivnosti in enosmerne upornosti lahko izračunamo kakovost tuljave pri različnih frekvencah. Recipročna vrednost kakovosti je izgubni faktor tuljave.

6.1 Zgled za izračun induktivnosti tipičnega induktivnega senzorja

D = 0,72 cm
l = 0,17 cm
N = 300 ovojev
k = 1 za zrak oziroma 2 ali 3 za feritni material

Uporabimo enačbo (6.1) in izračunamo induktivnost zračne tuljave:

$$L = \frac{1 \cdot \pi^2 \cdot 0{,}72^2 \cdot 300^2}{0{,}17 \cdot \left[1 + 0{,}45 \cdot \frac{0{,}72}{0{,}17} - 0{,}003 \cdot \frac{0{,}72^2}{0{,}17^2}\right]}$$

$$= 949\,725{,}87\ nH = 949{,}7\ \mu H$$

Z upoštevanjem koeficienta k in enačbe (6.1) izračunamo še induktivnost tuljave s feritnim lončkom:

$$L\,(k=3) = 3 \cdot 949{,}7\ \mu H = 2.849{,}1\ \mu H$$

6.2 Praktične meritve induktivnega senzorja

Tabela 2. Praktične meritve induktivnega senzorja

Frekvenca	Induktivnost, kakovost		
	Brez feritnega lončka	S feritnim lončkom 10G	S feritnim lončkom 26G
10 kHz	L = 930 µH Q = 3	L = 2.88 mH Q = 9,2	L = 2.87 mH Q = 9,2
100 kHz	L = 931 µH Q = 27,5	L = 2,89 mH Q = 73	L = 2.89 mH Q = 72

Induktivnost tuljave s feritnim jedrom se poveča za približno trikrat. Podobno je s kakovostjo Q, na katero najbolj vpliva vrsta feritnega materiala. Praktični rezultati se dovolj dobro ujemajo z izračunom.

7 Sklep

Induktivni senzorji so zelo uporabni za nekontaktna stikala v avtomatiki. So robustni in skoraj neobčutljivi za umazanijo in okolje. Imajo dolgo trajnostno dobo. Delujejo lahko v širokem frekvenčnem področju. Zaradi robustnosti in zanesljivosti lahko sklepamo, da bo njihova uporaba še dolgo nepogrešljiva v industrijski avtomatizaciji in profesionalni elektroniki. Električne izgube in kakovost induktivnih senzorjev določa izbrani feritni material. Računanje parametrov tuljav z odprtimi magnetnimi krogi je lahko le približno.

8 Literatura

/1/ Dieter Nührmann, Professionelle Schaltungstechnik, 3. Auflage, Teil 3, Optoelektronik, Fernsteuerschaltungen, Steuer- und Regeltechnik, točka 7.8, stran 137, 138, ISBN 3-7723-6713-5, Franzis' - Verlag, 1992

/2/ George Rose, Große Elektronik-Formel-sammlung, 19. Auflage, ISBN 3-7723-5339-8, Franzis' - Verlag, 1995, stran 130

Mag. Leopold Knez, univ. dipl. inž.,
tel. (01) 5833 114,
E-pošta: leopold.knez@iskra-feriti.si
Iskra Feriti, d. o. o.
Stegne 29, SI-1521 Ljubljana
tel. +386 1 5833 114
faks +386 1 5833 235

Prispelo (Arrived): 06.06.2002 *Sprejeto (Accepted): 25.05.2003*

UDK621.3:(53+54+621+66), ISSN0352-9045 Informacije MIDEM 33(2003)2, Ljubljana

HOME AUTOMATION ON THE MOVE

[1] Andrej Šoštarič, [1] Bojan Imperl, [2] Boro Jerabek

[1] HERMES SoftLab d.d., Ljubljana, Slovenia
[2] Gorenje d.d., Velenje, Slovenia

Key words: home automation, X.10, SMS, mobility, value added services, kitchen center

Abstract: In this article we would like to show how an arbitrary home and building electronic system based on the home automation standards such as X10 might be addressed and controlled by an appropriate mobile technology. Urge for mobility of users, which may be at the same time either the inhabitants of these homes or even administrators and supporters, is growing. The possibility to control and observe the status of home appliances while being on the move away from home using our mobile phones is becoming reality today. As an example we will introduce the prototype system, which gained a lot of attention on the last INFOS conference and was made functional throughout the cooperation of two Slovenian companies, Gorenje and HERMES SoftLab. While Gorenje developed a so-called kitchen center, an unique all-in-one home appliance controlled by the personal computer, HERMES SoftLab contributed the X10 PLC protocol environment and HERMES SoftLab's Smart Service Mediator (SSM) platform, well known from the mobile operators' world, which enable mobile users to control their automated home remotely using ordinary mobile phones and short messaging system (SMS). When developed, this prototype system presented one of the world's first attempts to integrate the home automation system with the GSM network using the SMS.

Hišna avtomatizacija na pohodu

Ključne besede: hišna avtomatizacija, X.10, SMS, mobilnost, storitve z dodano vrednostjo, kuhinjski center

Izvleček: V članku bi radi pokazali, kako lahko nek poljuben dom in stavbni elektronski sistem, ki temelji na standardih hišne avtomatizacije kot je X10, usmerjamo in nadzorujemo s pomočjo primerne mobilne tehnologije. Potreba po mobilnosti uporabnikov, ki so lahko hkrati prebivalci teh domov ali celo administratorji in vzdrževalci, vedno bolj narašča. Možnost upravljanja in opazovanja statusa hišnih naprav s pomočjo mobilnega telefona med uporabnikovo odsotnostjo z doma postaja dandanes stvarnost. Kot primer bomo predstavili prototip takšnega sistema, ki je na zadnji konferenci INFOS požel veliko zanimanja in sta ga v sodelovanju razvili dve slovenski podjetji, Gorenje in HERMES SoftLab. Medtem ko je Gorenje razvilo takoimenovan kuhinjski center, edinstveno, vse-v-enem hišno napravo, ki jo nadzoruje osebni računalnik, je HERMES SoftLab prispeval strojno rešitev, temelječo na standardu X10, in sporočilno platformo Smart Service Mediator (SSM), dobro znano v svetu mobilnih operaterjev. Vse to omogoča mobilnim uporabnikom nadziranje avtomatiziranega doma na daljavo z uporabo navadnega mobilnega telefona in pošiljanja kratkih sporočil (SMS). Ob razvoju je ta prototip predstavljal enega prvih poskusov integracije sistema hišne avtomatizacije z omrežjem GSM, ki temelji na pošiljanju kratkih sporočil.

Home automation

In recent years there have been several attempts worldwide to develop a home and building electronic system (HBES) based on the Power Line Carrier (PLC) technology. The PLC technology uses existing electrical power lines in home and buildings to send the control signals for controlling various home appliances. However the different system specifications have confused planning engineers, contractors, installers as well as resellers, end-users, building owners and investors. This situation is hindering market acceptance and growth. Consequently each system lacks the necessary volume success. In Europe specifically there are three solutions, which are candidates to become the home and building electronic system standard:

- BatiBUS - represented by BatiBUS Club International (BCI)
- EIB (European Installation Bus) - represented by European Installation Bus Association (EIBA)
- EHS (European Home Systems) - represented by European Home Systems Association (EHSA)

The three above mentioned associations have agreed to provide the technical basis for the convergence of these three systems so that in future there will be only one common system supported by relevant industrial companies. A common Association resulting from the amalgamation of BCI, EIBA and EHSA will promote the KNX standard.

In the USA and in the last few years also in Europe another system, X10, gained high popularity due to its simplicity, low price, and adoption by the manufacturers. X10 is a PLC protocol that allows compatible devices throughout the home to communicate with each other via the existing 110/220V electrical power lines. Using X10 it is possible to control lights and virtually any other electrical device or collect the data from the sensors (temperature, humidity, motion etc.) from anywhere in the house with no additional wiring.

X10 Power Line Carrier Protocol

The X10 PLC protocol /1/ defines the procedure for communication between the transmitting device and receiving device by sending and receiving signals over the power line wiring. These signals represent short RF bursts, a 120

kHz-coded signal superimposed on the 60Hz/50Hz electrical power line, with encoded digital information. The X-10 signals are synchronized to the zero-crossing point of the AC power line - they are transmitted within 200 µs of the zero crossing point. Power line interfaces provide 50Hz square wave with a max. delay of 100 µs from the zero crossing point to the AC power line. The maximum delay between signal envelope input and 120 kHz output bursts is 50 µs. A binary 1 is represented by a 1 ms burst of 120 kHz, at the zero crossing point. If burst is not presented in this period, a binary 0 is assumed. These 1 millisecond bursts are transmitted three times to cover the zero crossing points of all three phases in a three phase power distribution system, as shown in Figure 1.

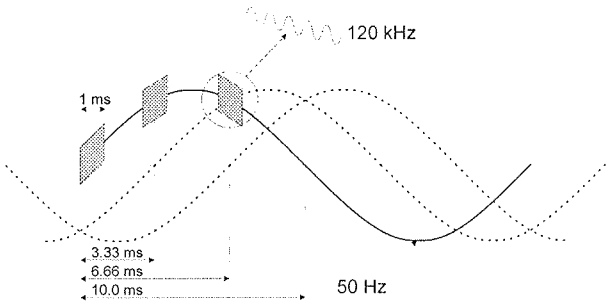

Figure 1: The Power Line Cycle and the X10 signals.

One cycle of the 50Hz power line carries one bit of information. In X10, transmission of the complete information consists of a sequence of three groups of bits (codes): start code, house code, and a number or function code (see Figure 2).

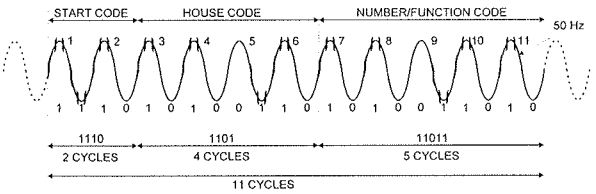

Figure 2: The X10 coding scheme.

The start code is a standard code denoting the start of the transmission and is transmitted within the first 2 power line cycles. The house code is a 4-bit code (any code from 0000 to 1111) and serves as the address of the target device to which the transmission is addressed. The number/function code is a 5-bit code (any code from 00000 to 11111). Transmission of the house code takes 4 power line cycles, while the transmission of the number/function code takes 5 power line cycles. The house codes and the number/function codes are transmitted in a true compliment form on alternate half cycles of the power line - if a binary 1 is transmitted on one half cycle (1 millisecond burst of signal) then binary 0 (no signal) should be transmitted on the next cycle (See Figure 3). The Start Code is always 1110, which is a unique code and unlike the house and number/function codes does not follow true complimentary relationship on alternate half cycles. The start code is transmitted within 2 power line cycles (see Figure 2).

The complete transmission (start code, house code, and a number/function code) hence requires 11 power line cycles and is always repeated twice with 3 power line cycles between each transmission: transmission of start, house, and number code followed by the transmission of the start, house, and function code. The house, number, and function codes are listed in Table 1.

	House codes
A	0110
B	1110
C	0010
D	1010
E	0001
F	1001
G	0101
H	1101
I	0111
J	1111
K	0011
L	1011
M	0000
N	1000
O	0100
P	1100

	Number codes
1	01100
2	11100
3	00100
4	10100
5	00010
6	10010
7	01010
8	11010
9	01110
10	11110
11	00110
12	10110
13	00000
14	10000
15	01000
16	11000

	Function codes
All units OFF	00001
All Lights ON	00011
ON	00101
OFF	00111
Dim	01001
Bright	01011
All Lights OFF	01101
Extended Code	01111
Hail Request	10001
Hail Acknowledge	10011
Pre-Set Dim	101X1
Extended Data	11001
Status=ON	11011
Status=OFF	11101
Status Request	11111

Table 1: The list of available house, number, and function codes.

We can connect a large number of X10 receiving devices to the power line. To each of them we can assign one of 16 available house codes and one of 16 available number codes giving 256 different possible combinations.

The X10 PLC home automation network consists of the following types of X20 devices:

Receiving devices (executing the commands, no feedback information): light switches, receptacles, chimes

Transmitting devices (transmitting signals to the power line: phone and PC controllers)

Transceiver devices (receiving data and report status): motion detectors, flood detectors, thermometers

X10 PLC Network devices: passive couplers, coupler repeaters, surge protectors, noise filters, and signal blocks that are installed in or near the electrical service panel. Such devices are necessary for providing consistent and reliable signaling performance, especially in the densely populated areas.

Kitchen center of Gorenje

Gorenje's kitchen center (Figure 3) is designed to become not only the central automation/information point of the kitchen but also the central point of the whole home. From outside it looks like a very modern and futuristically shaped kitchen-range. However, many are surprised when instead of a standard button-like control panel a modern flat panel touch screen silently rolls-out from the center whenever we want to monitor or control the system. By pressing the images on the touch screen we are able to turn on/off the oven or heating plates, control their temperature, start different cooking programs, set timers etc.

The brains of the kitchen center represent a personal computer hidden in the very bottom of the center and transparent from the user's point of view. Internal electronic devices (heating plates, oven) are controlled by a proprietary controller maid by engineers from Gorenje, which is connected to the computer's serial port /2/.

Another serial port is used for a X10 PLC modem, which connects the computer to the home's power line. This subsystem enables controlling of the X10 compliant home devices from the same point. The prototype system includes several light dimmers and switches as well as IR motion detectors. In general we could control also many other devices, such as heating and air-conditioning system, automatic doors, video and sound devices etc. /3/

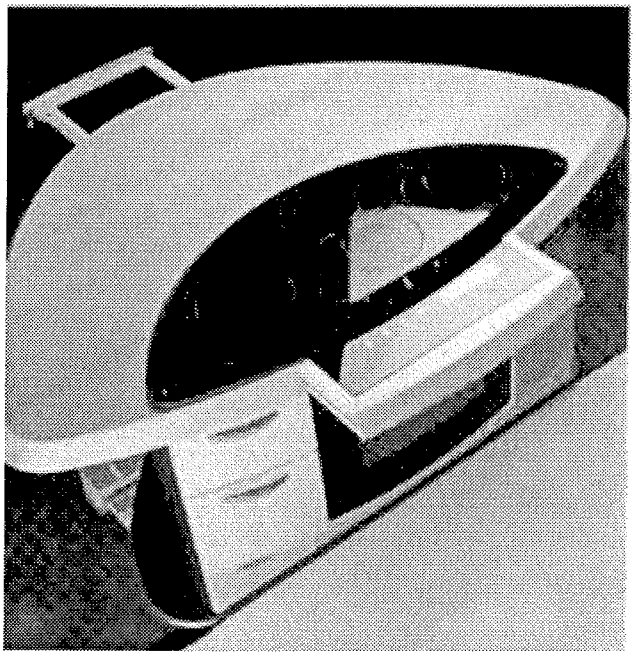

Figure 3: Kitchen center of Gorenje

Mobile phone as a remote control device

To have a complete control over the wide variety of home devices is at least a nice feature. But wouldn't it be nice if we turned on the air-conditioning system when we were still on our way home? Or we could even use our mobile phone to open the garage door remotely. Some suggestions would perhaps bring a smile to the reader while some others are definitely attracting much more attention. For instance, wouldn't it be very useful if we got an alarm in shape of a short message (SMS) or a voice call in case that motion or fire detectors register some problems? There are several proprietary and closed systems, which provide exactly those functionalities, but there are as many different standards as there are solutions. At the same time, the cost of several isolated and non-compliant solutions exceeds the cost of the solution we are about to introduce.

Today, almost everybody has a mobile phone. The penetration in some countries is reaching numbers higher than 70% of the whole population /4/. Mobile phone is not only voice-based communication device but is also becoming a payment instrument, electronic wallet, gaming device, and of course a special type of a remote controller.

On the other hand, engineers from HERMES SoftLab developed a messaging platform, of which main task is to connect a mobile user with information resources and applications anywhere on the Internet. Starting from the fact that Gorenje's kitchen center is controlled by a built-in personal computer, it seemed a logical step to connect that computer to the Internet and enable users to remotely control the home automation system.

But nonetheless, on the way to the final solution several problems were encountered, such as authentication and authorization issues, real-time message routing, security etc., which are successfully addressed and solved by the messaging platform.

Smart Service Mediator platform

SSM is a multi-channel platform that connects mobile users with the web servers using different communication channels /5/. While primarily it is being used for communication with short messages, voice, WAP, and HTTP channels are supported as well. Besides short messages, voice interaction is becoming more and more used, but in that case the cost of solution is higher because voice recognition system and text-to-speech synthesis must be involved.

Basically, there are two different types of SSM installations, depending on the usage model. SSM platform may be installed either at the mobile operator (Figure 4) or in home servers /6/. In the first case, home servers must be connected to the mobile operator's infrastructure via Internet, while in the second case an in-house GSM modem is needed. Both installation types have their advantages and disadvantages depending on cost, business models, Internet availability etc. First option is cheaper for the end user and is promoted by the mobile operator. Second option is operator independent, needs no Internet connection but is less

suitable for the individual use because of the higher complexity at the user's side. Anyway, the solution with the GSM modem might be appropriate for larger enterprises. In the prototype version web server was connected to the mobile operator's (Mobitel) SSM platform over the Internet.

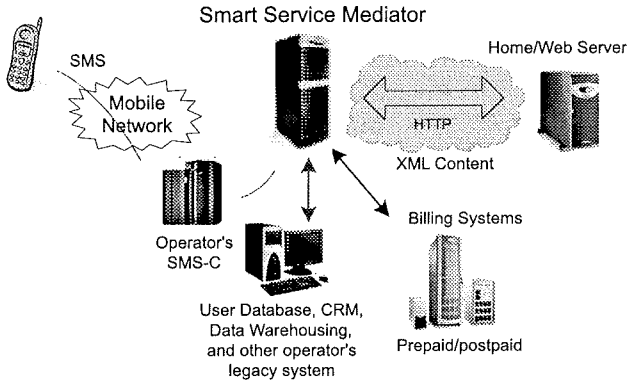

Figure 4: SSM platform as a part of mobile operator's service network.

SSM platform communicates with the external world using standard communication and security protocols, such as XML for message coding, HTTP and HTTPS for transport and message encryption. In Figure 4, reader can notice also a connection between the SSM and mobile operator's billing systems - SSM is used also as an additional revenue generator because it handles and counts the messages traveling through the system. To these messages we can attach service data records (SDR) meaning that users would pay more than just a cost of short messages for this extra service.

Following is a communication scenario between a mobile user and home automation system while remotely turning on the heating device:

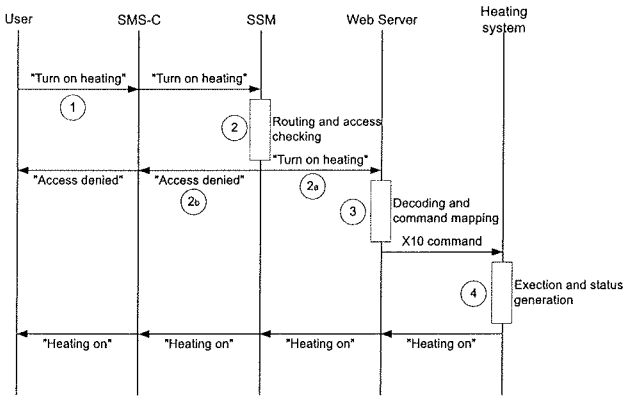

1. User initiates the action by sending an SMS with the predefined content structure (i.e. "Turn on heating" or "Heating on") to the certain number or to the so-called large account[1] (i.e. 1010). The message reaches the SMS Center (SMS-C), which is a vital part of the mobile operator's infrastructure and takes care of all in/outcoming SMS messages. SMS-C forwards the message to the SSM.
2. SSM performs two main tasks - it routes the messages to the relevant home web server depending on a LA number and performs the authorization checks. SSM enables an easy user grouping and generation of access check lists. Only authorized users are allowed to control the devices in a certain home automation environment. If the access is granted (step 2a) the message is routed to the destination web server determined by the URL specified in the SSM settings. Otherwise, user gets a message containing denial of a service (step 2b).
3. Web server parses the message sent by a mobile user. If the message is valid appropriate action is taken - in our case, an X10 command is sent via X10 PLC modem to the heating system with the aim to turn it on.
4. Heating system performs the action and returns the status, which is then forwarded back to the user.

The example shown above is only about turning on the heating system in a house. For controlling the kitchen center devices, such as oven, heaters, fan, and some other household devices, such as lights, alarm and dimmers, the following syntax is used:

command device arg

where

command	ON, OFF, STATUS, HELP (abbreviations allowed: ON, OFF, S, H)
device	ALARM/1..m/, LIGHT/1..n/, OVEN, (abbreviations allowed: A, L, O, S)
arg	If command = ALARM, arg can vary between SILENT and LOUD (set by default) If command = LIGHT, arg can vary between 1 to 10 (default is 10). Arguments from 1 to 9 dim the light (if lights are actually attached to dimmer X.10 devices). Arguments 0 and 10 have the meaning of turning the lights ON/OFF.

Following are some examples used in connection with the kitchen center:

- ON L1 30 (dim light1 to 30%)
- ALARM2 ON (turn on the second alarm in the house)
- OWEN OFF (switch the oven off)
- STATUS OWEN (get the oven status) etc.

1 *Large accounts (LA) or large account numbers are short mobile numbers, usually up to 4 digits long, which are used for easier dialing/addressing of mobile data services.*

All examples from above were used in a so-called pull mode, where users send messages and trigger some activities or status reports. However, SSM enables also push functionality, where messages can be sent to mobile users without their requests in case some special situation occurs - i.e. user can be notified with a short message triggered by the motion detector. Motion detectors are not the only originators of pushed messages. You can imagine some other devices, such as fire/smoke/water detectors, timers etc.

Conclusion

Mobile phones have definitely marked current generations in the same way radios, TV sets and cars did in the past. They have become a necessity alowing users of mobile phones to be constantly in contact with each other and in contact with information. The work described in the paper presents a step further - it alows users of mobile phones to be constantly in contact also with a number of different devices either at home or at work. Eventhough the integration of home appliances with the mobile network may seem an insignificant task, it requires a deep knowledge of a number of different technologies and tight cooperation of partners from a different areas. In this case, two inovative companies, HERMES SoftLab - a software engineering company, and Gorenje - a manufacturer of home appliances, have joined their effort and brought ideas to life. Integration of home appliances with the mobile network opens a variety of possibilities both in the business and in consumer environments and the full potential of the features it brings is yet to be discovered.

References

/1/ B. Berner, C Elliott. Approaching Home Automation, Smart Home Systems, 2001

/2/ B. Jerabek, Z. Cencen, U. Sonjak, Kuhinjski center prihodnosti, Gorenje, Velenje, November 2000.

/3/ A. Šoštarič, SMS - fun or something more?, Teleinfos conference, Ljubljana, May 2001.

/4/ The Demand for Mobile Value-Added Services, Mobile phone penetration, Gartner's report, February 2002.

/5/ Smart Service Mediator (SSM) White Paper, HERMES SoftLab d.d., Maribor, July 2002.

/6/ SMS Server (SSM Enterprise Edition) Administrators Guide, HERMES SoftLab d.d., Maribor, November 2001.

Dr. Andrej Šoštarič, dipl. ing.,
Senior Project Manager and Teaching Assistant at
University of Maribor
HERMES SoftLab d.d., Litijska 51,
1000 Ljubljana, Slovenia

Dr. Bojan Imperl, dipl. ing.,
Project Manager and Assistant Professor at
University of Maribor
HERMES SoftLab d.d., Litijska 51,
1000 Ljubljana, Slovenia

Boro Jerabek, dipl. ing.
Director of R & D Common Services
Gorenje d.d., Partizanska 12, Velenje, Slovenia

Prispelo (Arrived): 25.09.2002 *Sprejeto (Accepted):25.05.2003*

ABS-SENZORJI NA OSNOVI ALNiCO-MAGNETOV

Franc Koplan

Magneti Ljubljana, d.d., Ljubljana, Slovenija

Ključne besede: magneti, trajni magnetni materiali, AlNiCo-magneti, senzorji, sistem ABS (Anti - Lock Braking System), ABS-senzorji, Hall-senzorji, magnetouporovni senzorji, zobnik, merjenje hitrosti vrtenja, magnetni pretok, oprema za kontroliranje in preskušanje

Izvleček: Predstavljamo fizikalne osnove in princip delovanja ABS-sistema, zahteve za vgrajene AlNiCo-magnete, ki so ključni element senzorja. Ilustriramo izdelavo samega ABS-senzorja, najpomembnejše značilne elektromagnetne lastnosti senzorja kot osnovo za nadaljnji razvoj elektronskega krmilnega modula ali alternativnih rešitev ter sprememb samega senzorja. Predstavljena je tudi možnost podjetja, da ponudi proizvode z večjo stopnjo integracije za nove potrebe trga ter izsledke razvojno raziskovalnega dela na področju razvoja opreme za kontroliranje in preskušanje magnetov za potrebe drugih področij raziskovalnega dela, proizvodnje elektronskih komponent ter izdelovanja magnetnih sistemov.

ABS Sensor Applications Based on AlNiCo Magnets

Key words: magnets, permanent magnetic materials, AlNiCo magnets, sensors, Anti - Lock Braking System , ABS sensors, Hall sensors, magnetoresistive sensors, gear wheel, rotational speed measurement, magnetic flux, measuring and control equipment

Abstract: Organization Magneti Ljubljana presented the ABS - sensor application of its main production programme of AlNiCo magnets and its potential for the production of the sensors. The article is intended both to domestic organizations for further joint technological development and to successfull producers, which already produce sensors, and are looking for a reliable and capable partner to supply them with parts with higher degree of integration. The company has over 50 years of tradition, is sucessful in the world market and has the quality management system certified according to most important standards, including the automotive specification ISO / TS 16949. According to its policy the company develops new production programmes, including new materials, magnetic systems and equipment for production and control of magnetic products and similar electronic components for the new demands and expectations of the market.

The key sensors in the automotive applications and a scheme of the brake system of a vehicle are presented. The history, the benefits and the behaviour of the Anti-Lock Braking System are briefly described. The system usually contains 4 sensors and a common electronic unit, that handles the data from the sensors and controls the braking process, which is also appropriately described.

It is emphasized, that organization Magneti Ljubljana produces magnets, which are the key element of the ABS sensors. The company has the basic knowledge for the manufacturing processes of ABS sensors. It has already in 1999 taken part in the tender for the production of sensors for its largest customer.

The physical principles of the operation of the sensor, its construction and the behaviour of the induced voltage is described together with the typical requirements for used AlNiCo magnets. The most important typical electromagnetic properties of the sensor are illustrated and this illustration enables further development of the electronic control unit as well as the development of the alternative solutions or modifications of the sensor itself.

Some more contemporary and cheaper solutions for rotational speed measurements, offering important potential for further development and applications, were also mentioned and briefly described.

Since the magnetic, dimensional and visual properties of the magnets in the sensor are critical, the quality assurance in the company obtains the 0-ppm level by 100% sorting processes. These processes are supported by specially developped electronic measuring systems enabling high productivity. The organization has developed its own high speed magnetizing and demagnetizing equipment, fluxmeters and equipment for visual control including optical measurement of dimensions and geometry. This equipment could be of interest also to organizations, which develop magnetic materials, assemble magnets and produce magnetic systems or other similar electronic components.

1 Uvod

V prispevku želi podjetje Magneti Ljubljana, d.d. /1/ predstaviti uporabo in delovanje AlNiCo-magnetov, vgrajenih v ABS-senzorje, ter svoje možnosti za proizvodnjo tovrstnih senzorjev. Članek je namenjen tako domačim podjetjem za morebiten skupen nadaljnji razvoj in nastop na svetovnem trgu kot tudi podjetjem, ki že proizvajajo senzorje in iščejo zanesljivega in sposobnega partnerja za dobavljanje sestavnih delov z višjo stopnjo integracije. Podjetje ima 50-letno tradicijo, v zadnjem desetletju ima nenehno in relativno visoko stopnjo rasti fizičnega obsega proizvodnje in se ponaša z zavidljivimi poslovnimi uspehi ter certifikati najzahtevnejših sistemov vodenja kakovosti avtomobilske industrije, z ISO / TS 16949 vred. Kupci so renomirani svetovni proizvajalci, predvsem s področja senzorskih aplikacij v avtomobilski industriji, pa tudi električnih merilnih instrumentov, elektromotorjev, tahogeneratorjev itd. Skladno s svojo poslovno politiko podjetje razvija nove programe, kamor spada poleg razvoja materialov in samih magnetov tudi razvoj magnetnih sistemov in procesne proizvodne opreme ter opreme za magnetenje, preskušanje, delno ali popolno razmagnetenje in kalibriranje magnetnih sistemov /5/.

Raznovrstni trajni magneti so v avtomobilski industriji našli številna področja uporabe /4/, razvoj pa se še nadaljuje, še posebej v smeri nenehnega izboljševanja varnosti, za-

nesljivosti, ekonomičnosti in prijaznosti do uporabnika ter okolja. Ključni senzorji /2/ v avtomobilu so povezani s pozicijo (obese, pedal / plin, krmilje), hitrostjo gibanja vozila (ABS), temperaturo (notranja, regulacija klime, armatura, motor, prenos), hitrostjo gibajočih se delov (gredi, prenosi, avtomatska sklopka) , z vibracijami in udarci (motor, varovanje pred požarom). Na sliki 1 so shematsko prikazani sklopi senzorjev v avtomobilu.

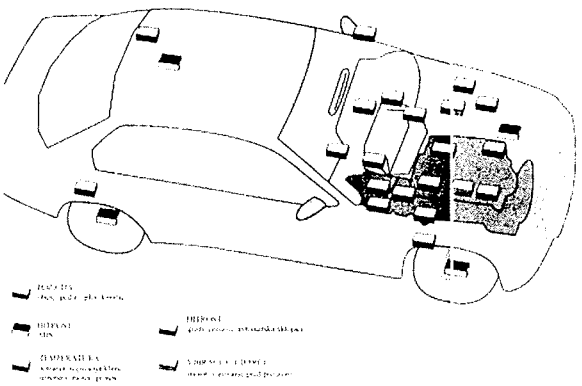

Slika 1: Senzorski sklopi v avtomobilu /2/

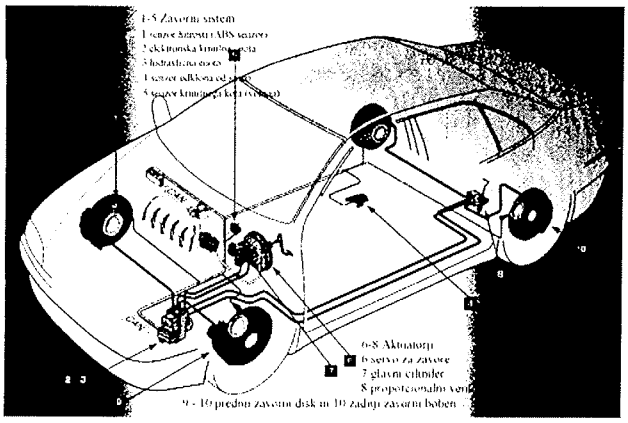

Slika 2: Shema zavornega sistema avtomobila /3/

Na sliki 2 je shematsko prikazan zavorni sistem avtomobila /3/, ki ga sestavljajo: senzor hitrosti vrtenja koles (ABS-senzor), elektronska krmilna enota, hidravlična enota, senzor odklona od smeri, senzor krmilnega kota (volana), aktuatorji in zavorni diski / bobni.

ABS je kratica za Anti - Lock Braking System, to je sistem, ki preprečuje blokiranje vrtenja koles med zaviranjem, s čimer zagotavlja večji zavorni učinek ter lažje vodenje vozila, povečano stabilnost vozila in ohranjanje varnostne razdalje. Navadno sistem sestavljajo skupno 4 senzorji na posameznih kolesih ter skupna elektronska enota, ki signale iz senzorjev obdela in vodi proces zaviranja. Elektronska enota pravilno deluje nad minimalno mejno hitrostjo, pri čemer z moduliranjem pritiska v zavorah, torej z zaviranjem in sproščanjem zavor, regulira zmanjševanje hitrosti vozila na ta način, da se hitrost kolesa obvladovano zmanjšuje, kolo pa se pri tem ne sme popolnoma zaustaviti, dokler je hitrost večja od mejne. V večini primerov se na ta način zagotovi najkrajša možna zavorna pot. Sistem ABS je bil razvit že leta 1930 za letala ter patentiran tudi za avtomobile. Zaradi izboljšanega vidika varnosti je pričel doživljati širšo uporabo v obdobju od 1975 do 1979, ko je bil v Združenih državah Amerike uveden v tovorna vozila. Leta 1980 so ga pričeli avtomobilski proizvajalci vgrajevati v osebna vozila, najprej v višji cenovni razred, z nadaljnjim razvojem in nižanjem stroškov pa je hitro našel svoje mesto tudi v avtomobilih nižjega cenovnega razreda.

ABS-sistem s 4 senzorji deluje na naslednji način:

- Ko elektronski modul na osnovi signala iz senzorja prepozna, da bo kolo blokiralo, s tuljavo zapre ventil, ki je navadno odprt, ter s tem prepreči nadaljnje dovajanje hidravlične tekočine in nadaljnje zaviranje kolesa.
- Elektronski modul nadaljuje opazovanje signala iz senzorja iz tega kolesa.
- Če se kolo ustavlja hitreje kot druga tri kolesa, odpre tuljavo ventila. Ujeta tlačna razlika se izravna v rezervoarju glavnega cilindra.
- Ko kolo znova dobi hitrost, modul vrne tuljavo v normalno stanje, ki omogoča dotok tekočine.

Podjetje Magneti Ljubljana, d.d. izdeluje AlNiCo-magnete, ki so bistveni del ABS-senzorja, zato bo v nadaljevanju predstavljen samo tovrstni senzor, razpolaga pa tudi s ključnim znanjem za proizvajanje samih senzorjev. Tako je podjetje v letu 1999 že konkuriralo za kooperacijsko proizvodnjo nekaterih tipov senzorjev za svojega največjega kupca magnetov.

2 Senzor ABS z AlNiCo-magnetom

2.1 Fizikalni princip delovanja

Dajalni sistem sestavljata zobnik iz mehkomagnetnega materiala, ki se vrti skupaj s kolesom, in sam senzor, kjer se zaradi vrtenja zobnika spreminja magnetni pretok, kar ima za posledico inducirano napetost. V nadaljevanju bodo predstavljeni časovni poteki inducirane napetosti na senzorju, posneti pri laboratorijski postavitvi merilnega sistema, prikazani na sliki 3.

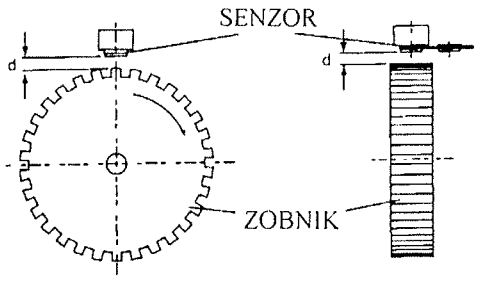

Slika 3: Lega senzorja glede na zobnik /6/

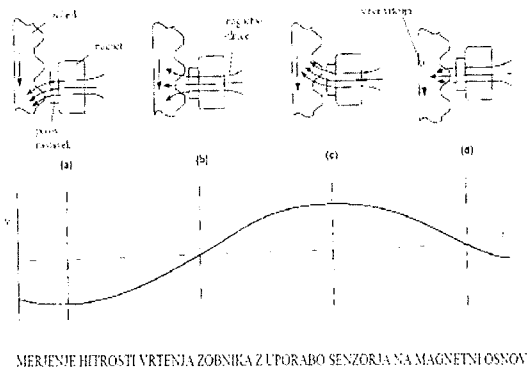

Slika 4: Spreminjanje magnetnega pretoka zaradi vrtenja zobnika ter potek inducirane napetosti /6/

2.2 Izdelava senzorja

Senzor sestavljajo:

- magnet
- polov nastavek
- spojni del za pritrditev polovega nastavka na magnet
- tuljavnik s kontakti
- tuljava
- priključni kabel z nosilcem, tesnili in mehansko zaščito.

Ključni del senzorja je AlNiCo-magnet valjaste oblike, ki je generator magnetnega polja. Po potrebi je ta magnet lahko tudi profilno brušen.

Na sliki 5 je prikazan značilni magnet pred vgradnjo v senzor, na slikah 6 - 8 pa izdelan, nezalit senzor brez kabelskih povezav za priključitev na elektronsko enoto.

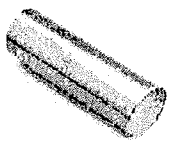

Slika 5: Liti AlNiCo-magnet za ABS-senzor

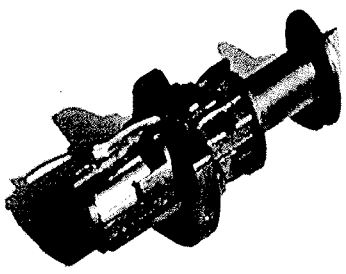

Slika 6: Zabrizgan magnet s polovim nastavkom in kontakti za priključitev na kabel

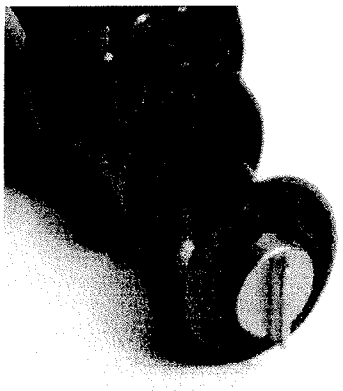

Slika 7: Polov nastavek za koncentracijo silnic

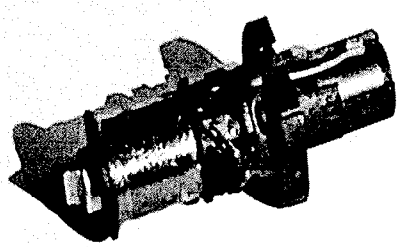

Slika 8: Izdelan, nezalit senzor s tuljavo

Značilni podatki za magnete so podani v tabeli 1. Navadno je uporabljen liti material, ki daje pri enakem volumnu nekoliko boljše magnetne lastnosti, in razmerje med premerom in dolžino 1:3, kar postavi delovno točko magneta nekoliko nad področje maksimalnega energijskega produkta.

Tabela 1: Najpomembnejše karakteristike AlNiCo-magneta

Karakteristika	Značilna vrednost
Premer valja	od 4 do 10 mm
Dolžina valja	od 15 do 40 mm
Remanenca Br - minimalno	od 1100 do 1250 mT
Koercitivnost $_BH_c$	od 45 do 60 kA/m
Maksimalni energijski produkt BH_{max}	od 32 do 40 kJ/m^3

Ker so magnetne lastnosti za pravilno delovanje senzorja kritične, v podjetju zagotavljamo zanje nivo 0 ppm s 100-odstotnim kontroliranjem in preskušanjem. Z ozirom na funkcijo ter način vgradnje so za magnet postavljene relativno visoke zahteve glede toleranc dimenzij in druge geometrije, videza, t.j. okrušitev in livarskih napak, pa tudi nivoja razmagnetenja. Za izpolnjevanje teh zahtev je bilo tre-

ba razviti visokoproduktivne elektronske merilne sisteme za magnetenje, merjenje magnetnega fluksa, razmagnetenje, vizualno kontrolo ter nekontaktno kontrolo dimenzij in geometrije. Ta oprema je zanimiva tudi za organizacije, ki se ukvarjajo z razvojem magnetnih materialov, vgradnjo magnetov in izdelavo magnetnih sistemov ter podobnih elektronskih komponent in je bila razvita v okviru lastnega razvoja procesne ter merilne opreme oziroma v okvirih projektov izboljšav v tehnoloških procesih v sodelovanju z Ministrstvom za gospodarstvo /5/. Na sliki 9 je prikazan del naprave za elektromagnetno preskušanje magnetov za ABS-senzorje.

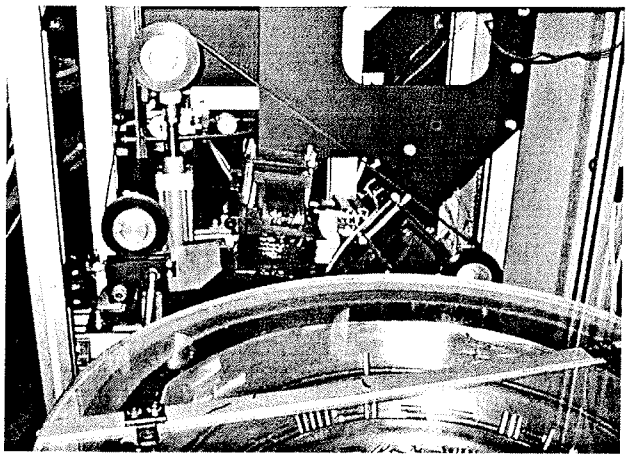

Slika 9: Naprava za EM-preskušanje magnetov za ABS-senzorje

Magnet mora biti čim bolj tesno povezan s polovim nastavkom iz mehkega železa, ki koncentrira silnice in s tem omogoča bolj izrazito spreminjanje magnetnega fluksa glede na razdaljo med vrhom polovega nastavka ter zobnikom.

Konstrukcija in izdelava tuljave je tehnološko zahtevna in se izvaja po posebnem programu navijanja.

Značilne karakteristike tuljave in izhodni signal senzorja so podane v tabeli 2:

TABELA 2	
Karakteristika	Tipične vrednosti
Upornost	od 0,5 do 2 kΩ
Induktivnost (1 kHz)	od 500 do 1200 mH
U, inducirana (tip. 400 r/min, reža 0,8 mm)	od 0,5 do 4,5 V

Glede na izhodno napetost imajo nekateri tipi senzorjev integrirane elektronske elemente za obdelavo inducirane napetosti, kar omogoča miniaturizacijo ter nižje skupne stroške izdelave senzorja, predvsem na račun cene vgrajenih magnetov.

V laboratoriju smo izvedli simulacijo delovanja senzorja (915 r/min, 70 zob) in posneli časovni potek inducirane napetosti ob prehodnem pojavu trenutne zaustavitve zobnika (slika 10).

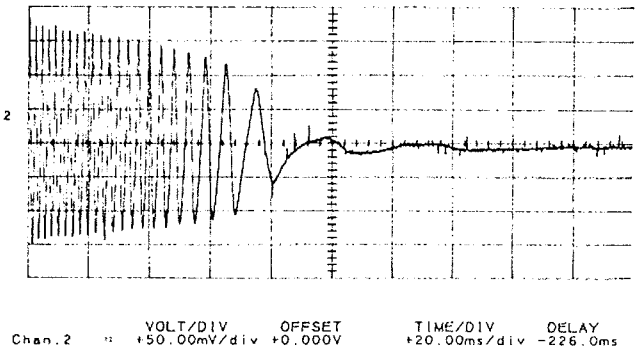

Slika 10:Prehodni pojav ob zaustavitvi zobnika

3 Sodobni načini merjenja hitrosti vrtenja na osnovi integriranih vezij oz. senzorjev

V zadnjem obdobju se v nižjem cenovnem razredu vse bolj uveljavljajo cenejše rešitve, temelječe predvsem na integriranih elektronskih elementih - Hallovih ter magnetouporovnih senzorjih /6/. Tu lahko še vedno ostane pasivni dajalnik - mehkomagnetni zobnik (slika 11) ali pa zobnik nadomestimo z multipolno namagnetenim plastomagnetnim aktivnim dajalnikom (slika 12).

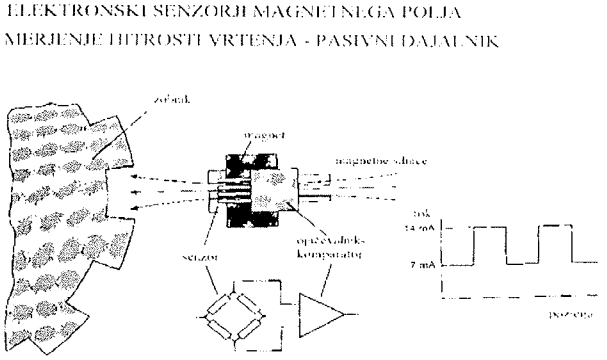

Slika 11:Sodobno merjenje hitrosti vrtenja s pasivnim dajalnikom in integriranim vezjem oz. magnetouporovnim senzorjem /6/

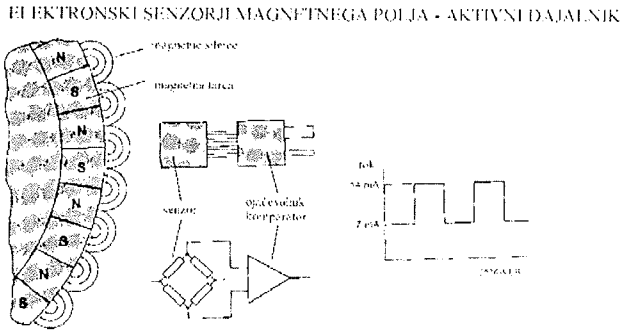

Slika 12:Sodobno merjenje hitrosti vrtenja z aktivnim dajalnikom in integriranim vezjem oz. magnetouporovnim senzorjem /6/

Predvidevamo, da ti novi proizvodi doslej uveljavljenih senzorjev z AlNiCo-magneti tudi v naslednjem srednjeročnem obdobju večinoma še ne bodo nadomestili, zato vidimo v programu izdelave ABS-senzorjev z AlNiCo-magneti novo priložnost za uspeh. Kupci namreč pri sebi instalirajo proizvode, temelječe na novih materialih, zmanjšujejo število svojih dobaviteljev oziroma celo prenašajo dele svojih proizvodnih programov k svojim ključnim dobaviteljem, da od njih prejmejo izdelke z višjo stopnjo integracije.

4 Sklep

Predstavljena je bila fizikalna osnova delovanja, izgradnja senzorja na osnovi paličastih AlNiCo- magnetov, značilne vrednosti njegovih najpomembnejših karakteristik za morebitno izdelavo elektronskega krmilnega modula ali alternativnih rešitev samega senzorja in možnost podjetja Magneti Ljubljana, d.d., da ponudi trgu proizvod z večjo stopnjo integracije ter si tako še naprej zagotovi poslovni uspeh na trgu.

5 Literatura

/1./ Magneti Ljubljana, d.d., The world - wide supplier of permanent metallic magnets [elektronski vir]. Magneti Ljubljana, 2002 [citirano 28. maj 2002; 12:00:00]. Dostopno na URL-naslovu: www.magneti.si

/2. / L' Electricfil Industrie: Sensors to meet the challenges of productivity, Beynost, 1997

/3. / Bosch: Bosch braking systems, Tokyo, 2000

/4. / S. Kobe, P. McGuiness: Application of permanent magnet materials, SLO-GER Meeting, Bled, 1998

/5. / F. Koplan: Računalniška podpora elektromagnetnemu preskušanju in vizualnemu sortiranju elektronskih komponent, Ljubljana, 2001

/6. / Philips Semiconductors: Data sheet - General rotational speed measurement, 1998

Franc Koplan, univ. dipl. inž. fizike in elektrotehnike
Magneti Ljubljana, d.d.
Stegne 37, SI-1000 Ljubljana, SLOVENIJA
tel. 386 (0)1 507 47 11
faks. 386 (0)1 511 12 95
e-pošta: f.koplan.svk@magneti.si

Prispelo (Arrived): 06.06.2002 *Sprejeto (Accepted): 25.05.2003*

A 12-BIT FLASH ADC

Anton Pleteršek

University of Ljubljana, Faculty of Electrical Engineering, Slovenia

Key words: digital-to-analog, converter, precision, accuracy, INL, DNL, linearity

Abstract: A 12 bit, single step flash digital-to-analog converter (DAC) in 0.6um CMOS was realized on 1.5mm2 silicon area and has power consumption of 0.5mW at 5V supply. Converter architecture based on resistor-string having 2**N resistor taps and layout-efficient coding scheme. The system features a precision, fast settling, offset canceling operational amplifier and has 0.002% linearity. The conversion time is 4us.

12-bitni bliskovni DAC

Ključne besede: digitalno-analogni, pretvornik, precizija, točnost, integralna nelinearnost, diferencialna nelinearnost

Izvleček: Bliskovni digitalno-analogni pretvornik, izdelan v standardni 0.6um tehnologiji CMOS na površini silicija1.5mm2 , ima minimalno porabo 0.5mW. Arhitekturo pretvornika sestavlja uporovna veriga z napetostnimi odcepi in CMOS stikali, ki so krmiljena na način, ki optimizira porabo silicija. Doseženo linearnost pretvornika (0.002%) zagotavlja ustrezno povprečenje, ki minimizira gradient spreminjanja upornosti polisilicija po silicijevi rezini. Z ustrezno optimizacijo internih zaklasnitev je dosežena hitrost pretvorbe 4us.

I. Introduction

The paper will discuss the digital-to-analog converter having the fast conversion time of 4μs at worst-case process. Concept based on resistors matching which guarantee the linearity of monolithic DAC to be in the 9 to 10 bit range. Performances can be extended to more then 12 bits, using so called layout averaging technique, which includes proper interleaving of passive components. Technique will be described in detail later in this paper. The result of such a technique is desensitizing the DAC to doping, thermal and misalignment gradients.

In present paper we will describe the layout efficient architecture of the 12 bit flash DAC with proposed algorithm to extend linearity to 0.003%. We will discuss the basic flash system, followed by section with detail description of the DAC converter blocks, DAC converter operational amplifier and the concept for offset compensation. The layout averaging and gradient-over-silicon analysis using Matlab and in final section the measurement and performances will be presented.

II. Basic Flash DAC

A single step flash DAC converter , based on resistive chain and digitally controlled switches are shown from Fig. 1. The input digital code is converted to switch-control signals. Only one switch is close at a time. Resistor-chain is supplied from constant, temperature and supply stable reference voltage. Ideally, here are only two current contacts - on bottom and on top of the chain where the voltage reference is connected. There are 2**N taps which are voltage contacts to switches and no current flows through them. The large number of switches with their parasitic capacitance loaded the sensitive - internal analog line. The resistance of the chain, the parasitic capacitance, switch resistance and internal - analog line (IVA) parasitic have influence on converter settling performances and therefore conversion time.

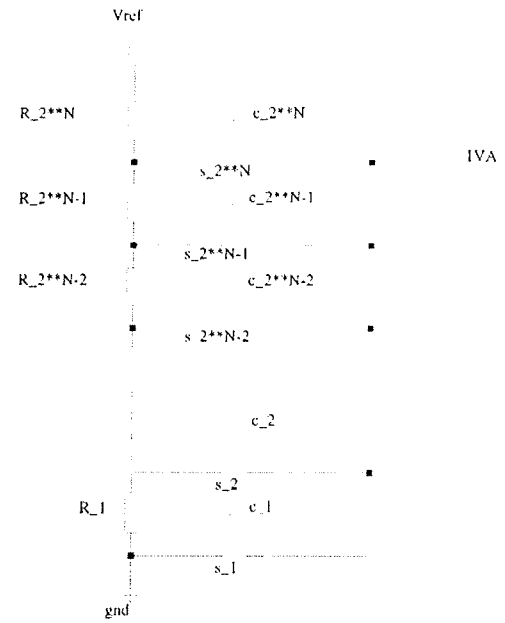

Fig. 1 DAC12 basic architecture.

It is therefore important to make the resistance small enough to speed up the conversion. Lower chain resistivity requires larger driving capability of the voltage reference. The optimum exists between switch resistance, chain resistance and capacitance. To reduce the number of switches, connected to the IVA, the so called tree-decoding scheme might be a solution. As we will show later in this paper,

the good compromise can be found between layout density and the settling performances. Using additional resistive parallelism, the equalizing of the settling performances over full scale can be achieved.

III. Circuit Realization

A. Layout efficient decoding

The principle is shown from Fig. 2. The 12 input NOR gate is realized by 12 N-channel devices in serial. The P-channel devices are omitted, the single PMOS current generator is used instead. There are 2**N current generators in the circuit, only one delivers current into system at a time. Overall required bias current is therefore single generator current which is in the range of 5uA for 12 bits converter. The complete decoding is optimized to fast controlled of the switch having on IAL side the capacitive loading, including the operational amplifier input capacitance.

The layout concept including four-bit intersection is in Fig. 2. Twenty metal lines (double metal process) passes the N-channel area. One kilo-bit block is organized as binary coded area from 1, 2, 4, and 8 bits sub-blocks inserted into 9-bit converter. Last - 10-th bit select between the two 9-bit converters. To get 12-bit converter, four such a 10-th stages are organized in proper way. Voltage reference was chosen to be 4.1V at 4.5V minimum supply. To minimize the parasitic, the switches are realized from negative reference side to be NMOS only, around mid-area switches are T-gates and on positive-reference side, switches are again single channel-PMOS only.

B. Interleaving and layout averaging

The principle of operation of presented DAC guarantee the monotonisity and therefore the analog output always increasing with increasing of the digital code. No matter how large is poly1 resistivity gradient, It will mainly influence on integral non-linearity (INL) and can be expressed as a difference between actual analog value (Vana_i) and ideal one (Vana_ideal) on internal analog bus (IVA - Fig. 1) and is equal to:

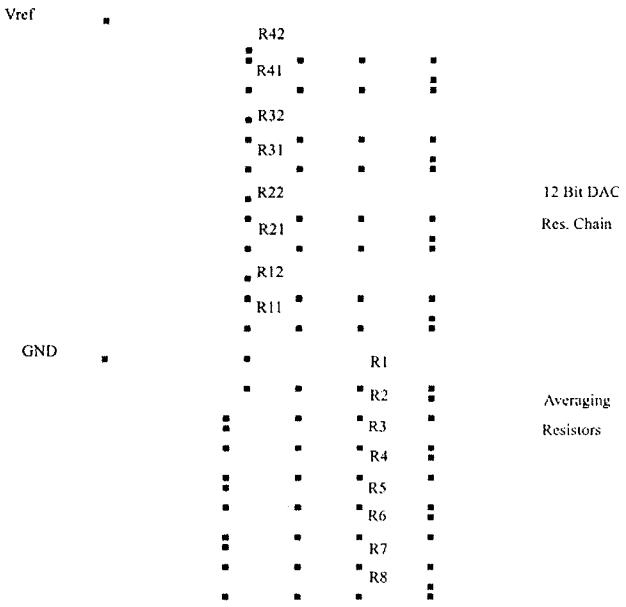

Fig. 3. Layout averaging. Dark dots represent the current-poly1-metal1 contacts. This scheme corresponds to "lay2" curves on MatLab analysis figures.

$$INL = V_{ANA\_i} - V_{ANA\_ideal} = \frac{V_{ref}}{2^N} \cdot \sum_{k=1}^{i} \frac{dR_k}{R}$$

R is resistor-unit (ideal), dRk is difference from unit value,

If we assume that all mismatch terms are zero over resistors chain, then the worst-case error will occur at the middle of the chain:

$$i = 2^{N-1}$$

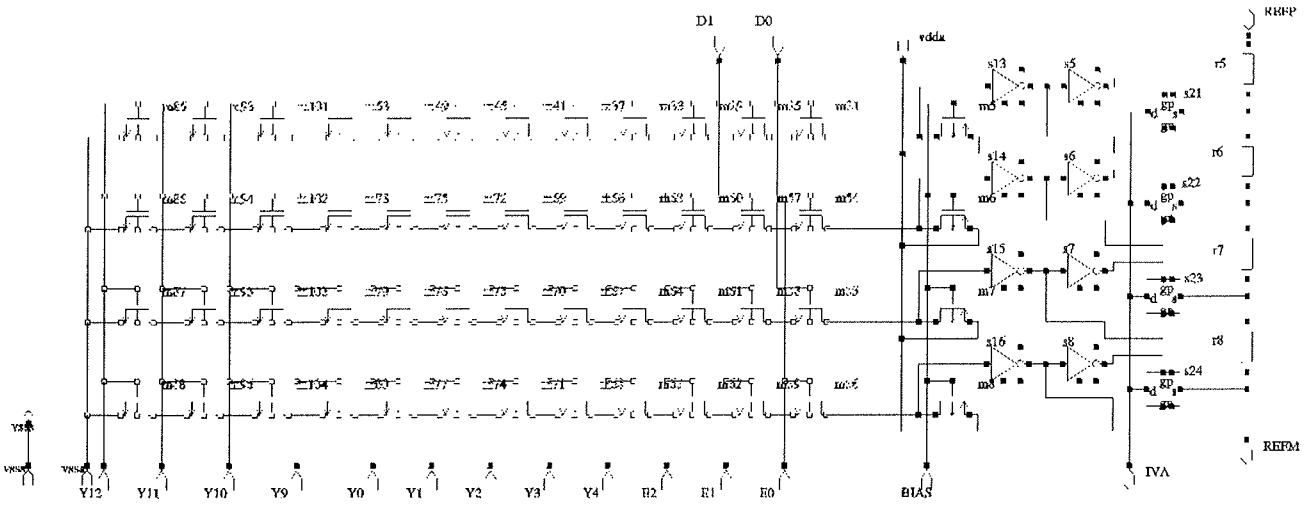

Fig. 2: Four - bit segment from 12 bit DAC

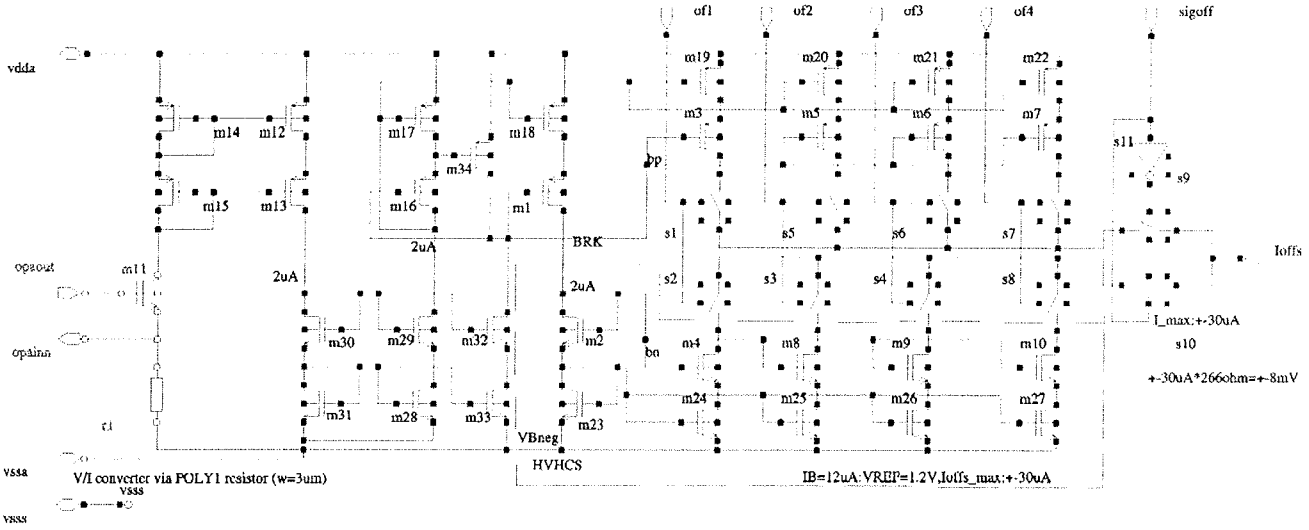

Fig. 4: Stable current generator for offset calibration. Binary weighted source and sink currents are generated from stable bandgap reference voltage.

And the maximum value of INL is:

$$INL_{\max} = \frac{V_{ref}}{2} \cdot \left[\frac{dR_k}{R}\right]_{\max}$$

It is evident that there is also an amplifier offset voltage contribution to INL. It contributes directly to INL. For high precision conversion, offset cancellation is a must (Fig. 4, Fig.5 and Fig. 6).

Maximum negative mismatch dominates at all the resistors in the lower half of the chain and the maximum positive mismatch occurs in the upper half of the chain or vice-versa, depends on resistivity gradient. Fig. 8 shows the INL error over all 12 bit on digital input.

Layout averaging principle uses additional parallel resistors to each sub-block of the DAC (Fig.3). The number of sub-blocks and the appropriate number of additional resistors define the possible layout mirroring and scrambling combinations. The different types of mismatches may occur randomly in X and Y direction on silicon. The sub-blocks mirroring and scrambling are therefore required in all directions (Fig. 8, Fig. 9, and Fig. 10). The number of sub-blocks is limited by the connectivity between sub-blocks and between the averaging resistors. The poly1-to-metal contact resistivity may vary from 2 Ohm to 20 Ohm, which could be more the one LSB unit resistor. Serial connections are required (metal1 and metal2), but they need to be done in proper way (temperature coefficient of Al metal resistivity). These contacts conduct the all-resistors main-chain current and may cause the majority of INL and DNL error.

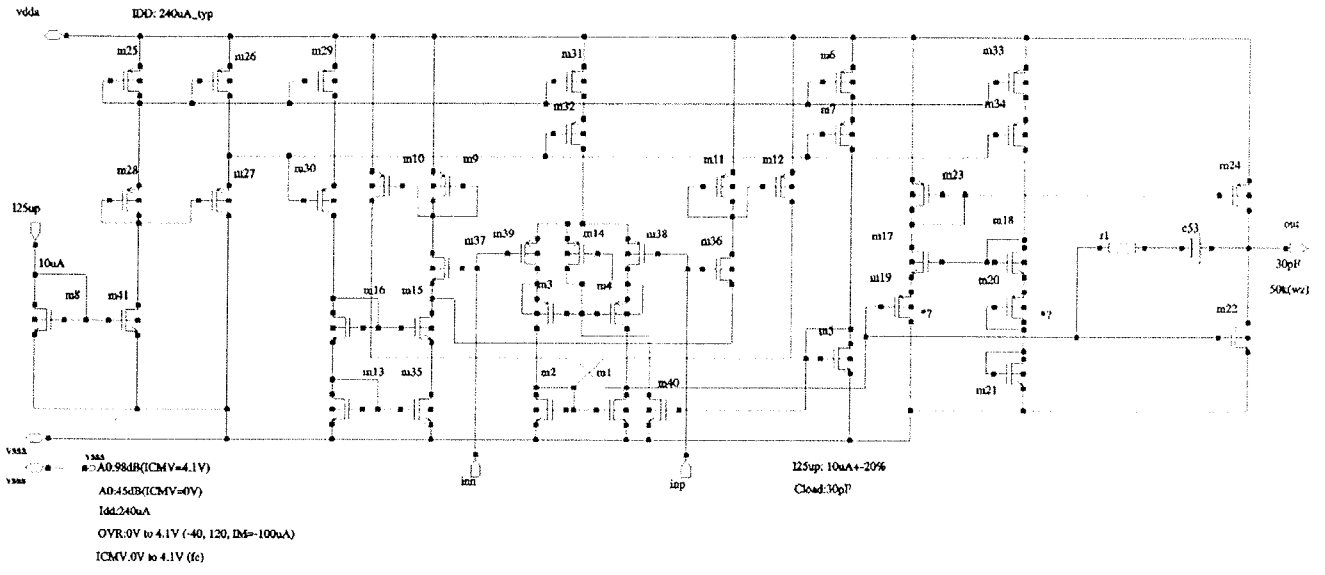

Fig. 5: High gain class AB amplifier having input voltage range from negative rail to 300mV from positive rail.

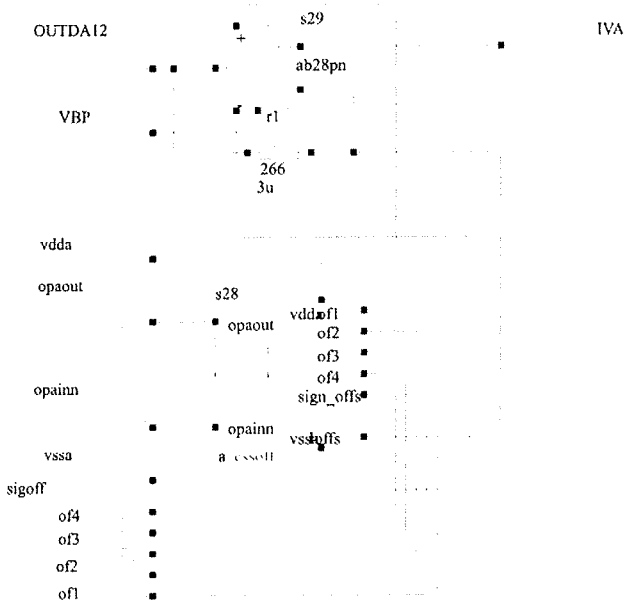

Fig. 6: Amplification of internally generated analog voltage Viva and offset correction circuitry.

Next important layout constraint is mismatch minimization. The resistor-unit value and its width on layout influence on analog output delay and on mismatch between units. Huge mismatch occurs when equal units have different neighbors.

IV. Conclusion

The required matching of resistors in chain using so called end-point analysis is relatively high and is derived from INL expression:

$$INL < 0.5LSB..... \frac{1}{2^N} [\%matching]$$

N is converter precision. The 12 bit DAC require 0.025% resistors matching which is theoretical and practical possible limit when all available techniques are implemented. That means the layout is very critical part of the analog circuit design. Again, theoretically is possible to realize the active element matching. As a result, the mismatch and drift occur and the conversion accuracy may again be much lower then is converter precision. Our first measurements using code density principle and end-point approach without layout averaging give an encouraging result for INL, which was within +-2LSB at more then 50% samples. Layout averaging may improve the result for more then +-1.5LSB as is shown from Fig. 8 to Fig. 10. Much better result gives so called "best-fit" approach. Nevertheless, the proposed layout averaging, as is shown from Fig. 3 for 12 bit flash DA converter, is a challenge for designers to improve the result where fast conversion is of the most importance in integrated system on silicon. The principle itself guaranty the DNL performance to be much better then +-0.5LSB.

The layout - four bit intersection is shown from Fig. 7.

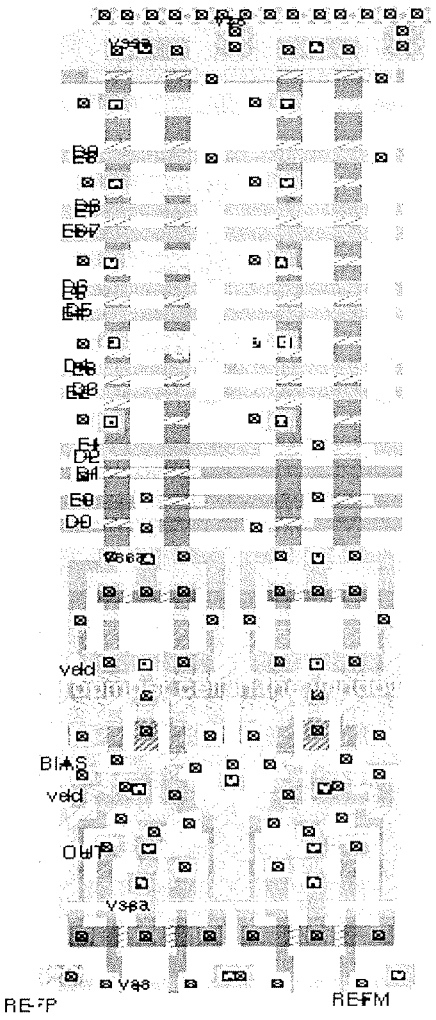

Fig. 7: Four - bit segment from the layout, as is shown from schematic in Fig. 2.

There are a number of different possible approaches like dual-ramp DAC /1/, where the accuracy depends on current generation accuracy, comparators offset and on clock frequency stability. Encouraging approach is a self-calibration method /2/, but it requires a long calibration period. It is clear that all improvements are possible mainly when using scaled down technologies which allows operation at much higher clock frequencies. Both principles may give conversion time better then 10us.

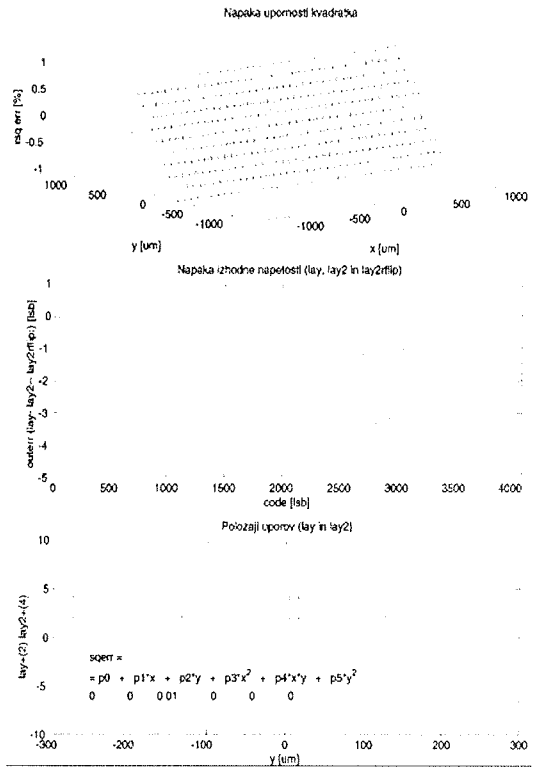

Fig. 8: Three curves are as follows: -4LSB maximum INL at the middle of the string, mirroring-parallelism - -1.5LSB and layout averaging 8:4 give accuracy of 1LSB. Gradient in Y direction is (0.5K-code-direction).

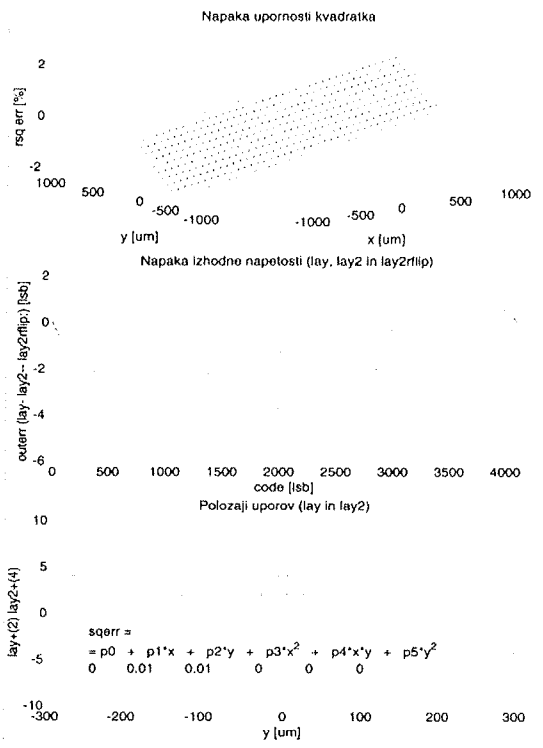

Fig. 9: Linear gradient in X/Y direction gives four max. and four minimums. They correspond to the number of segments that alternate in direction X.

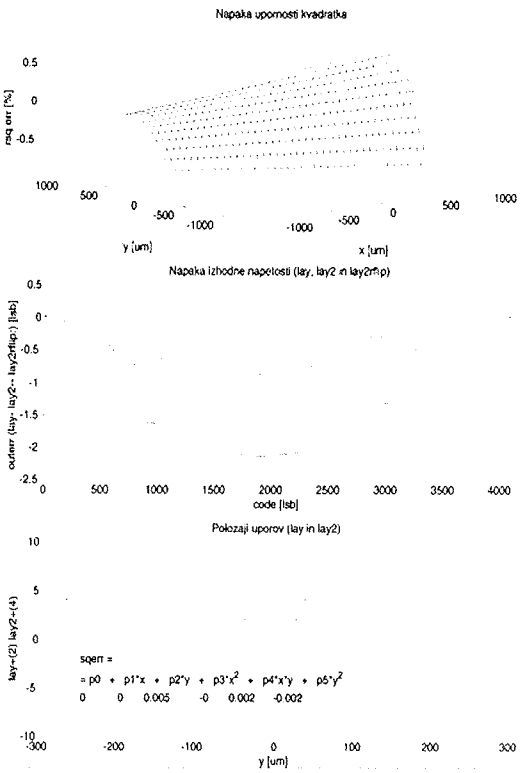

Fig. 10: Random mismatch and random weighting as is shown on first and last canvas. In X direction are resistors string of 0.5k codes, in Y direction are 8 times 0,5k codes and parallel string.

Acknowledgment

Author would like to thanks to Roman Benkovič for useful discussion and for mismatch analysis in MatLab.

This work was done in association with AMS AG, as a part of the complex analog-digital ASIC.

References

[1/ William D. Mack, M. Horowitz, R.A. Blauschild, "A 14 Bit Dual-Ramp DAC for Digital-Audio Systems", IEEE Journal of Solid-State Circuit, Vol. SC-17, No.6, Dec.1982, pp 1118-1126.

/2/ D.W.J. Groeneveld, H.J. Schouwenaars, H.A.H.Termeer, C.A.A.Bastiaansen, "A Self-Calibration Technique for Monolithic High-Resolution D/A Converters", IEEE, Journal of Solid-State Circuit, VOL. 24, No.6, Dec. 1989, pp1517-1522.

Anton Pleteršek
Faculty of Electrical Engineering,
Tržaška 25, 1000 Ljubljana, Slovenia
e-mail:anton@kalvarija.fe.uni-lj.si

Prispelo (Arrived): 06.06.2002 Sprejeto (Accepted): 25.05.2003

AUTOMATIC GAIN ADJUSTMENT IN CONTACTLESS COMMUNICATION SYSTEMS

V. Kunc, M. Atanasijević Kunc

Faculty of Electrical Engineering, University of Ljubljana, Ljubljana, Slovenia

Key words: automatic gain control

Abstract: Systems for contactless short range communications are more and more frequently used for different applications like access control, inventory and ticketing. Such systems comprise a RF transmitter emitting magnetic (electromagnetic) field and one or more transponders, which are supplied by the RF field. The transponder modulates the RF field to send information to the transmitter, which also comprises a reader system. The data transfer can be unidirectional (from transponder to reader) or bi-directional.

The receiver system in the transmitter senses the modulation of RF field caused by transponder(s) on the transmitter antenna. Since the distance from transmitter antenna to transponder can vary from practically zero to the maximum operation range, the dynamic range of receive signals is very high. The gain of receive channel must be high to successfully detect the small receive signal but high gain can cause problems in case of large input signals. The solutions to the problem are the clipping of the input signal or automatic gain control or receive channel. The proposed solution describes an automatic gain control, which is specially adapted for RFID applications, as it successfully exploits the special nature of signals in such systems.

Avtomatsko nastavljanje ojačenja v brezkontaktnih komunikacijskih sistemih

Ključne besede: avtomatska nastavitev ojačenja

Izvleček: Sistemi za brezkontakno komunikacijo skokovito pridobivajo na pomenu, saj njihova uporaba nezadržno narašča. Takšen sistem sestavlja oddajnik RF moči, ki oddaja elektromagnetno polje in eden ali več odzivnikov ki to polje uporabljajo za vir energije in preko modulacije RF polja pošiljajo podatke oddajniku. Pretok podatkov je lahko enosmeren, samo od odzivnika do oddajnika, ali pa v obe smeri.

Za sprejem podatkov od odzivnikov vsebuje oddajnik RF moči tudi sprejemni kanal. Sprejemnik opazuje signal na oddajni anteni in ojači vsako spremembo nivoja oddajnega signala. Na ta način sprejemnik zazna modulacije RF polja s strani odzivnikov. Ker je razdalja med sprejemnikom in odzivnikom lahko zelo različna, od praktično nič pa do maksimalne razdalje, ki še omogoča komunikacijo, je razpon možnih nivojev sprejemnega signala zelo velik. Ker seveda želimo zanesljivo sprejemati tudi najmanjše vhodne signale, ima spremna stopnja veliko ojačenje, kar lahko povzroči probleme pri visokih nivojih vhodnih signalov. Da bi preprečil napačno delovanje v takšnih primerih imamo na razpolago dve možni rešitvi. To je omejevalnik signala ali pa avtomatsko prilagoditev ojačenja nivoju vhodnega signala. Članek opisuje posebno izvedbo sistema za avtomatsko nastavitev ojačenja, ki je prilagojena za sprejemnike signala brezkontaktnih odzivnikov in uspešno izkorišča posebnosti signalov v teh sistemih.

1. Introduction

When designing an RFID receiver a maximum communication range is always one of major design goals. This implies that the receive gain is set as high as possible considering the input noise level. The result is that in case the transponder is close to reader antenna and the input signal level is much higher than the minimum one, the signal at the end stages of receive channel exceeds the liner region of amplifier stage thus causing problems in data communication. Two possible solutions for this problem exist.

The simplest possible solution is signal clamping. When the predefined level of the signal amplitude is reached the gain of the gain stage is decreased so that the amplitude can not increase further. This of cause causes signal distortion but since we are usually only interested in receiving digital data the distortion can be tolerated. A bigger disadvantage of clamping system becomes evident in case of communication where a significant level of disturbance signal is added to the communication signal. The disturbance signals usually do not exceed the signal clipping level so they appear at the end of receive gain chain amplified with full gain of receive channel. On the other hand the communication signals are usually higher than the clipping level so their amplitude is amplified with smaller gain. The obvious result is that the ratio of communication signal to disturbance signal can significantly degrade at the end of receive gain chain compared to the input. The communication signal recognition is aggravated or in worst case becomes impossible.

The second possibility is automatic gain adjustment of the receive channel where the receive gain is decreased in case of higher input signal levels. The gain than is the same for communication signal as well as for any possible disturbance signals resulting in no decrease of signal to disturbance ratio.

2. AGC system design

Automatic gain control (AGC) circuits are well established in telecommunication and audio systems. The basic design problem in AGC design is the impact of gain change on

the input signal. The input signal degradation due to AGC action must be kept at minimum and all important signal parameters (information content) should not be affected. To achieve this the nature of the input signal must be carefully studied and the AGC system designed for the particular input signals. The most important parameters are the gain change decision algorithm and the speed at which the gain is decreased and increased.

The classical AGC solution comprises compactors which determine if the signal amplitude at given gain stage is lower or higher than the predefined level for AGC action. If that level is exceeded the AGC reacts by rapid gain decrease. This mode of operation is called attack mode and the speed of gain decrease attack speed. The AGC system remains in this attack mode till the gain decrease results in signal amplitude below the AGC threshold level. At that point the AGC system enters second mode called decay mode. During decay the gain starts increasing back towards it original (high) level. In case the signal amplitude again exceeds AGC threshold level as a result of decay action or input signal increase the AGC systems returns to attack mode. At constant signal level the AGC system constantly switches between attack and decay mode so the decay speed must be orders of magnitude lower than attack speed to minimise the impact of mode switching on the input signal. The AGC system action is finally finished when the input signal is low enough that the decay action restores the default high gain and the AGC system is deactivated.

Our design solution of AGC system differs from above described classical one as it was designed for specific type of input signals existing in RFID communication. The protocol of RFID communication starts with the command sent from the reader to the transponder. The transponder reacts on the command and sends required data to the reader. The actual data is usually preceded by a preamble to prepare the reader for receiving the data. The coding format of the data is known so the AGC system has the information of the minimum and maximum possible time between two pulses. It is also reasonable to assume that the transponder is not able to change position in the RF field in the timeframe of data transfer so the same signal amplitude inside one data package can be expected. But immediately after the end of data transfer from one transponder a communication with different transponder, having completely different position in RF field and therefore different signal amplitude can start.

It is evident that the AGC system for such signals must have a fast attack speed to set the gain correctly well inside the preamble before the actual data receive starts. The second imperative is that also decay speed must be relatively high since the reader must be prepared to receive new data at completely different signal level in a short time after the first data transfer is finished.

To satisfy these requirements we devised an AGC system, which has three modes of operation instead of two as in classical solution. These modes are attack, decay and idle mode. The attack mode is started when the signal amplitude at the output of gain stage exceeds the defined threshold level. A rapid gain decrease is triggered and the signal amplitude is reduced below the threshold level. The conditions for attack mode are not preset anymore but the system does not enter usual decay mode. Instead the system waits in idle mode till conditions for decay or new attack are fulfilled. In idle mode the gain is not changing and is kept at the level defined by previous attack mode. The transition from idle mode to decay mode occurs if there are no incoming signals for a certain amount of time. The detection of data is performed using second comparator which has threshold level far below the AGC attack level (approximately one half of attack level) but still well above expected noise level. During data transfer package input pulses are always above idle mode comparator level. When the data transfer is finished these pulses stop and the idle mode comparator is not producing output pulses. If this condition persist longer than twice the maximum time space between two pulses as defined by data coding protocol the AGC system changes state from idle to decay. The decay is fast since the reader must be prepared for new data package from another transponder in relatively short time. The AGC action is finished when the gain is increased back to the default value.

The typical data receiving sequence using such AGC system starts with the preamble send by the tag. During preamble the receive channel evaluates if the signal is too high and reduces the gain accordingly by setting the AGC system to attack mode. Well before the preamble transmission from transponder is finished is the receive channel AGC system already in idle mode. It stays in idle mode all through data transfer since input signal above idle mode threshold is always present. After the data transmission is finished the AGC stays in idle mode for a defined time and changes state to fast decay mode. A case of short data transfer from three different transponders having different signal levels is presented on fig. 1.

In the upper canvas the output signal of the receive gain stage is shown. The receiving signal from the first transponder (shown in second canvas) was higher than the ACG limit presented as two straight lines on the same canvas. The attack mode is triggered. The flag presenting the attack mode is shown in canvas four. The attack is repeated every time the output signal exceeds the upper or lower limit. After two periods of incoming signal the gain is adjusted and the AGC system enters idle mode. Following pulses are received correctly with the gain set during attack time. The correctly received digitised signal is presented on the lowest canvas. After the receive signal stops the AGC system remains in idle for a time longer than two maximum receive signals periods. This is followed by a fast decay mode (the decay mode flag is presented on canvas three). Two more signal packages follow. The second one has higher amplitude than the first one so the AGC system must reduce the gain practically to the lowest possible. After the end of receive signal package another fast decay

cycle follows. The receive system is again ready for new receive signal package (third one) which has a low signal amplitude so no AGC action is needed.

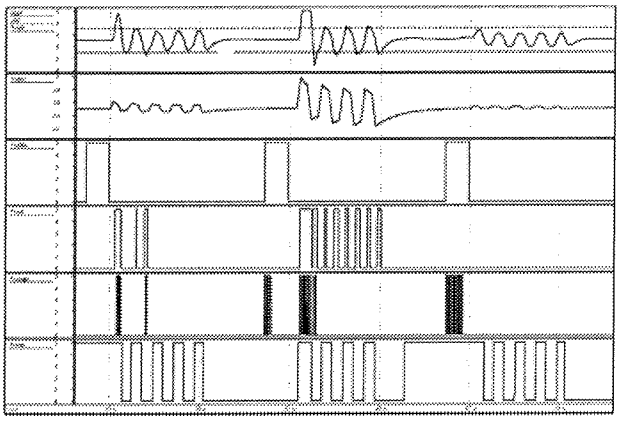

Canvas 1: Analog output signal after the AGC gain stage

Canvas 2: Analog input signal

Canvas 3: Fast decay mode flag

Canvas 4: Attack mode flag

Canvas 5: Clock signal for gain change counters (active during attack and decay)

Canvas 6: Digitised receive signal

3. Conclusion

The AGC system for contactless data communication system using RF powered transponders was designed based on the idea that only through a throughout knowledge of the nature of receive signal an optimum automatic gain control can be devised. The resulting system is perfectly suited for the task since it performs necessary gain adjustment only during the preamble of the incoming data package while there is absolutely no gain change during the actual data transfer. It also allows extremely fast gain recovery after the end of data transmission. All this ensures a reliable data receive in complete incoming signal amplitude range.

V.Kunc, M.Atanasijević Kunc
Faculty of Electrical Engineering
Tržaška 25, 1000 Ljubljana, Slovenia
E-mail: vinko@kalvarija.fe.uni-lj.si

Prispelo (Arrived): 06.06.2002 Sprejeto (Accepted): 25.05.2003

MICROSYSTEM FOR ELECTRICAL CURRENT SENSING

Albin Pevec, Janez Trontelj

University of Ljubljana, Faculty of Electrical Engineering, Ljubljana, Slovenia

Key words: integrated sensors, Hall sensors, current measurement, microsystems

Abstract: In this paper a method for measuring electrical currents with a magnetic microsystem is presented. With the use of two coils, core and a magnetic microsystem closed loop system can be constructed to measure the electrical current through the primary coil. The magnetic field, generated by the primary coil current is sensed by the sensor in the air gap and amplified. This signal is used to generate a current through the secondary coil and therefore compensating the magnetic field in the air gap.

Mikrosistem za merjenje električnega toka

Ključne besede: integrirani senzorji, Hall senzorji, merjenje toka, mikrosistemi

Izvleček: Članek predstavlja metodo merjenja toka z uporabo magnetnega mikrosistema. Z uporabo dveh tuljav, jedra in magnetnega mikrosistema je možno sestaviti zaprtozančni sistem, ki meri tok skozi primarno navitje. Tok skozi primarno navitje ustvari magnetno polje v jedru, katerega zazna senzor v zračni reži. Ta signal ustvari tok skozi sekundarno navitje in s tem kompenzira magnetno polje v zračni reži.

1. Introduction

There are various methods to measure electrical current. The most common methods include the use of a shunt resistor, a transformer or a magnetic sensor. Resistive shunts operate by giving a voltage proportional to the current going through the resistor. This offers good accuracy and low offset, but does not provide electrical isolation and can have high thermal drift. Due to this nonisolated method the resistor or the electronics can be destroyed due to transients. Transformers can be used to electrically isolate the measurement system from the main system, but the main disadvantage of this method is that this only works for AC currents. To extend the operation to DC or low frequency currents, a DC magnetic field sensing element must be added to the system. This can be achieved by adding a magnetic field sensor into the transformer core, by which the DC magnetic field is measured. If the magnetic field sensor signal is combined with the AC signal the measurement range of such a microsystem is extended into the low frequency region.

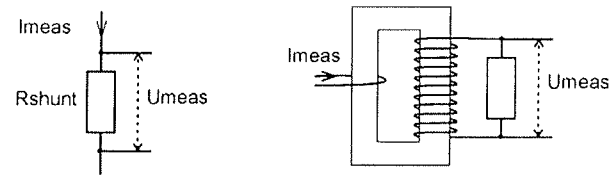

Fig. 1: Methods of current measurement - direct and galvanically separated

2. Closed loop system

The signals from the magnetic sensor and from the coil are combined in such a way, that the field in the magnetic core is always zero. This combination is a closed loop system.

In a closed loop current measuring system the sensor is placed in a compensating field which drives the field across the sensor to zero. The compensating field is generated by a secondary coil with N-turns. Therefore the current in the feedback (secondary) coil is proportional to the field from the primary current scaled by the turns ratio. Usually a shunt resistor is placed in series with the secondary coil to generate a voltage proportional to the measured current. The sensor is situated in the air gap. The magnetic sensor and the amplifying circuitry can be integrated on the same die, reducing the complexity of the wiring. The principle schematic of this closed loop system is shown on fig.2.

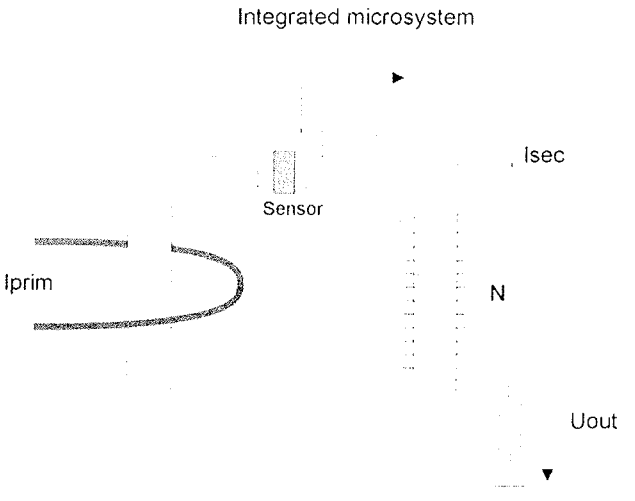

Fig. 2: Closed loop magnetic current sensing circuit

The output voltage for a single turn primary coil can be calculated from the following equation:

$$Uout = Rout \cdot I\,\mathrm{sec} = Rout \cdot Iprim \cdot \frac{1}{N}$$

The measured output voltage is dependent on the Rout shunt resistance and on the secondary coil N turn number. With these two parameters the measured secondary current can be scaled down to the values, deliverable by the integrated circuit.

The advantages for the closed loop system are:

- closed loop allows for higher accuracy
- the sensor always operates around zero magnetic field strength
- closed loop systems have higher bandwidths
- fast responses
- galvanic separation of the measuring system

3. Integrated microsystem for magnetic field sensing

To measure the magnetic field in the magnetic core gap a magnetic field sensor must be placed into the gap. Two types of sensors can be used:

- discrete sensors (for example magneto-resistive, Hall sensors)
- integrated sensors (integrated together with the processing and amplifying electronics)

The only requirement for the sensor is that it fits into the magnetic core air gap. Both types of sensors (discrete and integrated sensors) have been successfully used. The advantage of the integrated sensor system is the simpler wiring, due to the minimal on-chip wire length also the noise introduction is largely reduced. The disadvantage of the integrated version is the overall larger device, which must be fitted into the magnetic core gap.

The emphasis in this article is on the closed loop system with an integrated magnetic sensor, although the discrete version is very similar in operation. A N-well Hall sensor array was used as the sensing element. The Hall sensors can be easily integrated in standard CMOS processes. The array is made from 12 Hall sensors, each biased with 1mA. On the same die also the processing electronics and the current driving amplifiers are integrated. Figure 3. shows the block diagram of the presented integrated circuit, figure 4. the layout of the integrated circuit with the integrated Hall sensor array in the middle.

The magnetic sensor signal processing is similar for the Hall sensors and for the magneto-resistive sensors. Both sensor signals need to be alternated for offset compensating reasons. The sensor signal is amplified and buffered to provide current capability.

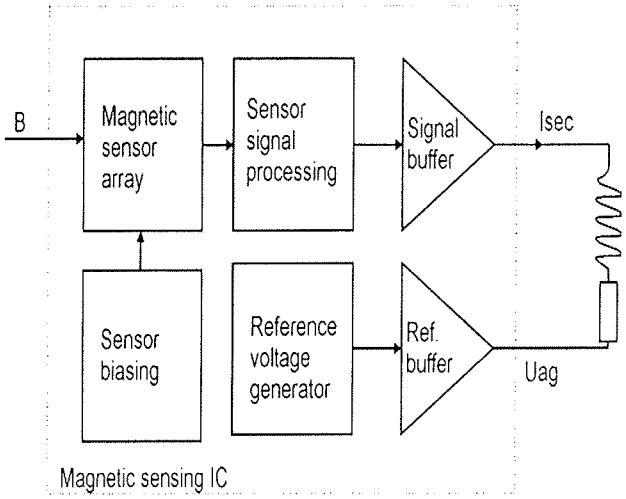

Fig. 3: Magnetic sensing integrated circuit block diagram

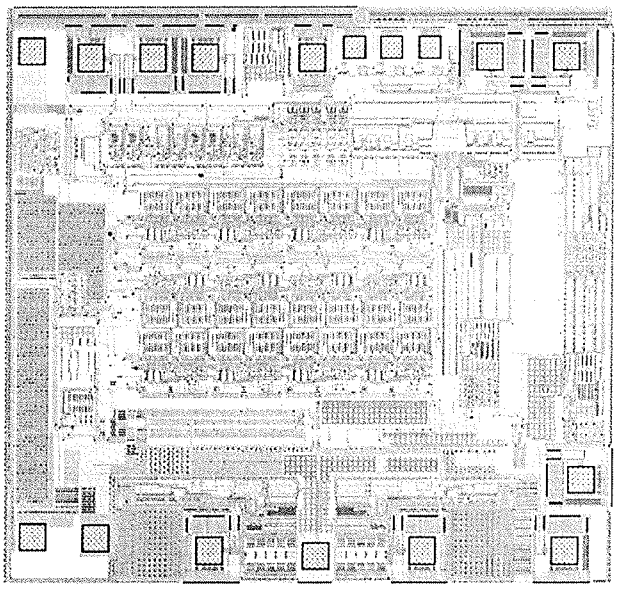

Fig. 4: Integrated microsystem for closed loop measurement

4. Simulation and measurement results

The magnetic core and the two coils have been modeled, enabling the SPICE simulation of the whole microsystem. With that the principle and the realization could be simulated. On fig 5. the step response (0 -> 25A) simulation is visible. The expected secondary coil current is 12.5mA (25A /N=2000). The simulated current is smaller due to the finite open loop gain of the amplifiers. On the secondary current the internal offset canceling circuitry settling is visible. This offset canceling is achieved by HF switching of the sensor signals.

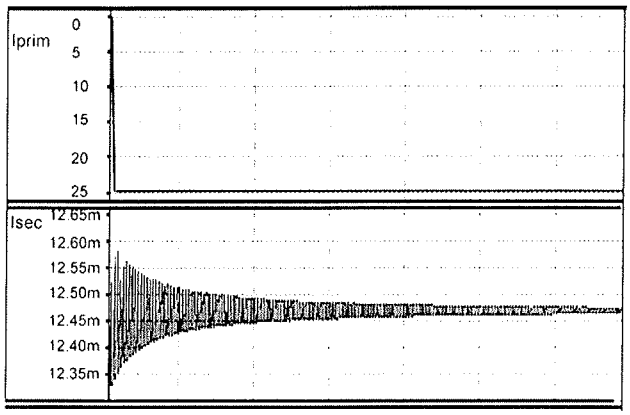

Fig. 5: Simulated 25A step response

On the following simulation the response to a 20A pulses with a frequency of 250Hz is shown. The response to these pulses is a combination of the secondary coil (HF response) and the sensor signal (LF response).

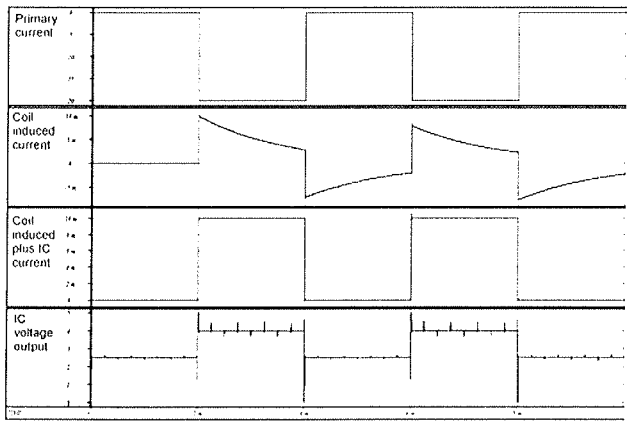

Fig. 6: Simulation of current pulses

The measured frequency response shows a flat frequency characteristics over the requested bandwidth. At lower frequencies the IC microsystem is the dominant contributor to the output signal, at higher frequencies the microsystem acts as a virtual ground and the signal comes from the current transformer. The frequency response is on fig.7. As can be seen, the frequency response shows variations below 0.6dB over the frequency range of up to 200kHz (the scale of the plot is 1dB/div). This means, that the mismatch between the secondary coil (dominant at high frequencies) and the sensor signal (dominant at low frequencies) is less than 0.6dB.

The measurement was made with a network analyzer and coils with a 5/2000 turn ratio. The primary current was measured on a 10Ω resistor, the secondary on a 100Ω. The expected result can be calculated :

$$\frac{Uout}{Uin} = \frac{I\sec \cdot Rout}{Iprim \cdot Rin} = \frac{5 \cdot 100\Omega}{2000 \cdot 10\Omega} = 0.025 \Rightarrow -32.04dB$$

The measured value is -32.27dB (at low frequencies) and shows good matching with the expected value.

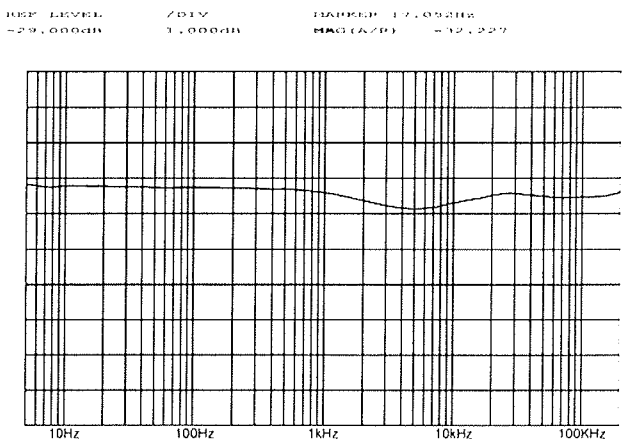

Fig. 7: Frequency dependency of the system

The positioning of the two coils largely influences the performance of the system, the best results are achieved when the primary and the secondary coil are overlapped and physically near to the sensor.

The frequency response of a non-optimal coil positioning can be seen on fig. 8, where the secondary coil was placed on the opposite side of the primary coil on the magnetic core. In this position the secondary coil induces less voltage and therefore the coil induced high frequency response is lower by almost 3dB.

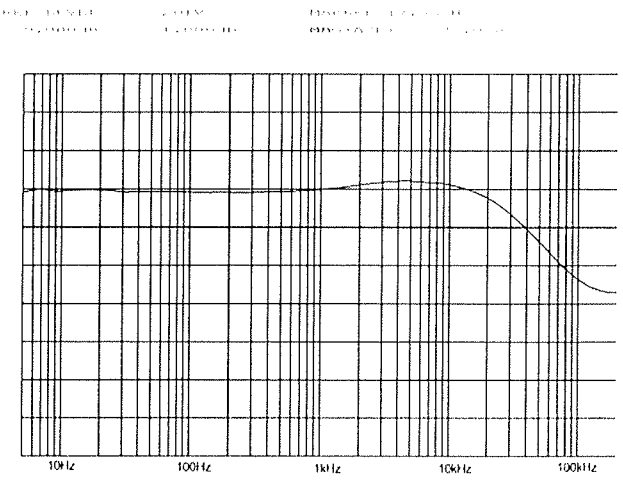

Fig. 8: Frequency dependency of the system with non-optimal coil position

5. Conclusion

It was shown, that a magnetic field sensing microsystem in a closed loop configuration for measuring currents has many distinct advantages over other methods. It combines the fast response times of the transformer method with the DC accuracy of the shunt resistor method. The Hall

magnetic sensor, processing electronics and the current amplifiers are all integrated on the same silicon die, creating an integrated microsystem. This die with the sensors is placed into the core air gap. With the use of the microsystem approach the interconnecting lines are largely shortened and therefore crosstalk and interference possibilities are reduced in comparison with the discrete sensor version. With an optimal positioning of the two coils on the magnetic core an matching error of 0.6dB between the low frequency sensor and the high frequency coil response can be achieved.

6. Literature

/1/ J. Trontelj, A. Pevec, J. Trontelj ml.: " Contactless current measurement with integrated Hall elements" ; The proceedings of the MIDEM 1997 conference

/2/ A. Pevec, J. Trontelj: "Microsystems with integrated capacitive, magnetic and optical sensors" Informacije MIDEM nr. 3-2002

/3/ W. Koon: "Current sensing for energy metering", Analog Devices, Application notes www.eetasia.com/ARTICLES/2002APR/2002APR08_AMD_DSP_EMS_TAC.PDF

/4/ Honeywell: "Magnetic current sensing", Honeywell, Application notes http://www.ssec.honeywell.com/magnetic/datasheets/an209.pdf

dr. Albin Pevec
prof. dr. Janez Trontelj

University of Ljubljana, Faculty of Electrical Engineering
Tržaška 25, Ljubljana, Slovenia
Tel: +386 (01) 4768337
Fax: +386 (01) 4264644
Email: albin@kalvarija.fe.uni-lj.si
Email: janez.trontelj1@guest.arnes.si

Prispelo (Arrived): 06.06.2002 *Sprejeto (Accepted):25.05.2003*

Čestitka prof. dr. Mariji Kosec za priznanje Ambasador Republike Slovenije v znanosti za leto 2003

20. junija 2003 je Slovenija dobila tri nove Ambasadorje Republike Slovenije v znanosti: Prof. dr. Marijo Kosec, Prof. dr. Damijana Miklavčiča in akademika prof. dr. Jožeta Trontlja. O odličnosti nagrajencev pričajo uradne utemeljitve, dostopne na spletnih straneh http://www.mszs.si/slo/ministrstvo/nagrade/ambasador/2003.asp.

Svečani dogodek nas je še toliko bolj razveselil, saj je med nagrajenci prvič tudi članica društva MIDEM, **prof. dr. Marija Kosec**, ki jo vsi člani dobro poznamo. Ne samo zato, ker je predsednica društva, temveč zaradi njene izžarevajoče energije in zagnanosti.

Prof. dr. Marija Kosec, izredna profesorica za materiale na Naravoslovnotehnični fakulteti, Univerze v Ljubljani, in vodja Odseka za elektronsko keramiko na Institutu „Jožef Stefan", je vodilna raziskovalka na področju elektronske keramike, pretežno feroelektrikov in piezoelektrikov. Med svetovne dosežke prištevajo rezultate njenih raziskav razumevanja sinteze sol-gel tankih plasti in prahov v sistemih $Pb(Zr, Ti)O_3$. S tem je odprla nove možnosti nizkotemperaturnih sintez (pri 400°C), kar je novost v svetu keramičnih materialov.

Rdeča nit njenega dela je odličnost in mednarodno uveljavljanje Slovenije in slovenske znanosti. Rezultate raziskav je prof. Koščeva objavila v 95 člankih, večinoma v uglednih revijah na področju materialov. Imela je 25 vabljenih predavanj na konferencah in 20 vabljenih predavanj na univerzah in inštitutih. Bila je sourednica 11 zbornikov s konferenc. Ima tri domače patente in en evropski patent. Njena dela so citirana več kot 500-krat. Z več prispevki je sodelovala v monografiji z naslovom "Sol-gel science and technology", ki je letos izšla pri založbi Kluwer.

Ena izmed njenih odlik je zagotovo sposobnost, da zna odlično povezovati osnovne raziskave z razvojnimi in uporabnimi. Prof. Marija Kosec je nosilka več kot 30 pogodb z industrijo, tako tujo kot domačo. O kvaliteti njenih raziskav pa govorijo tudi pogodbe s tujimi partnerji, kot je npr. razvoj prototipov iz feroelektrične keramike, ki omogočajo popolnoma nov način tiskanja (MAN Roland, Druckmachinen, Ausburg, Nemčija).

Prof. Koščeva s svojo raziskovalno aktivnostjo skrbi za stalno promocijo slovenske znanosti v svetu. V to kategorijo spadajo v prvi vrsti mednarodni projekti (NATO, 5. OP, COST) v vrednosti več kot milijon EUR. Pomembna je njena mednarodna pedagoška aktivnost. Bila je gostujoča znanstvenica leta 1993, predavateljica v okviru letne šole „Feroelektrične tanke plasti" leta 1995 in gostujoča profesorica leta 2001 s serijo predavanj „On ceramic processing", na elitni šoli École Polytehnique Fedérale de Laussanne (EPFL) v Laboratoriju za keramiko, ki ga vodi prof. Neva Setter. Prof. Koščeva sodeluje kot mentorica za diplomska dela, magisterije in doktorate tako z Univerzo v Ljubljani, kot v komisijah za zagovor doktorskih del po svetu, npr. v prej omenjeni EPFL, na Tehnični univerzi Copenhagen (Danska), Univerzi Oolu (Finska) in Univerzi v Corku (Irska).

Pod njenim vodstvom je bila skupina na Institutu »Jožef Stefan« imenovana za Marie Curie Training Site in si od Evropske unije pridobila naziv Centre of Excellence za naslednja štiri leta. Leta 1997 je uspešno organizirala mednarodno delavnico v okviru N.A.T.O., leta 2000 pa je predsedovala organizacijskemu odboru svetovnega kongresa o elektrokeramiki »Electroceramics VII«.

Prof. Koščeva je članica vrste odborov in komisij s področja keramike tako v Sloveniji kot tudi v svetu. Omeniti je treba njeno prestižno članstvo v IEEC Ferroelectric Committee, saj so v njem samo štirje člani iz Evrope. Je marljiva in prizadevna predsednica društva MIDEM, ki ga je že leta 1999 popeljala v ugledno mednarodno združenje IMPAS.

Kar koli se v svetu zgodi na področju elektronske keramike, še posebej na področju feroelektrikov, ne mine brez prof. Koščeve; naj bo to nova knjiga, posvetovanje, letna šola, večji projekt v okviru Evropske skupnosti ali pa samo zagovor doktorske disertacije.

Prof. Koščeva je z raziskovalnim delom dosegla neverjetno mednarodno odmevnost in z nastopanjem v mednarodnih znanstvenih krogih veliko prispevala k prepoznavnosti Slovenije v svetu in k povečanju njenega mednarodnega ugleda. Tudi društva MIDEM.

V imenu članov društva MIDEM ji izrekam **iskrene čestitke**!

Marko Topič

Posvet o novih tehnologijah
Symposium on new technologies

Igor Pompe

Zavod TC SEMTO, Stegne 25, 1000 Ljubljana, Slovenija, semto@guest.arnes.si

Zavod TC SEMTO je organiziral posvet o novih tehnologijah v dveh delih: 3. 6. 2003 v prostorih Univerze v Ljubljani, Fakultete za elektrotehniko, in 20. 6. 2003 v prostorih Instituta "Jožef Stefan (IJS). Namen posveta je bil seznaniti člane TC SEMTO z novimi tehnologijami in dejavnostjo nekaterih raziskovalno-razvojnih laboratorijev in skupin.

V nadaljevanju podajamo naslove in kratko vsebino prispevkov. Obširnejše bodo posamezni avtorji poročali v člankih, ki bodo objavljeni v revijah **Materiali in tehnologije** ali **Informacije Midem**.

Zavod TC SEMTO has organized Symposium on New Technologies in two parts: on June 3, 2003 in the premises of Univerza v Ljubljani, Fakulteta za elektrotehniko and on June 20, 2003 at Jožef Stefan Institute in Ljubljana. The aim of the symposium was information of TC SEMTO members about new technologies and activities of some of the research laboratories and groups.

The titles and abstracts of the lectures are published as follows. More details can be found in the articles that will be published in the reviews INFORMACIJE MIDEM and MATERIALI IN TEHNOLOGIJE.

Prispevki:

Prof. dr. Marija Kosec, Institut "Jožef Stefan": **Keramične tehnologije, keramične plasti iz raztopin**

Predstavljene so bile razne keramične tehnologije. Podrobneje je bil predstavljen postopek pridobivanja keramičnih plasti iz raztopin.

Dr. Peter Panjan, Institut "Jožef Stefan" : **Razvoj keramičnih prevlek za zaščito orodij in strojnih delov**

Predstavljena je bila paleta raznih nekaj mikrometrov debelih keramičnih trdih prevlek na površini orodja za zaščito pred abrazijsko, adhezijsko in kemotermično obrabo. S temi prevlekami se trajnost orodij poveča. Predstavljeni so bili tudi tehnološki postopki za nanašanje prevlek.

Dr. Uroš Cvelbar, Laboratorij za plazmo, Institut "Jožef Stefan": **Aktivacija površin polimernih materialov s kisikovo plazmo**

Obravnavan je bil postopek aktivacije površin polimernih materialov s kisikovo plazmo, da se doseže boljša omočljivost površine (lepše in lažje tiskanje ali boljše tesnjenje pri zalivanju ohišij).

Dr. Miran Mozetič, Laboratorij za plazmo, Institut "Jožef Stefan": **Perspektive široke industrijske uporabe plazemskega čiščenja**

Prikazan je bil postopek čiščenja površin z vodikovo plazmo. Možno je doseči atomsko čiste površine. Postopek je ekološko prijazna alternativa mokremu kemijskemu postopku, vendar zahteva relativno drage plazemske reaktorje.

Dr. Vojteh Leskovšek, Inštitut za kovinske materiale in tehnologije: **Nitriranje v plazmi**

Obdelan je bil postopek nitriranja v plazmi, postopek kemotermičnega modificiranja površin za utrjevanje strojnih delov in orodij, ki se jim s tem poveča trajno nihajna in upogibna trdnost, občutljivost jekla na zareze pa se zmanjša. Poveča se korozijska odpornost nizko in srednje legiranih jekel. Opisan je bil tehnološki proces. Parametri se prilagajajo kemični sestavi in predhodni toplotni obdelavi jekel. Nizke temperature nitriranja omogočijo, da jedro strojnega dela ali orodja tudi po nitriranju ohrani svoje prejšnje mehanske lastnosti.

Doc. dr. Drago Resnik, doc. dr. Danilo Vrtačnik, prof. dr. Slavko Amon, Laboratorij za mikrosenzorske strukture, Fakulteta za elektrotehniko, Univerza v Ljubljani: **Napredni načini mikroobdelave silicija za senzorske in aktuatorske mikrostrukture**

Prikazani so bili postopki obdelave silicija pri izdelavi silicijevih 3D-mikrostruktur, kjer se izkoriščajo poleg električnih tudi mehanske lastnosti silicija. Kombinacije novih mikro-

elektronskih materialov in naprednih tehnologij omogočajo realizacijo precizne površinske in globinske mikroobdelave zahtevnih silicijevih mikrostruktur.

Marija Zupan, univ. dipl. kem. tehnolog, IETP PT, Kranj: **Pet korakov do spajkanja brez Pb**

Predavanje je obsegalo razloge za vpeljavo spajkanja brez Pb v elektronski industriji, časovni načrt in korake, ki so potrebni za vpeljavo te tehnologije v proizvodnjo. Predstavljeni so bili ustrezni materiali in oprema ter merila za njihov izbor (plošče, zlitine spajk, prevleke itd..).

Doc. dr. Roman Kamnik, prof. dr. Tadej Bajd, Laboratorij za robotiko, Fakulteta za elektrotehniko, Univerza v Ljubljani: **Robotika v sodobnem svetu**

Podano je bilo stanje pri razvoju in uporabi robotike. Podani so bili osnovni pojmi iz robotike in osvetljeni vzroki za pospešen razvoj. Predstavljena je bila uporaba robotov v industrijskem okolju in delo Laboratorija za robotiko na Fakulteti za elektrotehniko v Ljubljani.

Dr. Vladimir Jovan, TC ARI: **Avtomatizacija v industriji**

Predstavljeno je bilo stanje avtomatizacije in informatizacije v slovenskih proizvodnih podjetjih. V nadaljevanju je avtor predstavil glavne razloge za vlaganja v avtomatizacijo in informatizacijo proizvodnje v slovenskih podjetjih, podal oceno rezultatov izvedenih projektov, izpostavil kritične aktivnosti teh projektov in opisal strategije njihovega izvajanja v slovenskih podjetjih. V drugem delu je predavatelj predstavil vrsto izvedbenih projektov avtomatizacije in informatizacije proizvodnje, ki sta jih izvedli dve skupini z Instituta "Jožef Stefan",in sicer Odsek za sisteme in vodenje ter Odsek za avtomatiko, biokibernetiko in robotiko. Ob koncu je bilo v kratkem predstavljeno delo Tehnološkega centra ARI (TC za avtomatizacijo, robotizacijo in informatizacijo proizvodnje).

Dr. Slavko Dolinšek, Fakulteta za strojništvo, Univerza v Ljubljani in Regionalni tehnološki center Zasavje: **Tehnologija DMLS (neposredno lasersko sintranje kovinskih prahov - od izdelave prototipnih orodij do hitre proizvodnje)**

Predstavljeno je bilo delo Regionalnega tehnološkega centra Zasavje (RTCZ) s poudarkom na neposrednem laserskem sintranju kovinskih prahov za hitro izdelavo orodij ali malih serij izdelkov zelo zahtevnih oblik. Predstavljene so bile možnosti izdelave delov in/ali orodij v RTCZ.

Dr. Martin Bizjak, Iskra Stikala: **Kontaktni materiali za nizkonapetostne stikalne aparate**

Obravnavani so bili kontaktni materiali za nizkonapetostne stikalne aparate v energetiki. Osnovni material je srebro, ki je lahko legirano s kovinami, lahko pa so srebru primešana zrnca ali vlakenca kovine ali kovinskih oksidov in grafita. Grafit je lahko primešan tudi v obliki drobnih palčk. Dodatki v srebru določajo lastnosti kotaktnega materiala.

Franc Koplan, univ. dipl. inž., Magneti; Paul McGuiness, Institut "Jožef Stefan": **Merjenje razmagnetilnih krivulj do 450 °C**

Predstavljeno je bilo delo, opravljeno v sodelovanju med IJS in podjetjem Magneti Ljubljana, katerega rezultat omogoča merjenje razmagnetilnih krivulj pri temperaturah merjencev do 450 °C . Nova tehnologija daje potencialnim uporabnikom konkurenčno prednost pri razvoju aplikacij z magneti pri visokih temperaturah.

Dr. Vincenc Nemanič, Institut "Jožef Stefan": **Novi nanomateriali - obetaven točkasti vir elektronov**

Predstavljeno je bilo delo na Odseku za tehnologijo površin in optoelektroniko IJS.

Predstavljene so bile katode s hladno emisijo iz ogljikovih nanocenk in drugih, novih materialov (npr. iz molibden sulfida).

Dr. Darko Makovec, Institut "Jožef Stefan": **Priprava MnZn-feritov s hidrotermalno obdelavo oksidov**

Podana je bila informacija o delu skupine z IJS in iz Iskre Feriti pri razvoju nove tehnologije priprave MnZn-feritnih prahov, ki temelji na hidrotermalnih reakcijah med izhodnimi oksidi. S hidrotermalno obdelavo oksidov je možno pripraviti fin feritni prah podobne sestave kot pri klasični metodi kalcinacije in mletja. Nova metoda je predvsem energijsko ugodnejša, ker dobljenih prahov ni treba intenzivno mleti kot pri klasičnem postopku.

Darko Belavič, univ. dipl. inž., Hipot: **Debeloplastne tehnologije**

Predstavljene so bile novosti v tehnologijah izdelave debeloplastnih vezij in izdelava LTCC-podlag .

Informacije MIDEM
Strokovna revija za mikroelektroniko, elektronske sestavine dele in materiale

NAVODILA AVTORJEM

Informacije MIDEM je znanstveno-strokovno-društvena publikacija Strokovnega društva za mikroelektroniko, elektronske sestavne dele in materiale - MIDEM. Revija objavlja prispevke s področja mikroelektronike, elektronskih sestavnih delov in materialov. Ob oddaji člankov morajo avtorji predlagati uredništvu razvrstitev dela v skladu s tipologijo za vodenje bibliografij v okviru sistema COBISS.
Znanstveni in strokovni prispevki bodo recenzirani.

Znanstveno-strokovni prispevki morajo biti pripravljeni na naslednji način:

1. Naslov dela, imena in priimki avtorjev brez titul, imena institucij in firm
2. Ključne besede in povzetek (največ 250 besed).
3. Naslov dela v angleščini.
4. Ključne besede v angleščini (Key words) in podaljšani povzetek (Extended Abstract) v anglešččini, če je članek napisan v slovenščini
5. Uvod, glavni del, zaključek, zahvale, dodatki in literatura v skladu z IMRAD shemo (Introduction, Methods, Results And Discsussion).
6. Polna imena in priimki avtorjev s titulami, naslovi institucij in firm, v katerih so zaposleni ter tel./Fax/Email podatki.
7. Prispevki naj bodo oblikovani enostransko na A4 straneh v enem stolpcu z dvojnim razmikom, velikost črk namanj 12pt. Priporočena dolžina članka je 12-15 strani brez slik.

Ostali prispevki, kot so poljudni cčlanki, aplikacijski članki, novice iz stroke, vesti iz delovnih organizacij, inštitutov in fakultet, obvestila o akcijah društva MIDEM in njegovih članov ter drugi prispevki so dobrodošli.

Ostala splošna navodila

1. V članku je potrebno uporabljati SI sistem enot oz. v oklepaju navesti alternativne enote.
2. Risbe je potrebno izdelati ali iztiskati na belem papirju. Širina risb naj bo do 7.5 oz.15 cm. Vsaka risba, tabela ali fotografija naj ima številko in podnapis, ki označuje njeno vsebino. Risb, tabel in fotografij ni potrebno lepiti med tekst, ampak jih je potrebno ločeno priložiti članku. V tekstu je treba označiti mesto, kjer jih je potrebno vstaviti.
3. Delo je lahko napisano in bo objavljeno v slovenščini ali v angleščini.
4. Uredniški odbor ne bo sprejel strokovnih prispevkov, ki ne bodo poslani v dveh izvodih skupaj z elektronsko verzijo prispevka na disketi ali zgoščenki v formatih ASCII ali Word for Windows. Grafične datoteke naj bodo priložene ločeno in so lahko v formatu TIFF, EPS, JPEG, VMF ali GIF.
5. Avtorji so v celoti odgovorni za vsebino objavljenega sestavka.

Rokopisov ne vračamo. Rokopise pošljite na spodnji naslov.

Uredništvo Informacije MIDEM
MIDEM pri MIKROIKS
Stegne 11, 1521 Ljubljana, Slovenia
Email: Iztok.Sorli@guest.arnes.si
tel. (01) 5133 768, fax. (01) 5133 771

Informacije MIDEM
Journal of Microelectronics, Electronic Components and Materials

INSTRUCTIONS FOR AUTHORS

Informacije MIDEM is a scientific-professional-social publication of Professional Society for Microelectronics, Electronic Components and Materials - MIDEM. In the Journal, scientific and professional contributions are published covering the field of microelectronics, electronic components and materials.
Authors should suggest to the Editorial board the classification of their contribution such as : original scientific paper, review scientific paper, professional paper...
Scientific and professional papers are subject to review.

Each scientific contribution should include the following:

1. Title of the paper, authors' names, name of the institution/company.
2. Key Words (5-10 words) and Abstract (200-250 words), stating how the work advances state of the art in the field.
3. Introduction, main text, conclusion, acknowledgements, appendix and references following the IMRAD scheme (Introduction, Methods, Results And Discsussion).
4. Full authors' names, titles and complete company/institution address, including Tel./Fax/Email.
5. Manuscripts should be typed double-spaced on one side of A4 page format in font size 12pt. Recommended length of manuscript (figures not included) is 12-15 pages
6. Slovene authors writing in English language must submit title, key words and abstract also in Slovene language.
7. Authors writing in Slovene language must submit title, key words and extended abstract (500-700 words) also in English language.

Other types of contributions such as popular papers, application papers, scientific news, news from companies, institutes and universities, reports on actions of MIDEM Society and its members as well as other relevant contributions, of appropriate length , are also welcome.

General informations

1. Authors should use SI units and provide alternative units in parentheses wherever necessary.
2. Illustrations should be in black on white paper. Their width should be up to 7.5 or 15 cm. Each illustration, table or photograph should be numbered and with legend added. Illustrations, tables and photographs must not be included in the text but added separately. However, their position in the text should be clearly marked.
3. Contributions may be written and will be published in Slovene or English language.
4. Authors must send two hard copies of the complete contributon, together with all files on diskette or CD, in ASCII or Word for Windows format. Graphic files must be added separately and may be in TIFF, EPS, JPEG, VMF or GIF format.
5. Authors are fully responsible for the content of the paper.

Contributions are to be sent to the address below.

Uredništvo Informacije MIDEM
MIDEM pri MIKROIKS
Stegne 11, 1521 Ljubljana, Slovenia
Email: Iztok.Sorli@guest.arnes.si
tel.+386 1 5133 768, fax.+386 1 5133 771